Grid Presentation for Heegaard Floer Homology of a Double Branched Cover

by

SAYONITA GHOSH HAJRA

(Under the Direction of Gordana Matić)

Abstract

Heegaard Floer homology, introduced by Peter Ozsváth and Zoltan Szabó, is an invariant of a closed oriented 3-manifold. Because of the complex nature of moduli spaces used in the definition, direct computations of this homology are difficult to achieve. In 2006, Sarkar and Wang proposed an algorithm to compute the Heegaard Floer homology groups of a closed oriented 3-manifold in a purely combinatorial way. Ozsváth, Stipsicz and Szabó improved on Sarkar-Wang's approach to show that using multi-pointed nice diagrams one can define a combinatorial stabilized hat-version of Heegaard-Floer homology, and combinatorially prove its invariance. Stipsicz gave a description of the stabilized hat-version of Heegaard Floer homology for a double branched cover of S^3 branched over a link based on the grid presentation of the link. Here we present an algorithm to compute this stabilized version. We define the extended grid homology groups associated to a link L and show combinatorially that the groups calculated by this algorithm are independent of certain choices made in constructing the extended grid diagram.

Index words: Heegaard Floer homology, Grid diagrams, Extended grid diagrams

Grid Presentation for Heegaard Floer Homology of a Double Branched Cover

by

SAYONITA GHOSH HAJRA

BSc, University of Calcutta, India, 2003

MSc, University of Calcutta, India, 2005

MA, The University of Toledo, 2009

A Dissertation Submitted to the Graduate Faculty

of The University of Georgia in Partial Fulfillment

of the

Requirements for the Degree

Doctor of Philosophy

Athens, Georgia

2014

Grid Presentation for Heegaard Floer Homology of a Double Branched Cover

by

SAYONITA GHOSH HAJRA

Professor:	Gordana Matić
Committee:	David Gay William Kazez Michael Usher

Electronic Version Approved:

Julie Coffield
Interim Dean of the Graduate School
The University of Georgia
August 2014

Dedication

I dedicate this work to my parents, Anjushree and Hiranmay Ghoshhajra.

Acknowledgments

I would like to thank my parents, Anjushree and Hiranmay Ghoshhajra, my sister, Ipsita, and her family, and my beloved husband, Santosh Kandel, for their love, trust and unconditional support. I would like to thank all of my friends, especially Susan Weldon, for their enormous help and support.

I would like to thank my advisor Dr. Gordana Matić for her continuous support, care, patience and for providing the opportunity to do the research.

I would like to thank my teachers and mentors, especially Dr. Edward Azoff, Dr. David Gay, Dr. William Kazez, Dr. Michael Usher, Dr. Angela Gibney, Dr. Daniel Krashen, Dr. Lisa Townsley for their suggestions and advices in my teaching and research. I would like to specially thank Dr. Sybilla Beckmann for holding my hands and introducing me to the world of educating future teachers. Also, a special thanks goes to Ms. Judy Milton for giving me the opportunity to hone my leadership and teaching qualities at UGA.

I would like to thank Department of Mathematics, Graduate School at the University of Georgia for giving me the opportunity to study here and for helping me with professional and personal development. I would like to thank Ms. Laura Ackerley for all her help in preparing my paperwork for graduation.

A special thanks to Allan Lacy for helping with the Sage code. I thank Kate Thompson for helping with the technology.

Contents

List of Figures

Chapter 1

Introduction

Heegaard Floer homology, introduced by Peter Ozsváth and Zoltan Szabó, is an invariant of a closed oriented 3-manifold. The definition of Heegaard Floer homology is based on Heegaard decompositions and Heegaard diagrams for 3-manifolds along with concepts from Lagrangian Floer homology [7]. Lagrangian Floer homology is defined for a symplectic manifold and a pair of Lagrangian submanifolds, where the generators are the intersection points of the Lagrangian submanifolds and the boundary maps count suitable pseudo-holomorphic disks. In the same spirit, Ozsváth and Szabó [16] defined Heegaard Floer homology that involves the symmetric product of the splitting Heegaard surface for a Heegaard decomposition of a 3-manifold as the symplectic manifold, and tori obtained as product of the boundaries of families of compressing discs as Lagrangian submanifolds. Because of the complex nature of moduli spaces involved, direct computations of these homology groups are difficult to achieve.

In 2006, Sarkar and Wang [22] proposed an algorithm to compute the Heegaard Floer homology of a closed oriented 3-manifold for specific Heegaard diagrams in a purely combinatorial way. Although they calculated the homology groups combinatorially, the combinatorial proof for the invariance of the homology under the "nice" moves was not done. Later Ozsváth, Stipsicz and Szabó [15] gave a combinatorial description of the hat-version of Heegaard Floer homology using pair-of-pants decompositions. In [15], Ozsváth, Stipsicz and Szabó showed that the stable hat-version of Heegaard Floer homology is a diffeomorphism invariant of the 3-manifold in a purely combinatorial way.

In 2009, Manolescu, Ozsváth and Sarkar [12] calculated all versions of link Floer homology of knots and links in S^3 using grid diagrams and in [13, 14], a topological invariance of this combinatorial version of link Floer homology is shown using combinatorial methods. In [5], a combinatorial proof for the invariance of knot floer homology over $\mathbb{Z}$ is shown using a Heegaard diagram for the pullback of a knot in S^3 in its cyclic branched cover. In the same spirit, Stipsicz [24] gave a description of the hat-version of Heegaard Floer homology based on the double branched cover construction and grid diagrams. Though not every 3-manifold admits a double branched cover presentation along a link in S^3 (e.g., 3-torus is not a 2-fold branched cover of S^3 [8]), the construction using double branched cover provides a wealth of interesting examples. Stipsicz gave a description of the stabilized hat-version of Heegaard Floer homology for a double branched cover of S^3 branched over a link based on the grid presentation of the link. We call the groups defined this way the extended grid homology $EGH(G)$ of the link L with extended grid diagram G. A way to combinatorially show that this algorithm defines a link invariant is to show that these groups are independent of the choices in the construction of the extended grid diagram and of the grid moves. We prove the following theorem:

Theorem 1.0.1. *The extended grid homology groups $EGH(G)$ based on the double branched cover construction are independent under the choice of the "cut lines", the choice of the "new curves", and under the cyclic permutation grid move.*

We develop a computer code to compute the hat-version of Heegaard Floer homology of the double branched cover of S^3 along a link in S^3.

We organize this dissertation as follows:

In Chapter 2, we recall the background material needed to understand this homology groups. We recall the preliminaries on Heegaard decompositions, (one-/ multi-pointed) Heegaard diagrams, and the Heegaard Floer homology groups based on one-pointed and multi-pointed Heegaard diagrams. Here we discuss the nice diagrams, nice moves, and the invariance of the stable version of the homology under those nice moves.

In Chapter 3, we discuss the grid diagrams, the three grid moves: cyclic permutation, commutation and stabilization, and the extended grid diagram.

In Chapter 4, we describe a grid diagram based link invariant $EGH(G)$ corresponding to the stabilized hat-version of the Heegaard Floer homology for the double branched cover.

In Chapter 5, we present our main result, Theorem 1.0.1.

In Chapter 6, we present an algorithm we use to devise a computer code to calculate $EGH(G)$. This code is in the developmental stage as due to memory handling issues it can at the moment handle only extended grids of size up to $n = 6$.

We thank Allan Lacy for his help with the Sage code.

Chapter 2

Preliminaries

2.1 Heegaard Decompositions and Heegaard Diagrams

Let Y be a closed, oriented, connected 3-manifold. A genus g handlebody U is the 3-manifold with boundary obtained by attaching g handles $\mathbb{D}_i^2 \times [0,1]$, $i = 1, 2, \ldots g$, to the 3-ball via a homeomorphism $h_i : \mathbb{D}_i^2 \times \{0,1\} \longrightarrow \partial B^3$ along $2g$ disjoint disks in the boundary of the ball. The boundary of the handlebody U is an oriented surface of genus g. We can glue together two handlebodies of genus g along their common boundary. $\mathbb{D}^2 \times \{\frac{1}{2}\}$ is a compressing disk in Y. More generally, we have:

Definition 2.1.1. *A compressing disk is an embedded disk $D \subset Y$ with $D \cap \partial Y = \partial D$ such that ∂D is homotopically nontrivial in ∂Y.*

Any 3-manifold with boundary is a handlebody if it can be cut down to a ball by cutting along compressing disks, i.e., if there exists compressing disks $D_i \subset Y$ with $\partial D_i \subset \Sigma_g = \partial Y$ such that $Y - \cup_{i=1}^{g} D_i \cong B^3$, then Y is a handlebody.

Definition 2.1.2. *(Heegaard decomposition for Y) If $Y = U_0 \cup_{\Sigma_g} U_1$ is obtained by gluing together two handlebodies U_0 and U_1 of genus g along their common boundary $\Sigma_g = \partial U_0 = -\partial U_1$, we say that U_1, U_2 is a Heegaard decomposition for Y.*

Theorem 2.1.1. *(Existence of Heegaard decompositions [23]) Let Y be a closed, oriented, connected 3-manifold. Then Y admits a Heegaard decomposition.*

Proof. Every 3-manifold admits a triangulation. The union of vertices and edges (the 1-skeleton) forms a graph in Y. Let U_0 be a small neighborhood of this graph. We can think of this neighborhood as obtained by taking a ball around each vertex and taking solid cylinders around each edge. Consider a maximal tree T in the 1-skeleton. A neighborhood of T, $B(T)$, is a 3-ball. The neighborhood of the edges not in T are attached to $B(T)$ as handles and the neighborhood of the union of the vertices and edges is a handlebody U_0. The closure of the complement of U_0 is a handlebody U_1 as it consists of the tubular neighborhood of the barycentres of the 3-simplices connected to the barycentres of the corresponding 2-simplices through handles. Also, the complement of U_0 in the faces of the triangulation are compressing disks for U_1 (Figure 2.1). Since, $\partial(U_0) = \partial(\overline{Y - U_0}) = \partial(U_1)$, the two handlebodies have the same genus. Therefore, $Y = U_0 \cup U_1$ is a Heegaard decomposition for Y. □

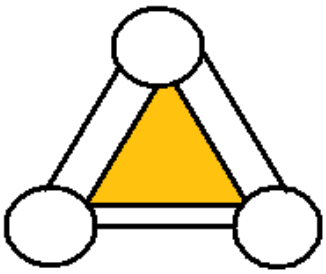

Figure 2.1: Compressing disk for U_1.

From the above proof, it is clear that the same 3-manifold admits a lot of different Heegaard decompositions.

Definition 2.1.3. *(Unknotted Arc) An arc γ is said to be a properly embedded unknotted arc in a 3-ball B^3 if there exists an embedded arc τ in $S^2 = \partial B^3$ and an embedded disc $D \subset B^3$ such that $\partial D = \gamma \cup \tau$.*

Definition 2.1.4. *(Stabilization) Given a Heegaard decomposition $Y = U_0 \cup_{\Sigma_g} U_1$ of genus g, we can construct a genus $(g+1)$ decomposition of Y by choosing two points in Σ_g and connecting those two points by an unknotted arc γ in U_1. Let U_0' be the union of U_0 and a tubular neighborhood N of*

γ. Let $U_1' = U_1 - N$. Then $Y = U_0' \cup_{\Sigma'} U_1'$ is called the stabilization of Y. The inverse operation is called destabilization.

Theorem 2.1.2. *([23]) Any two Heegaard decompositions for Y are related by a sequence of stabilizations (and destabilizations).*

Definition 2.1.5. *(Attaching Circles) A complete set of attaching circles $(\gamma_1, \ldots, \gamma_g)$ for a handlebody U is a collection of closed embedded curves in $\Sigma_g = \partial U$ such that the curves γ_i are disjoint from each other and bound disjoint embedded disks D_{γ_i} (called compressing disks) in U and $\Sigma_g - \gamma_1 - \cdots - \gamma_g$ is $2g$-times punctured spheres.*

In other words, boundary of the compressing disks are called attaching circles. We call these circles attaching circles because we can build the handlebody U from Σ_g by attaching disks D_{γ_i} along the attaching circles γ_i and then filling in by a ball.

Definition 2.1.6. *(Heegaard Diagram [17, 18]) Let $Y = U_0 \cup_{\Sigma_g} U_1$ be a genus g Heegaard decomposition for Y. A compatible Heegaard diagram $(\Sigma_g, \boldsymbol{\alpha}, \boldsymbol{\beta})$ is given by Σ_g together with a collection of curves $\alpha_1, \ldots, \alpha_g, \beta_1, \ldots, \beta_g$ with $\boldsymbol{\alpha} = (\alpha_1, \ldots, \alpha_g)$ a complete set of attaching circles for U_0 and $\boldsymbol{\beta} = (\beta_1, \ldots, \beta_g)$ a complete set of attaching circles for U_1 such that the $\boldsymbol{\alpha}$- and $\boldsymbol{\beta}$- curves intersect each other transversally.*

Let $\boldsymbol{\alpha} = (\alpha_1, \ldots, \alpha_g)$ and $\boldsymbol{\beta} = (\beta_1, \ldots, \beta_g)$ be two sets of attaching circles on a surface Σ_g. Consider $\Sigma_g \times [0,1]$ such that $\boldsymbol{\alpha}$ circles are on $\Sigma_g \times \{1\}$ and $\boldsymbol{\beta}$ circles are on $\Sigma_g \times \{0\}$. We can construct a 3-manifold by attaching a 2-handle $\mathbb{D}^2 \times [0,1]$ along each α_i and β_j and then capping off with two 3-handles. This shows how a Heegaard diagram determines a 3-manifold with a Heegaard decomposition.

Clearly, there exists many Heegaard diagrams for Y. To transform one Heegaard diagram to another, we can follow a sequence of so called Heegaard moves.

Definition 2.1.7. *([18]) Let $(\Sigma, \boldsymbol{\alpha}, \boldsymbol{\beta})$ be a Heegaard diagram. There are three different kinds of Heegaard diagram moves (Figure 2.2).*

- ***Isotopy:*** *A curve β_1 in a Heegaard diagram is isotopic to a curve β_2 if β_2 is obtained by isotoping β_1 such that β_2 remains transverse to the $\boldsymbol{\alpha}$-curves.*

- ***Handleslide of*** α_1 ***over*** α_2***:*** *Replace* α_1 *by* α_1'*, which is a simple closed curve disjoint from* $\alpha_1, \ldots, \alpha_g$ *such that* α_1', α_1*, and* α_2 *bound an embedded pair-of-pants in* $\Sigma - \alpha_3 - \cdots - \alpha_g$ *(A collection of disjoint curves* $\boldsymbol{\alpha}$ *in a closed surface* Σ *is called a pair-of-pants decomposition of* Σ *if every component of* $\Sigma - \boldsymbol{\alpha}$ *is diffeomorphic to the 2-sphere minus three disjoint disks).*

- ***Stabilization:*** *It is obtained by taking connected sum of* $(\Sigma, \boldsymbol{\alpha}, \boldsymbol{\beta})$ *with standard toric Heegaard diagram for* S^3*. The standard toric Heegaard diagram for* S^3 *is obtained by gluing the opposite edges of a square in a plane with one horizontal and one vertical line.*

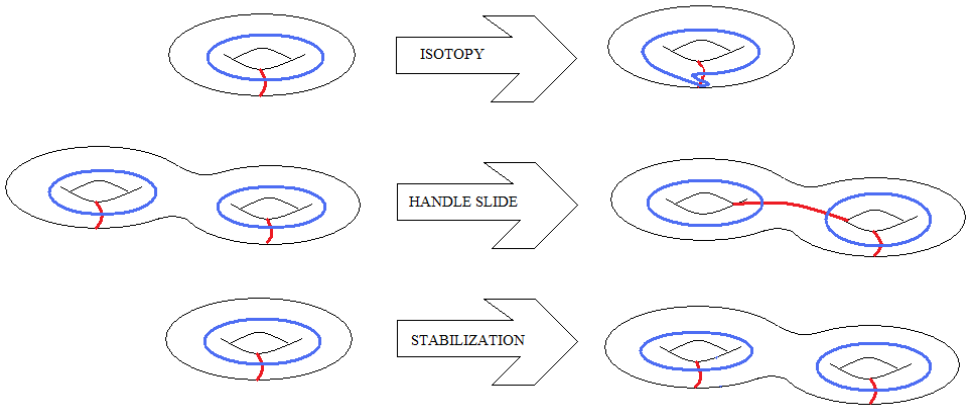

Figure 2.2: Heegaard moves on Heegaard diagrams.

Theorem 2.1.3. *([18])* • *If two Heegaard diagrams differ by isotopy, handleslide or stabilization, then the diagrams represent diffeomorphic 3-manifolds.*

• *Any two Heegaard diagrams which specify the same 3-manifold are diffeomorphic after a finite sequence of Heegaard moves.*

This suggests that a 3-manifold invariant can be defined by constructing an invariant of Heegaard diagrams that is preserved under the Heegaard moves.

2.2 Heegaard Floer Homology

In this section, we will review the invariant that was defined in [16, 17, 18]. The idea of the definition of the Heegaard Floer homology comes from the Lagrangian Floer homology theory [7]. We briefly discuss symplectic manifolds and Lagrangian submanifolds.

Definition 2.2.1. *Let X^{2n} be a smooth, oriented, even-dimensional manifold and $w \in \Omega^2(X)$ be a smooth 2-form such that w is closed and non-degenerate, i.e. $dw = 0$ and $w^n > 0$. Then the pair (X, w) is called a symplectic manifold and w is called a symplectic form.*

Definition 2.2.2. *A submanifold $L \subset X^{2n}$ of dimension n is a Lagrangian submanifold of (X, w) if $w|_{TL} = 0$.*

Floer [7] defined a homology theory for a symplectic manifold and a pair of Lagrangian submanifolds. The generators for this chain complex are the intersection points of the Lagrangian submanifolds and the boundary maps count appropriate pseudo-holomorphic disks. Ozsváth and Szabó [18] used the same idea to define Heegaard Floer homology groups.

Let $(\Sigma_g, \boldsymbol{\alpha}, \boldsymbol{\beta})$ be a Heegaard diagram for a closed, oriented 3-manifold Y with $|\boldsymbol{\alpha}| = |\boldsymbol{\beta}| = g$. Consider the g-fold symmetric product $Sym^g(\Sigma_g) = \Sigma_g \times \cdots \times \Sigma_g / S_g$, where S_g denotes the symmetric group on g letters. In other words, $Sym^g(\Sigma_g)$ consists of unordered g-tuples of points in Σ_g, where the same points can appear more than one time. Note that the action of S_g on $\Sigma_g \times \cdots \times \Sigma_g$ is not free along the diagonal consisting of $(x_1, \ldots, x_g)$, where there are repetition. In addition, the symmetric product $Sym^g(\Sigma_g)$ of a 2-dimensional surface Σ_g is a smooth manifold (typically symmetric products are not manifolds) and a complex structure on Σ_g induces a complex structure on $\mathrm{Sym}^g(\Sigma_g)$ [11]. We note that since α_i's are disjoint, $\alpha_1 \times \cdots \times \alpha_g$ is disjoint from the diagonal, and we consider g-dimensional tori $\mathbb{T}_\alpha = \alpha_1 \times \cdots \times \alpha_g / S_g$ and $\mathbb{T}_\beta = \beta_1 \times \cdots \times \beta_g / S_g$ in $Sym^g(\Sigma_g)$, i.e, $\mathbb{T}_\alpha$ consists of those g-tuples of points $\{x_1, \ldots, x_g\}$ for which $x_i \in \alpha_i$ for $i = 1, \ldots, g$. These tori are transverse to each other if all the $\boldsymbol{\alpha}-$ and $\boldsymbol{\beta}-$curves are.

Remark 2.2.1. *([11, 18]) $Sym^g(\Sigma_g)$ is a symplectic manifold and the tori $\mathbb{T}_\alpha$ and $\mathbb{T}_\beta$ are Lagrangian submanifolds.*

Next, we fix a reference point $z \in \Sigma_g - \boldsymbol{\alpha} - \boldsymbol{\beta}$ so that we can introduce Spin$^c-$structures. In [18], it is shown that the choice of z induces a natural map from $\mathbb{T}_{\boldsymbol{\alpha}} \cap \mathbb{T}_{\boldsymbol{\beta}}$ to the set of Spin$^c-$structures over Y, which induces a partition of $\mathbb{T}_{\boldsymbol{\alpha}} \cap \mathbb{T}_{\boldsymbol{\beta}}$.

Consider a Morse function on Y compatible with the $\boldsymbol{\alpha}$ and $\boldsymbol{\beta}$ curves. Then for each $\boldsymbol{x} = \{x_1, x_2, \ldots, x_g\} \in \mathbb{T}_{\boldsymbol{\alpha}} \cap \mathbb{T}_{\boldsymbol{\beta}}$, there is a g-tuple of flow lines connecting the index 1 and index 2 critical points through x_i. Also, there is a flow line connecting index 3 and index 0 critical point via z. Taking tubular neighborhoods of these $(g+1)$ flowlines, we get a collection of $(g+1)$ balls, outside of which the gradient vector field does not vanish. The gradient vector field can be extended as a nowhere vanishing vector field over Y. The homology class of this nowhere vanishing vector field, in the sense defined below, gives a Spin^c structure over Y.

Definition 2.2.3. *([17]) Let v_1 and v_2 be two nowhere vanishing vector fields. We say that v_1 is homologous to v_2 if there is a ball B in Y with the property that $v_1|Y-B$ is homotopic to $v_2|Y-B$.*

The above relation is an equivalence relation on the set of nowhere vanishing vector fields: It is obviously reflexive and symmetric relation. Suppose v_1 is homologous to v_2 and v_2 is homologous to v_3. Then there exists balls B_1, B_2 such that $v_1|Y-B_1$ is homotopic to $v_2|Y-B_1$ and $v_2|Y-B_2$ is homotopic to $v_3|Y-B_2$. If B_1 and B_2 are disjoint, then we can connect them by an arc and take the tubular neighborhood N of the arc. Then we get a ball $B = B_1 \cup N \cup B_2$ such that v_1 is homotopic to v_3 outside B. If B_1 intersects B_2, then we can always shrink one of the balls and make them disjoint.

Definition 2.2.4. *([17, 18]) We define the set of Spin$^c-$structures over Y as nowhere vanishing vector fields modulo this relation and denote this set by Spin$^c(Y)$.*

Theorem 2.2.1. *([17]) There is a one-to-one correspondence between Spin$^c(Y)$ and $H^2(Y,\mathbb{Z})$.*

We connect the ordinary Heegaard diagram with the above mentioned reference point z as follows:

Definition 2.2.5. *(Pointed Heegaard diagram [18]) Let $(\Sigma_g, \boldsymbol{\alpha}, \boldsymbol{\beta})$ be a Heegaard diagram for Y. We fix a reference point $z \in \Sigma - \boldsymbol{\alpha} - \boldsymbol{\beta}$. The collection $(\Sigma_g, \boldsymbol{\alpha}, \boldsymbol{\beta}, z)$ is called a pointed Heegaard diagram.*

Heegaard moves which are supported in a complement of z (for isotopies, the curves stay disjoint from z, and for handleslides, the pair-of-pants does not contain z) are called *pointed Heegaard moves* [18].

Proposition 2.2.1. *([18])* • *Any two pointed Heegaard diagrams which describe the same 3-manifold are diffeomorphic after a finite sequence of pointed Heegaard moves.*

• *For any 3-manifold (Y, s), $s \in Spin^c(Y)$, there exists a "strongly $s-$admissible" pointed Heegaard diagram for Y.*

• *Any two "strongly $s-$admissible" pointed Heegaard diagrams for (Y, s) can be connected by a finite sequence of pointed Heegaard moves, where all intermediate pointed Heegaard diagrams are "strongly $s-$admissible".*

Now we describe briefly how a one-pointed Heegaard diagram gives the topological invariant for the 3-manifold Y. Using certain constructions from Floer's theory, we define a chain complex $CF^\infty(Y, s)$, where $s \in \text{Spin}^c(Y)$. The chain group $CF^\infty(Y, s)$ is freely generated by pairs of the form $[x, i]$, where $x \in \mathbb{T}_{\boldsymbol{\alpha}} \cap \mathbb{T}_{\boldsymbol{\beta}}$ representing the given Spin^c-structure s, and $i \in \mathbb{Z}$ that tracks the intersection number of the holomorphic disks with $\{z\} \times Sym^{g-1}(\Sigma_g)$. The boundary maps $\partial^\infty : CF^\infty(Y, s) \longrightarrow CF^\infty(Y, s)$ count suitable holomorphic disks in $Sym^g(\Sigma_g)$, given by

$$\partial^\infty[\boldsymbol{x}, i] = \sum_{\boldsymbol{y}} \sum_{\{\phi \in \pi_2(\boldsymbol{x},\boldsymbol{y}) | \mu(\phi)=1\}} \#(\widehat{\mathcal{M}}(\phi))[\boldsymbol{y}, i - n_z(\phi)],$$

where $\pi_2(\boldsymbol{x}, \boldsymbol{y})$ denotes the set of homotopy classes of maps connecting $\boldsymbol{x}$ and $\boldsymbol{y}$, $\mu(\phi)$ is the Maslov index, $\widehat{\mathcal{M}}(\phi)$ denotes the 0-dimensional moduli space of holomorphic maps u from the unit disk $\mathbb{D}^2$ to $Sym^g(\Sigma_g)$ such that $-i$ maps to $\boldsymbol{x}$, i maps to $\boldsymbol{y}$, $u(\{z \in \partial\mathbb{D} | Rez \geq 0\}) \subset \mathbb{T}_{\boldsymbol{\alpha}}$ and $u(\{z \in \partial\mathbb{D} | Rez \leq 0\}) \subset \mathbb{T}_{\boldsymbol{\beta}}$, and $n_z(\phi)$ is the algebraic intersection number ($n_z(\phi) = \#\phi^{-1}(\{z\} \times Sym^{g-1}(\Sigma_g))$). There are other versions of chain complexes $CF^-(Y, s)$, $CF^+(Y, s)$ and $\widehat{CF}(Y, s)$ that are obtained by a natural filtration on $CF^\infty(Y, s)$ [18]. We denote the homology groups by $HF^\infty(Y, s)$, $HF^-(Y, s)$, $HF^+(Y, s)$, and $\widehat{HF}(Y, s)$ of the chain complexes $CF^\infty(Y, s)$, $CF^-(Y, s)$, $CF^+(Y, s)$, and $\widehat{CF}(Y, s)$ respectively.

We define a chain map $U : CF^\infty(Y, s) \longrightarrow CF^\infty(Y, s)$ as

$$U[x, i] = [x, i - 1]$$

and a map $(H_1(Y,\mathbb{Z})/\text{Tors})\otimes HF^\infty(Y,s) \longrightarrow HF^\infty(Y,s)$ that lowers the relative degree in $HF^\infty(Y,s)$ by one. These actions on $HF^\infty(Y,s)$ induce actions on $HF^-(Y,s)$, $HF^+(Y,s)$, and $\widehat{HF}(Y,s)$ and make these homology groups as $\mathbb{Z}[U]\otimes_{\mathbb{Z}}\Lambda^\star(H_1(Y,\mathbb{Z})/\text{Tors})$-modules. The seminal result of Ozsváth and Szabó is the following theorem.

Theorem 2.2.2. *(Theorem 1.1 in [18]) The homology groups $HF^\infty(Y,s)$, $HF^-(Y,s)$, $HF^+(Y,s)$, and $\widehat{HF}(Y,s)$ are topological invariants of Y and s.*

Because the groups were defined using a Heegaard diagram for Y, the proof requires showing the invariance of the homology groups under the three pointed Heegaard moves. The proof of the invariance uses ideas and methods from Lagrangian Floer homology, holomorphic disks and holomorphic triangles [18].

2.3 Multi-pointed Heegaard Diagrams and Homology Groups

In this section, we present a generalization of pointed Heegaard diagram to multi-pointed Heegaard diagram and the corresponding homology groups.

Definition 2.3.1. *([15]) A generalized Heegaard diagram for a 3-manifold Y is a triple $(\Sigma_g,\boldsymbol{\alpha},\boldsymbol{\beta})$, where $\boldsymbol{\alpha}$ and $\boldsymbol{\beta}$ are k-tuples of simple closed curves ($|\boldsymbol{\alpha}| = |\boldsymbol{\beta}| = k$, $k > g$) such that each α_i (similarly β_i) bounds a disk in the handlebody and cutting Σ_g along $\boldsymbol{\alpha}$ (similarly $\boldsymbol{\beta}$) gives disjoint union of punctured spheres.*

Definition 2.3.2. *(Multi-pointed Heegaard diagrams [15]) Let (Σ_g,U_0,U_1) be a genus g Heegaard decomposition for Y and let $(\Sigma_g,\boldsymbol{\alpha},\boldsymbol{\beta})$ be a corresponding generalized Heegaard diagram with $|\boldsymbol{\alpha}| = |\boldsymbol{\beta}| = k$. Choose $\boldsymbol{w} = \{w_1,w_2,...,w_{k-g+1}\} \subset \Sigma - \boldsymbol{\alpha} - \boldsymbol{\beta}$ such that each component of $\Sigma - \boldsymbol{\alpha}$ (and $\Sigma - \boldsymbol{\beta}$) contains a unique w_i. Then $(\Sigma_g,\boldsymbol{\alpha},\boldsymbol{\beta},\boldsymbol{w})$ is a multi-pointed Heegaard diagram and the points w_i's are called the basepoints of the Heegaard diagram.*

Example 2.3.1. ***(i) Standard spherical Heegaard diagram for S^3*** *[24]: Let α_1 and β_1 be two simple closed curves in S^2 intersecting each other transversely at two points. Let w_1 and w_2 be two points in $\Sigma - \alpha_1 - \beta_1$ such that the components they are in do not have common boundaries. Then*

$(\Sigma, \alpha, \beta, w = \{w_1, w_2\})$ *is the standard two-pointed spherical Heegaard diagram for* S^3. *Figure 2.3 shows the standard spherical Heegaard diagram for* S^3.

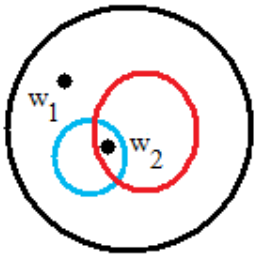

Figure 2.3: Standard spherical Heegaard diagram for S^3.

(ii) Standard toric Heegaard diagram for $\boldsymbol{S^3}$ *[24]: Consider a square in a plane with* n *horizontal and* n *vertical lines. A torus is obtained by gluing together the top-bottom, left-right sides of the square with* n-$\boldsymbol{\alpha}$ *and* n-$\boldsymbol{\beta}$ *simple closed curves. Placing* w_i *in each row and column such that each row and column has exactly one basepoint, we obtain a multi-pointed Heegaard diagram for* S^3 *(Figure 2.4).*

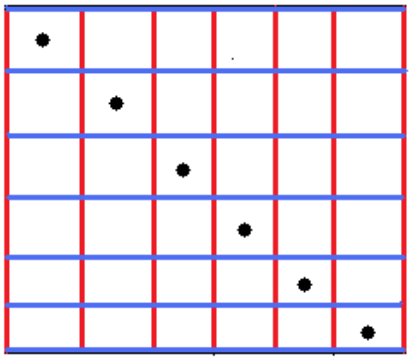

Figure 2.4: Standard toric Heegaard diagram for S^3 with $n = 6$.

Let $(\Sigma_g, \boldsymbol{\alpha}, \boldsymbol{\beta}, \boldsymbol{w})$ be a multi-pointed Heegaard diagram for a closed, oriented 3-manifold Y with $|\boldsymbol{\alpha}| = |\boldsymbol{\beta}| = k > g$ and $|\boldsymbol{w}| = k - g + 1$. Consider the k-fold symmetric product $Sym^k(\Sigma_g) =$

$\Sigma_g \times \cdots \times \Sigma_g / S_k$. Consider k-dimensional tori $\mathbb{T}_\alpha = \alpha_1 \times \cdots \times \alpha_k / S_k$ and $\mathbb{T}_\beta = \beta_1 \times \cdots \times \beta_k / S_k$ in $Sym^k(\Sigma_g)$.

Let $\widehat{CF}(\Sigma_g, \boldsymbol{\alpha}, \boldsymbol{\beta}, \boldsymbol{w})$ be the free $\mathbb{Z}/_2$-module generated by the points $\boldsymbol{x} = (x_1, \ldots, x_k)$ in $\mathbb{T}_\alpha \cap \mathbb{T}_\beta$ and the boundary maps $\partial : \widehat{CF}(\Sigma_g, \boldsymbol{\alpha}, \boldsymbol{\beta}, \boldsymbol{w}) \longrightarrow \widehat{CF}(\Sigma_g, \boldsymbol{\alpha}, \boldsymbol{\beta}, \boldsymbol{w})$ are given by counting certain holomorphic disks as follows:

$$\partial(\boldsymbol{x}) = \sum_{\boldsymbol{y}} \sum_{\{\phi \in \pi_2^0(\boldsymbol{x}, \boldsymbol{y}) | \mu(\phi) = 1\}} \#(\widehat{\mathcal{M}}(\phi))\boldsymbol{y},$$

where $\pi_2^0(\boldsymbol{x}, \boldsymbol{y})$ denotes the set of homotopy classes of maps connecting $\boldsymbol{x}$ and $\boldsymbol{y}$ such that $n_{w_i}(\phi) = 0, \forall i$.

Theorem 2.3.1. *([18, 20]) The homology $\widehat{HF}(Y)$ of the chain complex $\widehat{CF}(\Sigma_g, \boldsymbol{\alpha}, \boldsymbol{\beta}, \boldsymbol{w})$ with $k = g$ is an invariant for the 3-manifold Y. In general, for a rational homology 3-sphere,*

$$H_*(\widehat{CF}(\Sigma_g, \boldsymbol{\alpha}, \boldsymbol{\beta}, \boldsymbol{w})) \cong \widehat{HF}(Y) \otimes H_*(T^{k-g}),$$

where $H_*(T^{k-g})$ is the singular homology of the $(k-g)$-dimensional torus with coefficients in $\mathbb{Z}/_2$.

2.4 Nice Heegaard Diagrams and Nice Moves

Even though Heegaard Floer theory is a powerful tool in the study of 3- and 4-dimensional topology, it is extremely difficult to compute these invariants directly as it is hard to calculate $\#(\widehat{\mathcal{M}}(\phi))$ for a general domain ϕ. Calculations have been done for many families of 3-manifolds using techniques like surgery triangle for the Heegaard Floer homology [18]. Sarkar and Wang [22] gave a combinatorial algorithm to compute Heegaard Floer homology groups using certain (multi) pointed Heegaard diagrams, which they called "nice" Heegaard diagrams. They proved that every closed, oriented 3-manifold admits a "nice" Heegaard diagram and any (multi) pointed diagram can be changed to a "nice" Heegaard diagram by a sequence of isotopies and handleslides (Theorem 1.2 in [22]). Using Sarkar and Wang's idea of "nice" Heegaard diagrams, Ozsváth, Stipsicz and Szabó [15] constructed a class of Heegaard diagrams using pair-of-pants decompositions to give a combinatorial proof for the invariance of the stable Heegaard Floer homology, which is free from the theory of pseudo-holomorphic disks.

Definition 2.4.1. *([15, 22]) Let $(\Sigma, \boldsymbol{\alpha}, \boldsymbol{\beta}, \boldsymbol{w})$ be a multi-pointed Heegaard diagram. An elementary domain is a connected component of $\Sigma - \boldsymbol{\alpha} - \boldsymbol{\beta}$. An elementary domain without a basepoint is called nice if it is either a bigon or a rectangle.*

We discuss the three moves, which are the modification of the pointed Heegaard moves. Before that we present the definition for a nice embedded arc.

Definition 2.4.2. *(Definition 3.3 in [15]) Suppose that $\mathcal{D} = (\Sigma, \boldsymbol{\alpha}, \boldsymbol{\beta}, \boldsymbol{w})$ is a nice diagram. An embedded arc $\gamma = (\gamma(t))_{t\in[0,1]}$ is nice if*

i) $\gamma(0)$ is on an $\boldsymbol{\alpha}$-curve and $\gamma(1)$ is in the interior of a bigon or an elementary domain D_f containing a basepoint.

ii) the elementary domain D_1 containing $\gamma(0)$ on its boundary is either a bigon or it contains a basepoint and it does not contain any other $\gamma(t)$, for small t.

iii) $\gamma - \gamma(0)$ is disjoint from all the $\boldsymbol{\alpha}$-curves, γ is transverse to α at $\gamma(0)$, and γ intersects $\boldsymbol{\beta}$-curves transversally.

iv) for any elementary domain D, at most one component of $D - \gamma$ is not a bigon or a rectangle, and if there is such a component, it contains a basepoint.

v) the component of $D_f - \gamma$ containing $\gamma(1)$ is either a bigon, or it contains a basepoint.

vi) if $D_1 = D_f$, then we assume that the component of $D_1 - \gamma$ containing $\gamma(1)$ also contains a basepoint.

We discuss the three nice moves [15].

- **Nice isotopy:** An isotopy along an embedded nice arc is called a nice isotopy (Figure 2.5).
- **Nice handleslide:** The result of sliding α_1 over α_2 along an embedded arc η is a pair of curves (α_1', α_2), where α_1' is the connected sum of α_1 and α_2 along η (Figure 2.6). η defines a nice handleslide if the interior of η lies in a single rectangle and $\eta(0)$ lies on the boundary of an elementary domain containing a basepoint (Figure 2.6).

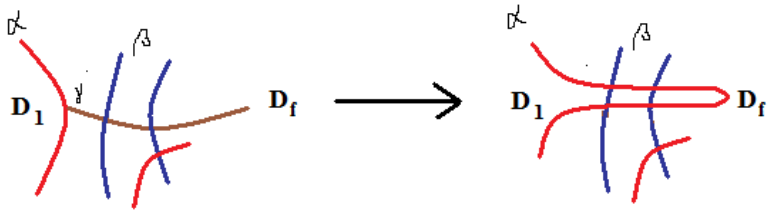

Figure 2.5: Nice isotopy.

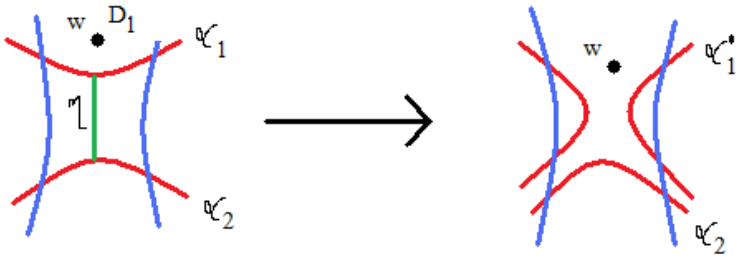

Figure 2.6: Nice handleslide.

- **Nice stabilization**: There are two types of stabilizations of the multi-pointed Heegaard diagram: *Type-b* stabilization and *Type-g* stabilization. A *type-b* stabilization is the connected sum of $(\Sigma, \boldsymbol{\alpha}, \boldsymbol{\beta}, \boldsymbol{w})$ with the standard spherical Heegaard diagram for S^3 (Figure 2.7). A *type-b* stabilization does not change the Heegaard surface Σ. It increases the number of $\boldsymbol{\alpha}$-curves, $\boldsymbol{\beta}$-curves and the number of basepoints. A *type-g* stabilization is the connected sum of $(\Sigma, \boldsymbol{\alpha}, \boldsymbol{\beta}, \boldsymbol{w})$ with the standard one-pointed toric Heegaard diagram for S^3 (Figure 2.8). A *type-g* stabilization increases the genus of the surface Σ and the number of $\boldsymbol{\alpha}$- and $\boldsymbol{\beta}$-curves. It does not change the number of basepoints.

A nice move will mean any one of the above three moves. The following theorem gives the invariance of the nice multi-pointed Heegaard diagrams under the nice moves.

Theorem 2.4.1. *(Theorem 3.8 in [15]) Suppose D' is obtained from a nice multi-pointed Heegaard diagram D by a nice move. Then D' is a nice multi-pointed Heegaard diagram.*

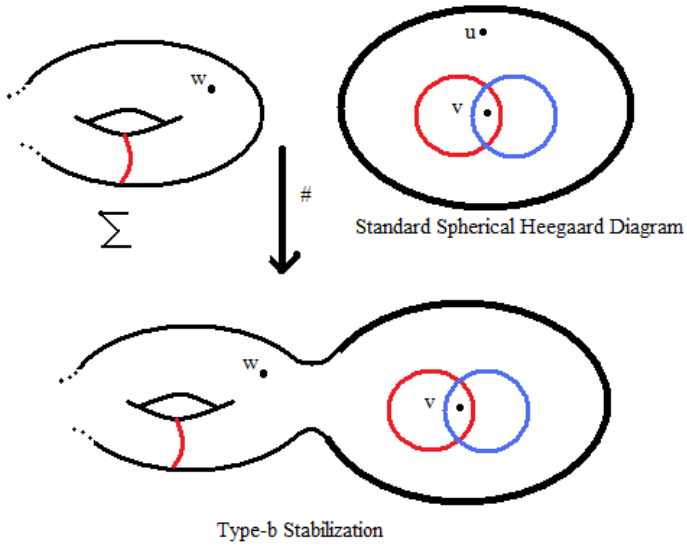

Figure 2.7: Type-b Stabilization.

The next definition names the condition on two nice diagrams of the same underlying manifold that are connected by nice moves.

Definition 2.4.3. *([15]) Two nice diagrams $\mathcal{D}'$ and $\mathcal{D}''$ of a 3-manifold are called "nicely connected" if there is a sequence of nice diagrams $(\mathcal{D}_i)_{i=1}^n$ such that $\mathcal{D}_1 = \mathcal{D}'$ and $\mathcal{D}_n = \mathcal{D}''$ and the consecutive $\mathcal{D}_i$'s differ by a nice move.*

Definition 2.4.4. *([15]) Let Y be a 3-manifold with a Heegaard decomposition such that the two handlebodies are given by pair-of-pants decompositions $\boldsymbol{\alpha}$ and $\boldsymbol{\beta}$ of the Heegaard surface Σ. The triple $(\Sigma, \boldsymbol{\alpha}, \boldsymbol{\beta})$ is called a pair-of-pants generalized Heegaard diagram or a pair-of-pants diagram for Y. If all the $\boldsymbol{\alpha}$ and $\boldsymbol{\beta}$-curves are homological nontrivial in $H_1(\Sigma, \mathbb{Z}/2\mathbb{Z})$, then we call the pair-of-pants diagram an essential pair-of-pants diagram for Y.*

In [15], Ozsváth, Stipsicz and Szabó provided an algorithm to change any essential pair-of-pants diagram for a 3-manifold, not containing $(S^1 \times S^2)$-summand, to a nice diagram. This nice Heegaard diagram for Y is said to be derived from the essential pair-of-pants diagram. The following theorem shows that nice diagrams for a fixed 3-manifold are connected by nice moves.

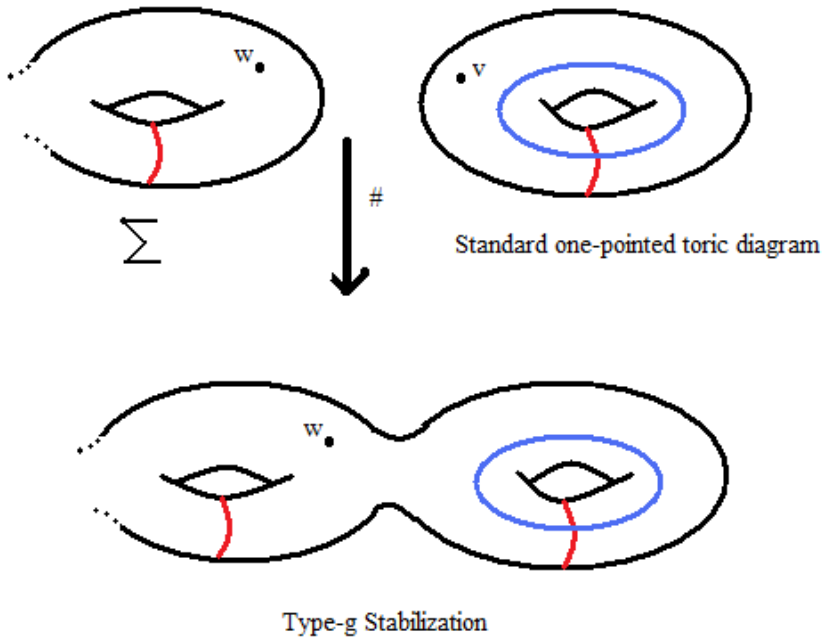

Figure 2.8: Type-g Stabilization.

Theorem 2.4.2. *([15]) Any two multi-pointed nice Heegaard diagrams for Y, not containing $(S^1 \times S^2)$-summand, are nicely connected.*

Based on these diagrams, we present a quick review of the combinatorial Heegaard Floer homology that uses only combinatorial methods and is independent of the theory of holomorphic disks.

2.5 Combinatorial Heegaard Floer Homology Groups

Let $\mathcal{D} = (\Sigma_g, \boldsymbol{\alpha}, \boldsymbol{\beta}, \boldsymbol{w})$ be a nice multi-pointed Heegaard diagram for a closed, oriented 3-manifold Y with $|\boldsymbol{\alpha}| = |\boldsymbol{\beta}| = k > g$ and $|\boldsymbol{w}| = k - g + 1$. Let $\widetilde{CF}(\mathcal{D})$ be the $\mathbb{Z}/_2$-vector space generated by the set S of intersection points $\boldsymbol{x} = \{x_1, \ldots, x_k\} \in \Sigma$, where every $\boldsymbol{\alpha}$- and $\boldsymbol{\beta}$- curve contains exactly one point x_i.

Let $\boldsymbol{x}, \boldsymbol{y} \in \widetilde{CF}(\mathcal{D})$. We define the boundary map

$$\widetilde{\partial_{\mathcal{D}}} : \widetilde{CF}(\mathcal{D}) \longrightarrow \widetilde{CF}(\mathcal{D})$$

as follows:

$$\widetilde{\partial_{\mathcal{D}}}(\boldsymbol{x}) = \sum_{\boldsymbol{y} \in S} |\mathfrak{M}_{\boldsymbol{x},\boldsymbol{y}}|.\boldsymbol{y},$$

where

$$\mathfrak{M}_{\boldsymbol{x},\boldsymbol{y}} = \begin{cases} \emptyset & \text{if } \boldsymbol{x} = \boldsymbol{y} \text{ or } \boldsymbol{x}, \boldsymbol{y} \text{ differ in at least 3 coordinates} \\ \text{Empty bigons} & \text{if } \boldsymbol{x}, \boldsymbol{y} \text{ differ in exactly one coordinate } x_i \neq y_i \text{ and } x_k = y_k, \forall k \neq i \\ \text{Empty rectangles} & \text{if } \boldsymbol{x}, \boldsymbol{y} \text{ differ in exactly two coordinates } x_i \neq y_i,\ x_j \neq y_j \text{ and } x_k = y_k, \forall k \neq i, j \end{cases}$$

and $|\mathfrak{M}_{\boldsymbol{x},\boldsymbol{y}}|$ is the cardinality of the set $\mathfrak{M}_{\boldsymbol{x},\boldsymbol{y}}$ (mod 2).

Theorem 2.5.1. *([15]) $(\widetilde{CF}(\mathcal{D}), \widetilde{\partial_{\mathcal{D}}})$ is a chain complex.*

The combinatorial Heegaard Floer homology is the homology group $\widetilde{HF}(\mathcal{D}) = H_*(\widetilde{CF}(\mathcal{D}), \widetilde{\partial_{\mathcal{D}}})$ of the chain complex $(\widetilde{CF}(\mathcal{D}), \widetilde{\partial_{\mathcal{D}}})$.

Theorem 2.5.2. *(Theorem 7.1 in [15]) Suppose a nice diagram $\mathcal{D}_2$ is obtained from a nice diagram $\mathcal{D}_1$ either by a nice isotopy, a nice handleslide or a nice type-g stabilization, then $\widetilde{HF}(\mathcal{D}_1) \cong \widetilde{HF}(\mathcal{D}_2)$. If $\mathcal{D}_2$ is obtained from $\mathcal{D}_1$ by a nice type-b stabilization, then $\widetilde{HF}(\mathcal{D}_2) \cong \widetilde{HF}(\mathcal{D}_1) \otimes (\mathbb{Z}/_2 \oplus \mathbb{Z}/_2)$.*

We prepare the ground for the other main result of this section. With that purpose, we first introduce a definition from algebra.

Definition 2.5.1. *([15]) Two pairs $(V_1, w_1), (V_2, w_2)$ of $\mathbb{Z}/_2$ vector spaces V_1 and V_2 with $w_1 \geq w_2$ ($w_i \in \mathbb{Z}$) are said to be equivalent if $V_1 = V_2 \otimes (\mathbb{Z}/_2 \oplus \mathbb{Z}/_2)^{\otimes(w_1 - w_2)}$. The equivalence class of the pair (V, w) is denoted by $[V, w]$.*

Let Y be a closed, oriented 3-manifold. We first assume that Y contains no $(S^1 \times S^2)-$ summand. Let $\mathcal{D}_1$ and $\mathcal{D}_2$ be two multi-pointed nice Heegaard diagrams for Y with basepoints $b(\mathcal{D}_1)$ and $b(\mathcal{D}_2)$

respectively, and their corresponding homologies be $\widetilde{HF}(\mathcal{D}_1)$ and $\widetilde{HF}(\mathcal{D}_2)$. Then, by Theorem 2.4.2, Theorem 2.5.2, $[\widetilde{HF}(\mathcal{D}_1), b(\mathcal{D}_1)] = [\widetilde{HF}(\mathcal{D}_2), b(\mathcal{D}_2)]$. Hence, the following definition is well-defined.

Definition 2.5.2. *(Definition 8.1 in [15]) Let Y be a 3-manifold, which contains no $(S^1 \times S^2)-$ summand. Let $(\Sigma, \boldsymbol{\alpha}, \boldsymbol{\beta})$ be an essential pair-of-pants diagram for Y and let $\mathcal{D}$ be a multi-pointed nice Heegaard diagram for Y with basepoints $b(\mathcal{D})$ derived from $(\Sigma, \boldsymbol{\alpha}, \boldsymbol{\beta})$. We define the stable Heegaard Floer group $\widehat{HF}_{st}(Y)$ as the equivalence class $[\widetilde{HF}(\mathcal{D}), b(\mathcal{D})]$.*

We consider a more general closed, oriented 3-manifold. By Kneser-Milnor theorem, Y can be decomposed as a connected sum of another 3-manifold Y', which contains no $(S^1 \times S^2)-$summand, with n copies of $(S^1 \times S^2)$. Also, by the Kneser-Milnor theorem, Y determines n and Y' uniquely. Hence, $\widehat{HF}_{st}(Y)$ will depend only on $\widehat{HF}_{st}(Y')$ and n. This gives the validity of the following definition and proves the following theorem.

Definition 2.5.3. *(Definition 8.1 in [15]) Let $Y = Y' \# n(S^1 \times S^2)$, where Y' does not contain any $(S^1 \times S^2)-$summand. Let $\mathcal{D}$ be a multi-pointed nice Heegaard diagram for Y' with basepoints $b(\mathcal{D})$ derived from an essential pair-of-pants diagram for Y'. Then the stable Heegaard Floer homology $\widehat{HF}_{st}(Y)$ is defined as $[\widetilde{HF}(\mathcal{D}) \otimes (\mathbb{Z}/_2 \oplus \mathbb{Z}/_2)^n, b(\mathcal{D})]$.*

The main result of [15] is a combinatorial proof of:

Theorem 2.5.3. *([15]) The stable Heegaard Floer homology group $\widehat{HF}_{st}(Y)$ is a diffeomorphism invariant of Y.*

Chapter 3

Grid Diagrams

In this chapter we give a brief overview of the planar grid diagrams. Planar grid diagrams are combinatorial representations of knots and links in $\mathbb{S}^3$ [12, 13, 14]. In the late 19th century, Karl Hermann Brunn used this technique to study knots and links [2]. Later grid diagrams were used by Dynnikov to recognize unknots [6]. This chapter describes the basic construction of the grid diagrams for a knot or link as it appears in the combinatorial knot Floer homology [12], and various moves in the grid diagram [4]. Details can be found in [14].

3.1 Planar Grid Diagrams

Definition 3.1.1. *([12]) A planar grid diagram Γ is a $n \times n$ square grid in the plane, together with a collection of n X's and n O's in the small squares in the grid satisfying the following:*

- *Each row contains exactly one X and exactly one O.*
- *Each column contains exactly one X and exactly one O.*
- *No square contains both an X and an O.*

Here n is called the grid number of the grid diagram Γ. We can obtain a "toroidal grid diagram" by identifying the left and right segments, top and bottom segments of the grid.

One can obtain a link L in S^3 from a grid diagram by joining the X's and O's in each column and row by vertical and horizontal line segments such that at every point of intersection, the vertical

segments always cross over the horizontal segments. Figure 3.1 shows a planar grid diagram for the Hopf link with $n = 4$.

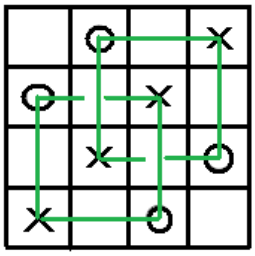

Figure 3.1: Planar grid diagram for Hopf link.

Lemma 3.1.1. *([1, 3]) Every link in S^3 admits a grid diagram.*

Proof. We take an arbitrary projection of L. We can isotope L so that the projection has only horizontal and vertical segments. We need to make sure that at each of the crossings the vertical segments cross over the horizontal segments. Any horizontal over-crossing can be changed into undercrossing by isotoping the vertical and the horizontal segments as shown in Figure 3.2. We can move the different horizontal (and vertical) segments so that they are not collinear, then denote the turns by X's and O's and, isotoping further if needed to insure that at most two corners are on any horizontal/vertical line, we obtain a grid diagram for L. □

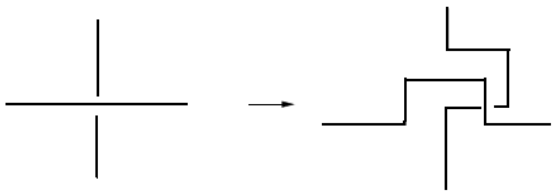

Figure 3.2: Modifying horizontal over-crossing to under-crossing.

3.2 Grid Moves

There are three elementary moves on grid diagrams that are enough to go between any two grid diagrams for the same link, a result due to Cromwell [4]. They are cyclic permutation, commutation and stabilization.

- **Cyclic Permutation**: One can obtain a new diagram $\mathbb{G}'$ by cyclically permuting the rows and the columns of a planar grid diagram $\mathbb{G}$ (Figure 3.3).

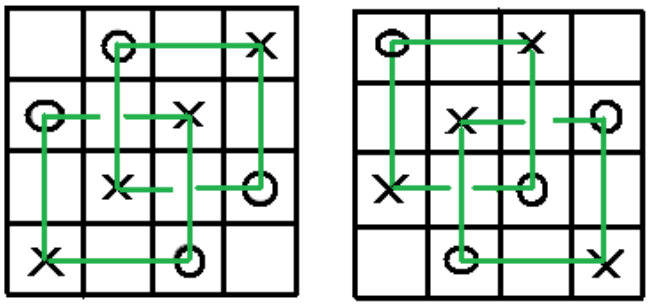

Figure 3.3: Cyclic permutation in a Hopf link by moving the top row to the bottom row. In S^3 this amounts to isotoping the top arc to the bottom by swinging it through the upper half space.

- **Commutation**: Consider two consecutive columns in a grid diagram. There are two ways an X and an O in one column can be joined by a vertical line in the associated torus. If the segment between X and O from the adjacent column is contained in one of those two arcs, then the commutation move allows us to switch the two columns (Figure 3.4). Commutation can be alternatively done by the analogous move on two rows. Commutation move results in either planar isotopy (Figure 3.5), Reidemeister second move (Figure 3.6) or a Reidemeister third move (Figure 3.7).

- **Stabilization**: A stabilization of an $n \times n$ grid $\mathbb{G}$ is a $(n+1) \times (n+1)$ grid diagram $\mathbb{G}'$ obtained by splitting a row and a column of $\mathbb{G}$ in two. A way to get $\mathbb{G}'$ is to erase the points from the row and column containing the point along which we want to stabilize. Then split the empty row and empty column in two by adding a horizontal and a vertical line. We

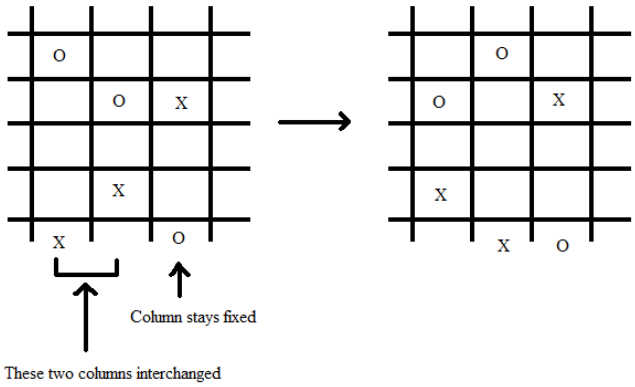

Figure 3.4: Commutation move.

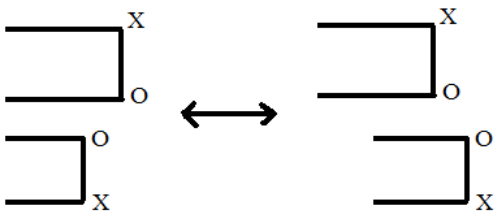

Figure 3.5: Commutation move resulting in planar isotopy. Here we do commutation of the two columns.

can stabilize at any corner point (Figure 3.8). There are four different ways to stabilize a particular corner point and to place new points in the newly formed cells of $\mathbb{G}'$. Figure 3.9 shows different stabilizations at the X corner point in the down-left position in the grid. The different stabilizations are northwest NW, northeast NE, southwest SW and southeast SE positions. Stabilization changes the projection of the link either by a planar isotopy or by the first Reidemeister move (Figure 3.10). The inverse of stabilization is called destabilization.

Theorem 3.2.1. *([4, 6]) Let G_1 and G_2 be two grid diagrams representing two isotopic links. Then G_1 can be obtained from G_2 by a finite sequence of grid moves.*

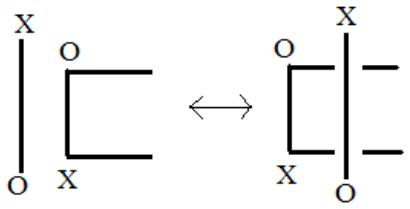

Figure 3.6: Commutation move on the two columns resulting in second Reidemeister move in the grid diagram.

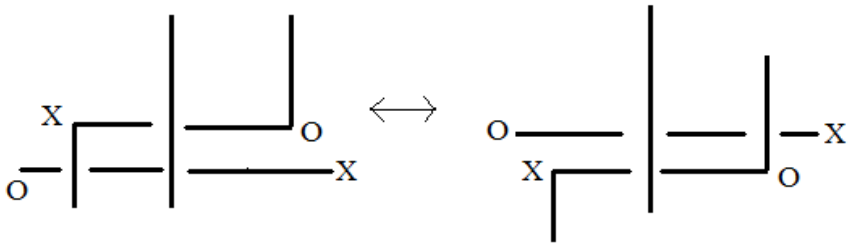

Figure 3.7: Commutation move on the two rows resulting in third Reidemeister move in the grid diagram.

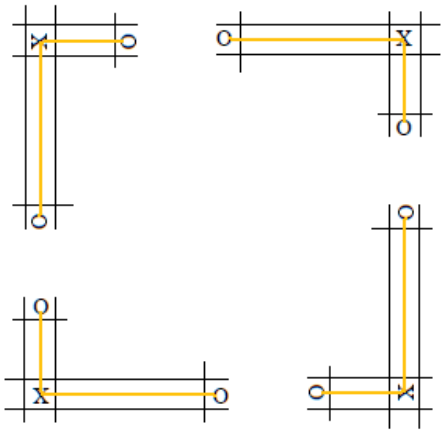

Figure 3.8: The four different positions for X at the corner.

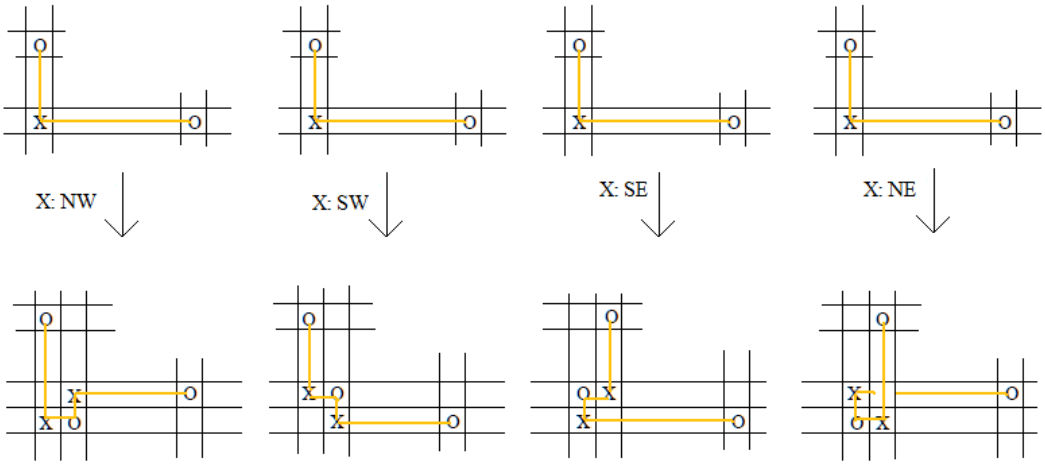

Figure 3.9: Stabilization Move.

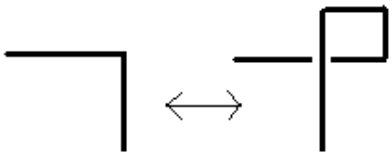

Figure 3.10: First Reidemeister move in the grid diagram.

3.3 Extended Grid Diagrams

Consider a link L in S^3. Take a $(n \times n)$-toroidal grid diagram for L in S^3. We call the vertical circles α-curves, the horizontal circles β-curves, and the O's and X's basepoints. Each annular region between two α-curves contains two basepoints, O and X. In each such annular region, we will insert a new α-circle parallel to the old α-circles such that it separates the two basepoints. We introduce similar β-circles to obtain a new type of grid diagram, called an *extended grid diagram* with a $(2n \times 2n)-$ grid, where each row and each column contain exactly one basepoint (Figure 3.11).

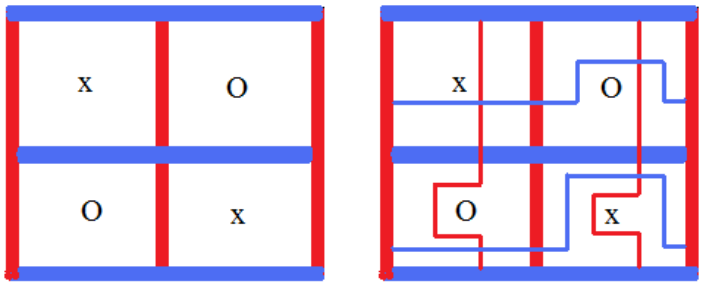

Figure 3.11: Extended grid diagram for the unknot.

By adding the new curves in $\mathbb{T}^2$, the grid diagram for L is changed into a multi-pointed Heegaard diagram for S^3 as each component of $\mathbb{T}^2 - \boldsymbol{\alpha}$ and $\mathbb{T}^2 - \boldsymbol{\beta}$ contains exactly one basepoint.

Remark 3.3.1. *We made a choice of the new curves in the construction of the extended grid diagram. There are, up to isotopy relative to base points, exactly two choices for each new curve.*

Chapter 4

Extended Grid Homology

In this chapter, we give an exposition of the construction of the combinatorial hat-version of Heegaard Floer homology based on the double branched cover construction as introduced in [24].

4.1 Adapted Diagrams

Consider a link L in S^3. We will study the double branched cover Y of S^3 branched along L from the perspective of the extended grid presentation for L.

Consider an extended toric grid diagram for L. We cut the extended toric grid diagram along α_0 and β_0 to obtain a planar extended grid diagram G. Join the basepoints X and O in the annular region between two old $\boldsymbol{\alpha}$-curves by arcs called cut lines such that the arcs do not intersect β_0, and they do not intersect the intersection points of $\boldsymbol{\alpha}$ and $\boldsymbol{\beta}$ (Figure 4.1, Figure 4.2).

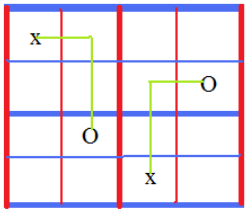

Figure 4.1: Extended grid diagram for the unknot.

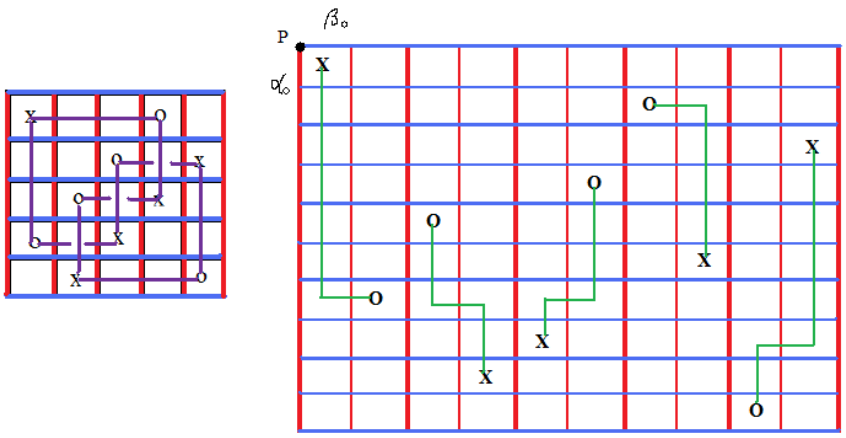

Figure 4.2: An extended grid diagram for the trefoil with cut lines connecting the basepoints.

We will use these cut lines to understand the lifts of the new curves in G to the double branched cover and the construction of the chain complex of the extended grid homology $EGH(G)$.

Theorem 4.1.1. *([24]) The pull-back of the extended grid diagram to the double branched cover Y gives a Heegaard diagram D for Y with only octagons and rectangles as elementary domains. We get a nice Heegaard diagram for Y with a basepoint in each octagon, and the basepoints are exactly corresponding to O's and X's.*

Proof. Let $S^3 = H_0 \cup H_1$, where H_0 and H_1 are two solid tori glued along their common boundary $\mathbb{T}^2$. Let Σ_g be the branched cover of $\mathbb{T}^2$ branched along the basepoints. Using the Euler characteristics and facts from covering maps,

$$\chi(\Sigma_g) = 2\chi(\mathbb{T}^2) - 2n, \tag{4.1}$$

which implies $g = n + 1$. The old α-circle (and β-circle) that bounds a disk in the solid torus H_0 (and H_1) lifts to two disjoint copies of circles in the 3-manifold, bounding disks in the handlebody. A Seifert surface for a knot intersects the cut line, hence, the new $\boldsymbol{\alpha}$-circle intersecting the cut line

joining the two basepoints X and O in a single point lifts to a single circle bounding a disk in the handlebody (Figure 4.3). Hence, the double branched cover of the solid torus is a handlebody of genus $(n+1)$.

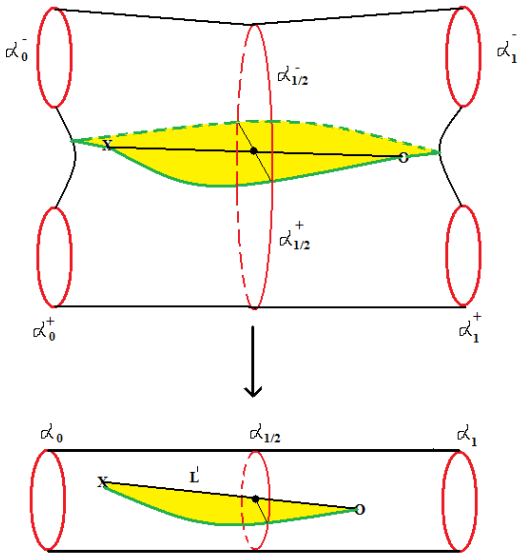

Figure 4.3: Lift of old α-circles and new α-circles. The green line represents the cut line. The segment $L' \subset L$ joining X and O represented by the black line lies inside the solid torus and the yellow shaded region representing the Seifert surface for the knot lifts to two copies. Here two copies of the α-curves are represented by $+$ and $-$ in the lift.

Hence, we get 3n disjoint $\boldsymbol{\alpha}$-curves (similarly $\boldsymbol{\beta}$-curves) in the genus $(n+1)$ surface Σ_g. Each $\mathbb{T}^2 - \boldsymbol{\alpha}$ component in the extended grid lifts to a pair-of-pants diagram each containing a single basepoint. Hence, the 3n $\boldsymbol{\alpha}$-curves (similarly 3n $\boldsymbol{\beta}$-curves) give a pair-of-pants decomposition of the surface Σ_g, which in turn gives a pair-of-pants diagram $\mathcal{D}$ for Y. Since all the $\boldsymbol{\alpha}$- (similarly $\boldsymbol{\beta}$-) curves are homologically essential in the torus, all are homologically essential in $\mathcal{D}$. An elementary domain in the toric diagram lifts to an elementary domain in $\mathcal{D}$. An elementary domain in $\mathcal{D}$ either covers a rectangle in the extended grid diagram which does not contain a basepoint or it covers a rectangle in the extended grid diagram containing a basepoint. In the former case, the elementary domain in $\mathcal{D}$ is a rectangle and in the latter case, the elementary domain in $\mathcal{D}$ is an octagon (Figure

4.4). We get a nice diagram as each pair-of-pants component contains a unique octagon containing a base-point (Figure 4.4). □

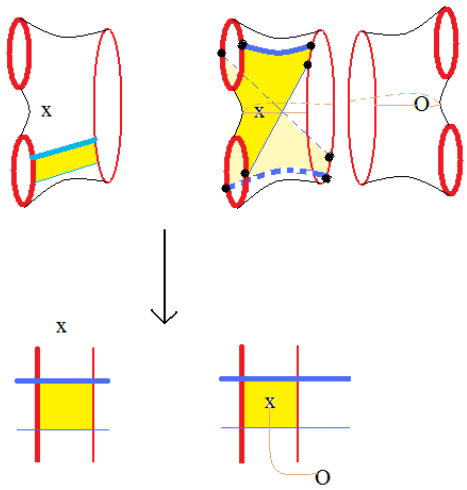

Figure 4.4: Elementary domains in the toric diagram and its lift.

Definition 4.1.1. *An Heegaard diagram $\mathcal{D}$ for Y, which is a double branched cover of S^3 branched along a link L, that is obtained by using the double branched cover as above is called an adapted diagram.*

We present a detailed pictorial description of an adapted diagram D for the double branched cover Y of S^3 branched along $L \subset S^3$. Consider an extended grid diagram G for L. Take two copies of G with cut lines, and call them G^+ and G^-. Then D can be thought of as union of G^+ and G^- glued across the cut lines (Figure 4.5) satisfying the following conditions:

- any curve which meets a cut line in G^+, comes out in G^- and vice versa.
- each new α curve in G lifts to a simple closed curve in $G^+ \cup G^-$.
- each new β curve in G lifts to a simple closed curve in $G^+ \cup G^-$.
- each old α curve in G lifts to two disjoint $\boldsymbol{\alpha}$ curves, α_1 and α_2 in $G^+ \cup G^-$.
- each old β curve in G lifts to two disjoint $\boldsymbol{\beta}$ curves, β_1 and β_2 in $G^+ \cup G^-$.

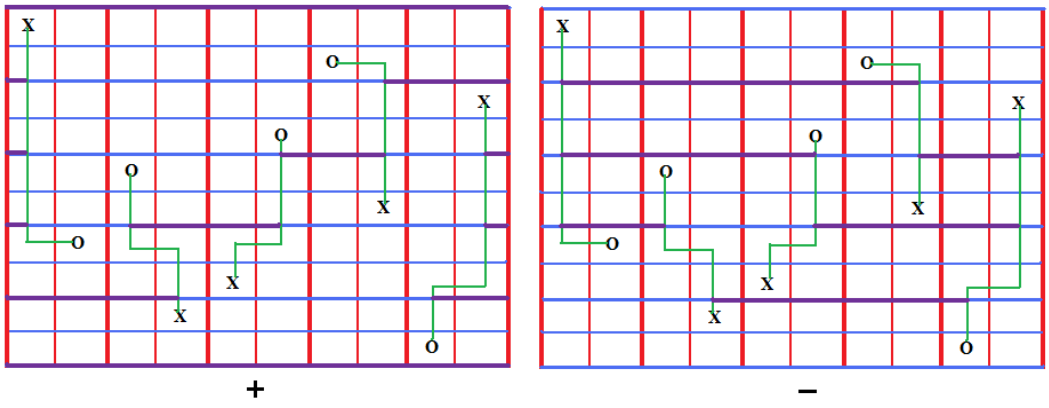

Figure 4.5: A pictorial representation of an adapted diagram for the double branched cover. The thick lines represent old curves, while the thin lines represent new curves. When a curve in G^+ meets the cut line joining X and O, it comes out from the other side of the cut line in G^- and vice versa.

4.2 The Chain Complex $EGC(G)$

4.2.1 The Generators of $EGC(G)$

We discuss the generators for the chain complex $EGC(G)$. To each intersection point p of the $\boldsymbol{\alpha}$- and $\boldsymbol{\beta}$- curves in the extended grid, we associate p^+ and p^-, denoting the two corresponding points in G^+ and G^-.

Definition 4.2.1. *The set of generators $S(G)$ for the chain complex $EGC(G)$ is the set of unordered $3n$-tuples $\boldsymbol{x} = \{x_{ij}^k\}$ of intersection points such that*

- *x_{ij} is an intersection point $\beta_i \cap \alpha_j$ in the extended grid and $k \in \{+, -\}$.*
- *every new $\boldsymbol{\alpha}-$ and $\boldsymbol{\beta}-$curve in the grid admits exactly one coordinate of $\boldsymbol{x}$.*
- *every old $\boldsymbol{\alpha}-$ and $\boldsymbol{\beta}-$curve in the grid admits exactly two coordinates of $\boldsymbol{x}$.*
- *if two coordinates of $\boldsymbol{x}$ are on the same old $\boldsymbol{\alpha}-$curve, then they have opposite signs.*

- *if* $x_{ij}^{k_{ij}}$ *and* $x_{it}^{k_{it}}$ *are two coordinates of* $\boldsymbol{x}$ *on* β_i*, then*

$$k_{it} = (-1)^{(N_{x_{ij}x_{it}}+1)} k_{ij},$$

where $N_{x_{ij}x_{it}}$ *is the number of intersection of the cut lines with* β_i *in between* x_{ij} *and* x_{it}*.*

We note that both x_{ij}^+ and x_{ij}^- can appear in $\boldsymbol{x}$ if both β_i and α_j are old curves and x_{ij} is the only intersection point on both of those old curves in the extended grid.

All the conditions together ensure that there are $3n$ intersection points from $3n$ $\boldsymbol{\alpha}$ and $\boldsymbol{\beta}$ curves such that each $\boldsymbol{\alpha}-$ and $\boldsymbol{\beta}-$curve intersects exactly once. Each $\boldsymbol{x} = \{x_{ij}^k\} \in \mathbb{T}_\alpha \cap \mathbb{T}_\beta$ corresponds to the intersection points on $G^+ \cup G^-$, with x_{ij}^+ belonging to G^+ and x_{ij}^- belonging to G^-. Since the inverse image of a new curve under the branched cover map is a single new curve, we get only one-coordinate of $\boldsymbol{x}$ on the new curve, either in G^+ or in G^-. The last two conditions for the generators guarantee that the two entries from the same old curve are on different components of the inverse image of the old curve in the extended grid (see the two golden dots and the two green dots in Figure 4.6). Hence, the set of intersection points $\mathbb{T}_\alpha \cap \mathbb{T}_\beta$ of the adapted diagram $\mathcal{D} = G^+ \cup G^-$ for Y is in one-to-one correspondence with the set of generators $S(G)$ for the chain group $EGC(G)$.

Remark 4.2.1. *We can give additive notation for the relations above if we put* $k = 0$ *for - and* $k = 1$ *for + which we will use later. The last condition for the generators can then be written as:*

for any two coordinates $x_{ij}^{k_{ij}}$ *and* $x_{it}^{k_{it}}$ *of* $\boldsymbol{x}$ *on* β_i*,* $k_{it} = (k_{ij} + N_{x_{ij}x_{it}} + 1)$ *mod* 2*.*

4.2.2 The Differential

We define a differential $\partial' : EGC(G) \longrightarrow EGC(G)$ by

$$\partial'(\boldsymbol{x}) = \sum_{\boldsymbol{y} \in S(G)} \#rect^o(\boldsymbol{x}, \boldsymbol{y}).\boldsymbol{y} \tag{4.2}$$

where $\boldsymbol{x} \in S(G)$, $rect^o(\boldsymbol{x}, \boldsymbol{y})$ denotes the set of empty rectangles (rectangles not containing any basepoint and not containing any coordinate of $\boldsymbol{x}, \boldsymbol{y}$ in the interior or in the boundary) from $\boldsymbol{x}$ to $\boldsymbol{y}$, and $\#rect^o(\boldsymbol{x}, \boldsymbol{y})$ denotes the cardinality of that set mod 2.

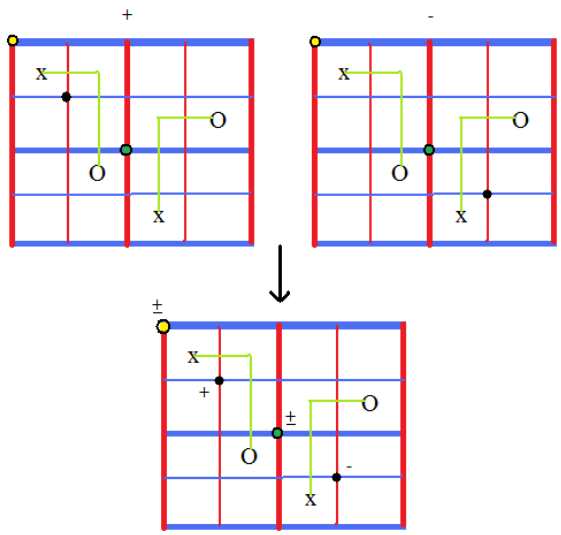

Figure 4.6: Figure showing generators in the lift.

We discuss possible types of rectangles in the torus. $rect^o(\boldsymbol{x}, \boldsymbol{y})$ is empty if $\boldsymbol{x}$ and $\boldsymbol{y}$ differ in more than two coordinates. Suppose now that $\boldsymbol{x}$ and $\boldsymbol{y}$ differ at two coordinates, where the coordinates are $(x_{ij}^{k_{ij}}, x_{ts}^{k_{ts}})$ and $(y_{tj}^{k_{tj}}, y_{is}^{k_{is}})$. If the four points $(x_{ij}, y_{is}, x_{ts}, y_{tj})$ are not all distinct, then $rect^o(\boldsymbol{x}, \boldsymbol{y}) = \emptyset$. If the four points $(x_{ij}, y_{is}, x_{ts}, y_{tj})$ are all distinct, then there are four rectangles R_1, R_2, R_3 and R_4 in the extended grid connecting them (as shown by A, B, C and D in Figure 4.7).

We will first discuss the first type of rectangle as shown in Figure 4.7 - type A. In order for a rectangle of type A in the grid to lift to a rectangle in the double cover, the following conditions need to hold true:

- $k_{is} = (-1)^{N_{x_{ij}y_{is}}} k_{ij}, k_{is} = (-1)^{N_{y_{is}x_{ts}}} k_{ts}, k_{tj} = (-1)^{N_{x_{ij}y_{tj}}} k_{ij}, k_{tj} = (-1)^{N_{y_{tj}x_{ts}}} k_{ts}$
- the rectangle does not contain any basepoint.
- when a cut line connecting two basepoints partitions a rectangle, then each of the parts gets an opposite sign.

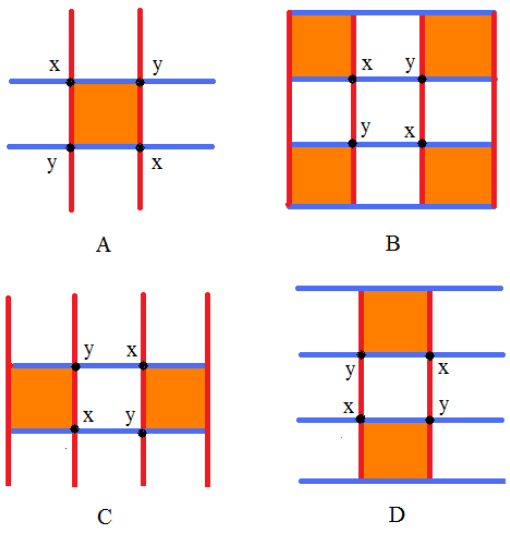

Figure 4.7: Different squares in the extended grid diagram.

- if there is a coordinate $x_{mn} = y_{mn}$ that lies in the rectangle (including the boundary of the rectangle), then the sign of x_{mn} is opposite to the sign of the smaller domain it sits in.

The first condition ensures that all the corner points of a rectangle are compatible with each other, i.e. that a rectangle in the extended grid is the projection of the rectangle in $\Sigma_g \subset Y$. The third condition implies that if a cut line partitions a rectangle, which is in G^+, then the portion of the rectangle after meeting the cut line comes out from G^- and vice versa (Figure 4.8). All these conditions together ensure that the rectangle in the lift contains no basepoint and no other coordinates of $\boldsymbol{x}$ and $\boldsymbol{y}$.

We next discuss rectangles of type C and D from Figure 4.7 . The last three conditions required for rectangles of type A remain the same for other types. In case of type C, the conditions for an empty rectangle are the following:

- $k_{tj} = (-1)^{N_{x_{ij}y_{tj}}} k_{ij}, k_{is} = (-1)^{N_{y_{is}x_{ts}}} k_{ts}$
- $k_{is} = (-1)^{N_{y_{is}x_{ij}}} k_{ij}$, if x_{ij} and y_{is} are on the old β-curve.

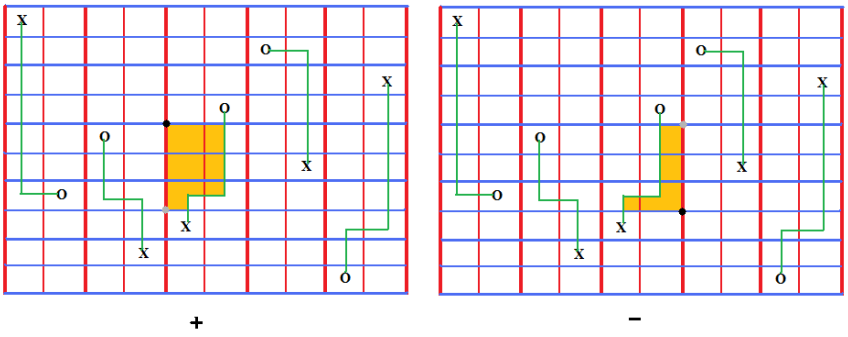

Figure 4.8: Rectangle of Type A. Figure showing a rectangle from $\boldsymbol{x}$ to $\boldsymbol{y}$, where $\boldsymbol{x}$ is represented by black dot and $\boldsymbol{y}$ is denoted by grey dot. Here the line joining the basepoints separates the rectangle.

- $k_{is} = (-1)^{(N_{y_{is}x_{ij}}+1)}k_{ij}$, if x_{ij} and y_{is} are on the new β-curve.
- $k_{tj} = (-1)^{N_{y_{tj}x_{ts}}}k_{ts}$, if x_{ts} and y_{tj} are on the old β-curve.
- $k_{tj} = (-1)^{(N_{y_{tj}x_{ts}}+1)}k_{ts}$, if x_{ts} and y_{tj} are on the new β-curve.

The last condition has this form because there are odd number of intersections of the cut lines with the new curves. There is an odd number of intersections of the cut lines with the new curves because a new curve in the extended grid lifts to one single curve. Hence, if there are N cut lines between y_{is} and x_{ij}, then there will be $N+1 \pmod 2$ cut lines between x_{ij} and y_{is}. Figure 4.9 shows a rectangle of type C.

In case D, the conditions for an empty rectangle are the following:

- $k_{is} = (-1)^{N_{x_{ij}y_{is}}}k_{ij}, k_{tj} = (-1)^{N_{y_{tj}x_{ts}}}k_{ts}$
- $k_{tj} = (-1)^{N_{y_{tj}x_{ij}}}k_{ij}$, if x_{ij} and y_{tj} are on the old α-curve.
- $k_{tj} = (-1)^{(N_{y_{tj}x_{ij}}+1)}k_{ij}$, if x_{ij} and y_{tj} are on the new α-curve.
- $k_{is} = (-1)^{N_{x_{ts}y_{is}}}k_{ts}$, if x_{ts} and y_{is} are on the old α-curve.
- $k_{is} = (-1)^{(N_{x_{ts}y_{is}}+1)}k_{ts}$, if x_{ts} and y_{is} are on the new α-curve.

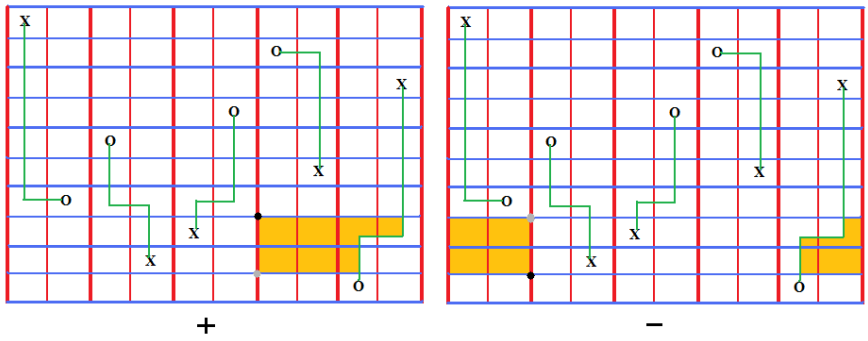

Figure 4.9: Rectangle of Type C. Figure showing a rectangle from $\boldsymbol{x}$ to $\boldsymbol{y}$, where $\boldsymbol{x}$ is represented by black dot and $\boldsymbol{y}$ is denoted by grey dot. Here the line joining the basepoints separates the rectangle.

Figure 4.10 shows a rectangle of type D.

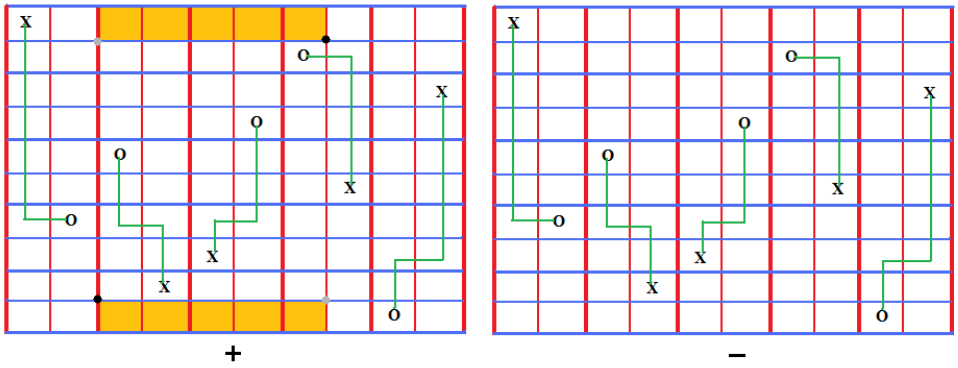

Figure 4.10: Rectangle of Type D. Figure showing a rectangle from $\boldsymbol{x}$ to $\boldsymbol{y}$, where $\boldsymbol{x}$ is represented by black dot and $\boldsymbol{y}$ is denoted by grey dot.

In case B, the conditions for an empty rectangle are the following:

- $k_{is} = (-1)^{N_{x_{ij}y_{is}}} k_{ij}$, if x_{ij} and y_{is} are on the old β-curve.
- $k_{is} = (-1)^{(N_{x_{ij}y_{is}}+1)} k_{ij}$, if x_{ij} and y_{is} are on the new β-curve.
- $k_{tj} = (-1)^{N_{x_{ts}y_{tj}}} k_{ts}$, if x_{ts} and y_{tj} are on the old β-curve.
- $k_{tj} = (-1)^{(N_{x_{ts}y_{tj}}+1)} k_{ts}$, if x_{ts} and y_{tj} are on the new β-curve.

- $k_{tj} = (-1)^{N_{x_{ij}y_{tj}}} k_{ij}$, if x_{ij} and y_{tj} are on the old α-curve.
- $k_{tj} = (-1)^{(N_{x_{ij}y_{tj}}+1)} k_{ij}$, if x_{ij} and y_{tj} are on the new α-curve.
- $k_{is} = (-1)^{N_{y_{is}x_{ts}}} k_{ts}$, if x_{ts} and y_{is} are on the old α-curve.
- $k_{is} = (-1)^{(N_{y_{is}x_{ts}}+1)} k_{ts}$, if x_{ts} and y_{is} are on the new α-curve.

Figure 4.11 shows a rectangle of type B.

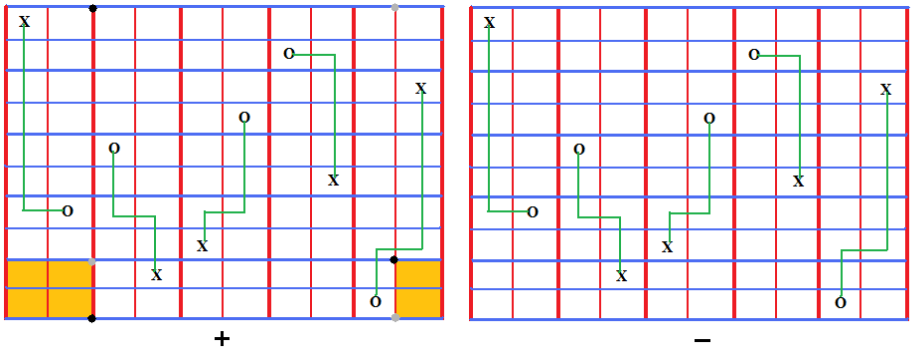

Figure 4.11: Rectangle of Type B. Figure showing a rectangle from $\boldsymbol{x}$ to $\boldsymbol{y}$, where $\boldsymbol{x}$ is represented by black dot and $\boldsymbol{y}$ is denoted by grey dot.

This gives a combinatorial way to count empty rectangles in the lift. We will describe an algorithm that encodes the combinatorics in chapter 6.

Proposition 4.2.1. *The map $\partial' : EGC(G) \longrightarrow EGC(G)$ satisfies $\partial' \circ \partial' = 0$. The extended grid homology $EGH(G)$ is the homology of the chain complex $(EGC(G), \partial')$.*

Proof. The proof is based on analyzing how empty rectangles interact with each other (See Lemma 4.4.6 in [14]). We can write

$$\partial' \circ \partial'(x) = \sum_{\boldsymbol{z} \in S(G)} \sum_{\{\tau \in \pi(\boldsymbol{x},\boldsymbol{z}) | \boldsymbol{z} \cap Int(\tau) = \emptyset, \tau \cap \mathbb{X} = \emptyset, \tau \cap \mathbb{O} = \emptyset\}} N(\tau)\boldsymbol{z} \tag{4.3}$$

where $N(\tau)$ is the number of ways τ can be decomposed as two empty rectangles. There can be atmost four points where $\boldsymbol{x}$ and $\boldsymbol{z}$ could differ as a rectangle switches two points. We consider three cases.

Case 1: $\boldsymbol{x} - (\boldsymbol{x} \cap \boldsymbol{z})$ contains four distinct points. In this case, τ consists of two disjoint rectangles r_1 and r_2. There are exactly two ways to decompose τ, first r_1 and then r_2 or first r_2 and then r_1 (Figure 4.12). Hence, $N(\tau) = 2$.

Figure 4.12: Case 1: The domain τ as two disjoint rectangles.

Case 2: $\boldsymbol{x} - (\boldsymbol{x} \cap \boldsymbol{z})$ contains three distinct points. In this case, τ has six corners, five $90°$ and one $270°$. One can decompose τ in two different ways by decomposing τ along the $270°$ corner (Figure 4.13). Hence, $N(\tau) = 2$.

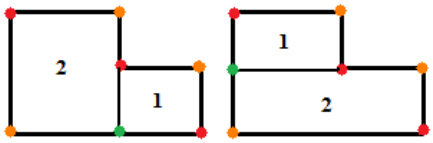

Figure 4.13: Case 2: Two ways of decomposing τ.

Case 3: $\boldsymbol{x} - (\boldsymbol{x} \cap \boldsymbol{z})$ contains no points. This case does not exist as τ will be an annulus in the extended grid and it will contain a basepoint.

Hence, we have $\partial' \circ \partial' = 0$. □

Proposition 4.2.2. *$EGH(G)$ is the stabilized hat-version of Heegaard Floer homology group of the double branched cover using the adapted diagram $\mathcal{D}$, i.e., $EGH(G) = \widehat{HF}_{st}(Y_L)$, where Y is the double branched cover of S^3 branched along a link $L \in S^3$.*

Proof. We need to show that the map ∂' is equal to the boundary map ∂ of the chain complex of the stabilized hat-version of Heegaard Floer homology group of the double branched cover of S^3 along a link L. From Theorem 2.5.1 we know that ∂ can be computed by counting the empty bigons and rectangles in a Heegaard diagram $\mathcal{D}$ for a 3-manifold Y. In our case, adapted diagram

$\mathcal{D}$ contains only rectangles and octagons and all octagons contain a basepoint. We need to show that every empty rectangle in the lift is a lift of an empty rectangle downstairs, i.e. it projects injectively to an empty rectangle in the extended grid.

Let R be an empty rectangle in $\mathcal{D}$ with four corner points a_1, a_2, a_3, a_4. Suppose that the branched covering map is not injective on the side of the rectangle connecting a_1 and a_2 along an $\boldsymbol{\alpha}$-curve α_i, then the rectangle in the extended grid might overlap. Hence, the whole α_i is used to join a_1 to a_2. However, that would imply that the image of the elementary domain in the extended grid contains a basepoint and hence would contradict the emptyness of R. □

4.2.3 Relative Grading

Let $(\Sigma_g, \boldsymbol{\alpha}, \boldsymbol{\beta}, \boldsymbol{w})$ be a nice multi-pointed Heegaard diagram.

Definition 4.2.2. *A domain D is a formal linear combination $D = \sum_i n_i D_i$ of the elementary domains D_i, where n_i is the multiplicity of D_i in D.*

Given $z \in (\Sigma_g - \boldsymbol{\alpha} - \boldsymbol{\beta})$, the local multiplicity $n_z(D)$ of D at z is the multiplicity of the elementary domain D_i containing z in D. We define $n_w(D) = \sum_i n_{w_i}(D)$.

Definition 4.2.3. *Let $\boldsymbol{x}, \boldsymbol{y}$ be two generators in $\mathbb{T}_{\boldsymbol{\alpha}} \cap \mathbb{T}_{\boldsymbol{\beta}}$. A domain connecting $\boldsymbol{x}$ to $\boldsymbol{y}$ is a formal linear combination of elementary domains such that the boundary of D consists of an union of sequence of $\boldsymbol{\alpha}$ and $\boldsymbol{\beta}$ curves, $\partial(\partial D \cap \boldsymbol{\alpha}) = \boldsymbol{y} - \boldsymbol{x}$ and $\partial(\partial D \cap \boldsymbol{\beta}) = \boldsymbol{x} - \boldsymbol{y}$.*

In [9], Lipshitz gave a formula to compute the Euler measure for a domain as well as the Maslov index. For any domain D,

$$e(D) = \chi(D) - \frac{K}{4} + \frac{L}{4}, \tag{4.4}$$

where $\chi(D)$ is the Euler characteristics of the domain, K is the number of acute (convex) corners in D, and L is the number of obtuse (concave) corners in D. We note that if D_i is an elementary domain which is a $2n$-gon, this corresponds to defining $e(D_i)$ as $1 - \frac{n}{2}$ and extending linearly to all domains (linear combinations of elementary domains) with $n_{w_i} = 0$, $i = 1, 2, \ldots, k - g + 1$. Then $e(D)$ is the Euler measure of D.

Definition 4.2.4. *([15]) Suppose D be a domain connecting two generators $\boldsymbol{x}$ and $\boldsymbol{y}$. Then the point measure $p(D)$ of D is the sum of $p_{x_i}(D)$ and $p_{y_j}(D)$ for each $\boldsymbol{x}$ (and $\boldsymbol{y}$) coordinate x_i (and y_j), where $p_{x_i}(D)$ (and $p_{y_j}(D)$) is the average of the multiplicities of the four domains that meet at x_i (and y_j).*

The Maslov index $\mu(D)$ of a domain D is the sum of the Euler measure $e(D)$ and the point measure $p(D)$.

$$\mu(D) = e(D) + p(D) \tag{4.5}$$

Note that the Maslov index of the domain is additive. The Maslov index of the domain induces a relative grading on the set of generators $S(G)$:

$$\mu(\boldsymbol{x}, \boldsymbol{y}) = \mu(D) \tag{4.6}$$

for a domain D connecting $\boldsymbol{x}$ to $\boldsymbol{y}$.

Definition 4.2.5. *Let $\boldsymbol{x}, \boldsymbol{y}$ be two generators in $S(G)$. If there is a rectangle D connecting $\boldsymbol{x}$ and $\boldsymbol{y}$, the relative grading between $\boldsymbol{x}$ and $\boldsymbol{y}$ satisfies*

$$\mu(\boldsymbol{x}, \boldsymbol{y}) = 1. \tag{4.7}$$

We choose a generator x_0, where x_0 has only one intersection point of the old $\boldsymbol{\alpha}$ and old $\boldsymbol{\beta}$ curves in the extended grid and the intersection points in the new curves lifts to the positive region in the lift.

We define $\mu(x_0) = 0$ and for any $y \in S(G)$, we define the $\mathbb{Z}$ grading as

$$\mu_{x_0}(y) = \mu(x_0, y) \tag{4.8}$$

Theorem 4.2.1. *$(EGC(G), \partial')$ is a chain complex and the differential ∂' changes the $\mathbb{Z}$ grading by one. $EGC(G) = \bigoplus_{\mu_{x_0} \in \mathbb{Z}} EGC_{\mu_{x_0}}(G)$, where μ_{x_0} is the $\mathbb{Z}$ grading.*

Chapter 5

Main Results

5.1 Invariance of EGH under Choice of Cut Lines

We show combinatorially that the extended grid homology for a double branched cover of S^3 branched along a link $L \subset S^3$ is independent of the choice of the lines joining X and O. We call these lines joining basepoints cut lines. We will choose the cut lines to be straight lines coming out from the top basepoint in the extended grid, going straight down to the row containing the lower basepoint in that column of the original grid, and then turning left (or right) depending on the position of the lower basepoint (Figure 5.1). We call these cut lines Type-1 cut lines. We could choose the cut lines differently as shown in Figure 5.2 by starting from the topmost basepoint in the extended grid in between two old α-curves and instead of going straight down, turning left or right, depending on the location of the lower basepoint that lies in between the two old α-curves and then coming down straight to the second basepoint. We call these Type-2 cut lines.

Let G be an extended grid diagram for a link with Type-1 cut lines and G' be another extended grid diagram for the same link with Type-2 cut lines. Let $\widetilde{G}$ and $\widetilde{G'}$ be the Heegaard diagrams for the 3-manifold obtained from the lifts of the extended grid diagrams G and G' respectively.

Theorem 5.1.1. *If G and G' be extended grid diagrams of a link L in S^3 branched along L, where G and G' have type-1 and type-2 cut lines respectively, then there is an isomorphism between $EGH(G)$ and $EGH(G')$.*

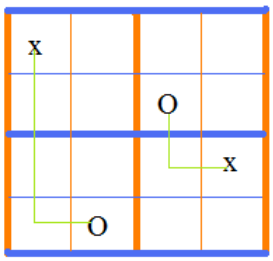

Figure 5.1: Extended grid diagram for the unknot with Type-1 cut lines.

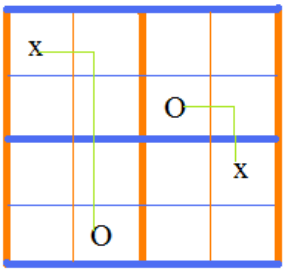

Figure 5.2: Extended grid diagram for the unknot with Type-2 cut lines.

To prove Theorem 5.1.1, we define a map $\phi_1 : EGC(G) \longrightarrow EGC(G')$ by $\phi_1(\boldsymbol{x}) = \phi_1(\{x_{ij}^k\}) = \{x_{ij}^{\phi_{ij}(k)}\}$, where

$$\phi_{ij}(k) = \begin{cases} k & \text{if } N_1 = N_2, \\ k+1 (\text{mod } 2) & \text{if } N_1 \neq N_2, \end{cases}$$

where $N_1 =$ the number of intersection points of β_i with the cut lines that lie between $\alpha_0 \cap \beta_i$ and $\alpha_j \cap \beta_i$ in G, $N_2 =$ the number of intersection points of β_i with the cut lines that lie between $\alpha_0 \cap \beta_i$ and $\alpha_j \cap \beta_i$ in G', and for the generators $\{x_{ij}^k\}$ we refer to Remark 4.2.1.

Lemma 5.1.1. *The map ϕ_1 is well-defined.*

Proof. By well-defined we mean that ϕ_1 maps generators to generators. For $k = 0$ and 1 both, i.e., x_{ij} is the intersection of two old curves in the lift, it is clear that $N_1 = N_2$.

The map ϕ_1 keeps the position of the coordinates of the generators, the only change is in the sign of the exponent. The change in sign occurs in between the old $\alpha-$curves as the cut lines only change between two old $\alpha-$curves (Figure 5.3). From definition 4.2.1, it is clear that the first four conditions hold true. We only need to show the last condition, i.e., on an old $\boldsymbol{\beta}$-curve, the exponents are compatible under the map ϕ_1.

Let x_{ij}^m and x_{ip}^n be two entries on an old $\boldsymbol{\beta}$-curve β_i in G. Then, $n = m + (N_1^p - N_1^j) + 1$ (mod 2), where N_1^p (similarly N_1^j) is the number of intersection points of β_i with the cut lines that lie

between $\alpha_0 \cap \beta_i$ and $\alpha_p \cap \beta_i$ (similarly $\alpha_j \cap \beta_i$) in G. Let $x_{ij}^{m'}$ and $x_{ip}^{n'}$ be the images of x_{ij}^{m} and x_{ip}^{n} respectively, under the map ϕ_1.

Case 1: If $N_2^p = N_1^p$ and $N_2^j = N_1^j$, where N_2^p (similarly N_2^j) is the number of intersection points of β_i with the cut lines that lie between $\alpha_0 \cap \beta_i$ and $\alpha_p \cap \beta_i$ (similarly $\alpha_j \cap \beta_i$) in G', the fifth condition for generators is true by the definition of ϕ_1.

Case 2: Assume that $N_2^p \neq N_1^p$ and $N_2^j \neq N_1^j$. Then $N_2^p = N_1^p + 1 \pmod 2$, $N_2^j = N_1^j + 1 \pmod 2$, $n^{'} = n + 1 \pmod 2$, and $m^{'} = m + 1 \pmod 2$.

So, $m^{'} + N_2^p - N_2^j + 1 = (m+1) + (N_1^p + 1) - (N_1^j + 1) + 1 \pmod 2 = m + (N_1^p - N_1^j) + 1 + 1 \pmod 2 = n + 1 \pmod 2 = n^{'}$. This shows that the two exponents are compatible under the map ϕ_1.

Case 3: Either $N_2^p \neq N_1^p$ or $N_2^j \neq N_1^j$. If $N_2^p \neq N_1^p$. Then $N_2^p = N_1^p + 1$, and $n^{'} = n + 1 \pmod 2$.

So, $m^{'} + N_2^p - N_2^j + 1 = m + (N_1^p + 1) - N_1^j + 1 \pmod 2 = m + (N_1^p - N_1^j) + 1 + 1 \pmod 2 = n + 1 \pmod 2 = n^{'}$.

Hence, ϕ_1 maps generators to generators. □

Lemma 5.1.2. *The map $\phi_1 : EGC(G) \longrightarrow EGC(G')$ is a chain map.*

Proof. We recall that for any $x \in S(G)$,

$$\partial \boldsymbol{x} = \sum_{\boldsymbol{y} \in S(G)} \sum_{rect^{\circ}(\boldsymbol{x}, \boldsymbol{y})} \boldsymbol{y}$$

where $rect^{\circ}(x, y)$ is the collection of empty rectangles (not containing any basepoints as defined in chapter 4).

We want to show that ϕ_1 commutes with the boundary map. ϕ_1 keeps the position of the coordinates in a generator, the only change is in the signs of the exponent. Recalling the rules for the rectangles, it is clear that the sign of the exponents are compatible under the map ϕ_1. Geometrically, we can see the composite map $\phi_1 \circ \partial$ slides the rectangles in the Heegaard diagram for Y across the cut lines (Figure 5.3, Figure 5.4). □

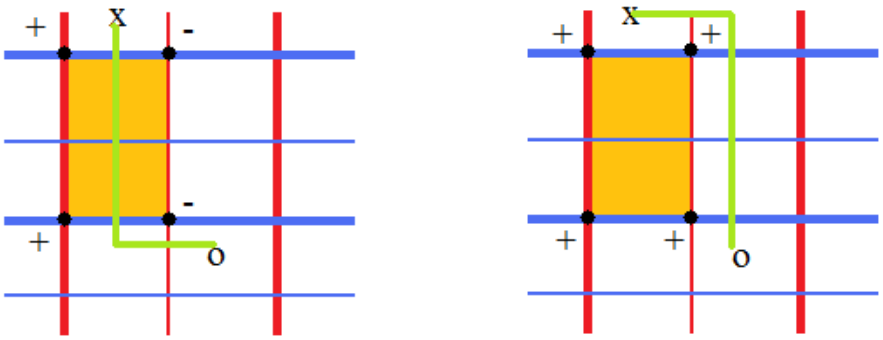

Figure 5.3: Rectangles in Type-1 and Type-2 cut lines in the extended grid diagram.

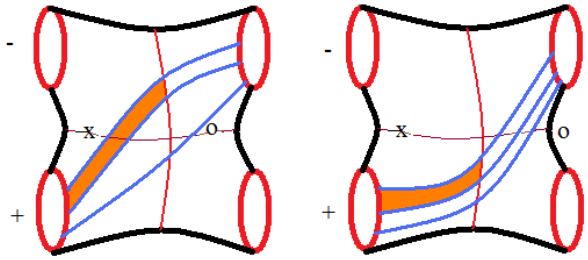

Figure 5.4: The figure on the left shows the rectangle under the boundary map ∂ and the picture on the right shows the rectangle under the map $\phi_1 \circ \partial$.

Similarly, we define a chain map $\phi_1^{'} : EGC(G') \longrightarrow EGC(G)$ by $\phi_1'(\boldsymbol{x}) = \phi_1'(\{x_{ij}^k\}) = \{x_{ij}^{\phi'_{ij}(k)}\}$, where

$$\phi'_{ij}(k) = \begin{cases} k & \text{if } N_1 = N_2, \\ k+1 (\text{mod } 2) & \text{if } N_1 \neq N_2, \end{cases}$$

where $N_1 =$ the number of intersection points of β_i with the cut lines that lie between $\alpha_0 \cap \beta_i$ and $\alpha_j \cap \beta_i$ in G', and $N_2 =$ the number of intersection points of β_i with the cut lines that lie between $\alpha_0 \cap \beta_i$ and $\alpha_j \cap \beta_i$ in G.

Proof of Theorem 5.1.1. Using lemma 5.1.2, we have two chain maps, ϕ_1 and ϕ_1', and ϕ_1' is the inverse of ϕ_1. Hence, $EGH(G) \cong EGH(G')$.

A similar argument holds true for any other pair of choices of cut lines joining X and O. Hence, the extended grid homology EGH is independent under the choice of the cut lines.

5.2 Invariance of EGH under Choice of New Curves Separating X and O

Here we show that the combinatorial extended grid homology $EGH(G)$ of a double branched cover of S^3 branched along a link $L \subset S^3$ is independent of the choice of the new curves separating X and O.

We will show the independence for the choice of the new β-curves. The proof that same is true for the choice of the new α-curves is similar. A new β-curve can be introduced in the grid diagram separating X and O in two different ways as shown in Figure 5.5. We call the first picture Type A and the second Type B in Figure 5.5. In Type A, the leftmost basepoint in the row of the new curve appears above the new β-curve and the rightmost basepoint appears below the new β-curve. In Type B, the leftmost basepoint appears below the new β-curve and the rightmost basepoint above the new β-curve.

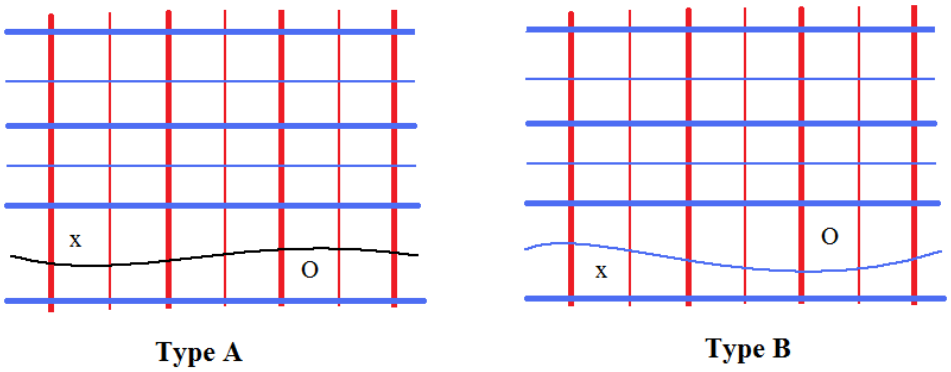

Figure 5.5: New curves separating the two basepoints X and O.

Let H_1 be an extended grid diagram for a link $L \subset S^3$ where one of the new $\boldsymbol{\beta}-$curves, β_{i_0}, is of Type A. Let $\widetilde{H_1}$ be a lift of H_1 and the set of generators $S(H_1)$ be the set of unordered 3n-tuples of intersection points between the α- and β-curves satisfying the conditions for the generators (see definition 4.2.1).

We draw the extended grid diagram H_2 by replacing the specified new β-curve of type A, β_{i_0}, by a new β-curve of Type B which we will call γ_{i_0}. We will draw the two types of curves in the same extended grid diagram, and call this diagram $H_{1,2}$. Let $\widetilde{H_{1,2}}$ be the lift of $H_{1,2}$. The lifts to the double branched cover of the two curves β_{i_0} and γ_{i_0} intersect each other exactly at four points (two in each $H^+_{1,2}$ and $H^-_{1,2}$ respectively). We call those points $\{a_1, b_1, a_2, b_2\}$, where a_1, b_1 are in the positive region and a_2, b_2 are in the negative region in the lift (Figure 5.6). We can isotope β_{i_0} and γ_{i_0} so that their intersections are not on any vertical α-curves and they intersect transversally at a right angle.

Proposition 5.2.1. *If H_1 and H_2 are the extended grid diagrams of a link L in S^3 branched along L, where H_2 is obtained from H_1 by replacing a Type-A β-curve with a Type-B β-curve (we denoted γ), then there is an isomorphism between $EGH(H_1)$ and $EGH(H_2)$.*

To prove this, we first need to define a chain map from $EGC(H_1)$ to $EGC(H_2)$. For that, we will use a pentagon counting map. This is an adaptation of a pentagon counting map that appeared in the proof for commutation invariance of the grid homology in [14]. The pentagons we will count live in the diagram $H_{1,2}$.

Definition 5.2.1. *(Embedded pentagon [14]) An embedded pentagon "pent" in $H_{1,2}$ is a domain with boundary which is a union of five embedded arcs in $\boldsymbol{\alpha} \cup \boldsymbol{\beta} \cup \gamma_{i_0}$ such that two of the edges and a vertex they meet at are in $\beta_{i_0} \cup \gamma_{i_0}$, and at any of the five corner points p, where two of the arcs intersect, the intersection of "pent" with a neighborhood of p is one of the four quadrants determined by the two intersecting curves at p (Figure 5.6).*

A pentagon "pent" is an embedded pentagon connecting $\boldsymbol{x}$ to $\boldsymbol{y'}$ if

- *$\boldsymbol{x}, \boldsymbol{y'}$ have exactly (3n-2) coordinates in common,*
- *$\partial((\partial pent) \cap \boldsymbol{\alpha}) = \boldsymbol{y'} - \boldsymbol{x}$.*

The collection of pentagons from $\boldsymbol{x}$ to $\boldsymbol{y'}$ is denoted $pent(\boldsymbol{x}, \boldsymbol{y'})$. A pentagon in $pent(\boldsymbol{x}, \boldsymbol{y'})$ is *empty* if it does not contain any point of $\boldsymbol{x}$ or $\boldsymbol{y'}$ in its interior or in the boundary and it does not contain any basepoint X or O in its interior. The set of empty pentagons from $\boldsymbol{x}$ to $\boldsymbol{y'}$ is denoted by $pent^{\circ}(\boldsymbol{x}, \boldsymbol{y'})$.

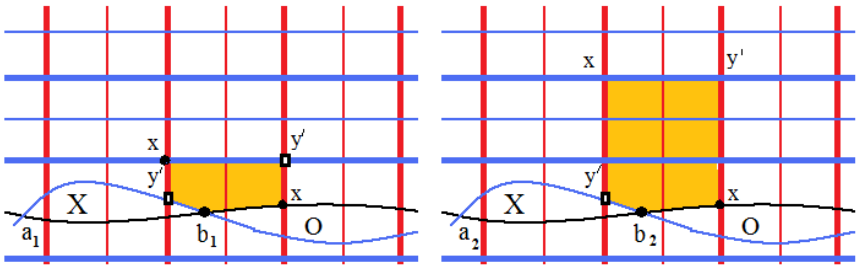

Figure 5.6: Pentagons changing $\boldsymbol{x}$ to $\boldsymbol{y'}$.

Any pentagon from some $\boldsymbol{x} \in S(H_1)$ to some $\boldsymbol{y'} \in S(H_2)$ must have an edge in the type A β_{i_0}-curve and an adjacent one in the type B γ_{i_0}-curve, intersecting at one of the intersection points b_1 or b_2 in $\beta_{i_0} \cap \gamma_{i_0}$. One of the other intersection points, either a_1 or $a_2 \in \beta_{i_0} \cap \gamma_{i_0}$, is a vertex of any pentagon from any generator for $\widetilde{H_2}$ to $\widetilde{H_1}$. Here we define the from-to relationship in the same way as we did for the boundary map, the "from" vertex being in the top left and bottom right corners. Suppose now that $\boldsymbol{x}$ and $\boldsymbol{y'}$ are connected by a pentagon. Then they differ at two coordinates, where the coordinates are $(x_{ij}^{k_{ij}}, x_{ts}^{k_{ts}})$ and $(y_{tj}^{'k_{tj}}, y_{is}^{'k_{is}})$. There are four types of pentagons in the extended grid diagram (Figure 5.7).

If the two generators do not differ at exactly two coordinates, then $pent^{\circ}(\boldsymbol{x}, \boldsymbol{y'}) = \emptyset$. If they differ at exactly two coordinates, and the four corresponding points $(x_{ij}, y'_{is}, x_{ts}, y'_{tj})$ are all distinct, then there are four possible types of pentagons in the extended grid connecting them (as shown by A, B, C and D in Figure 5.7). We discuss the type A pentagons first. In order for a pentagon in the grid to lift to a pentagon in the double cover, the following conditions need to hold true:

- $k_{is} = (-1)^{N_{x_{ij} y'_{is}}} k_{ij}, k_{is} = (-1)^{N_{y'_{is} x_{ts}}} k_{ts}, k_{tj} = (-1)^{N_{x_{ij} y'_{tj}}} k_{ij}$
- the pentagon does not contain any basepoint.

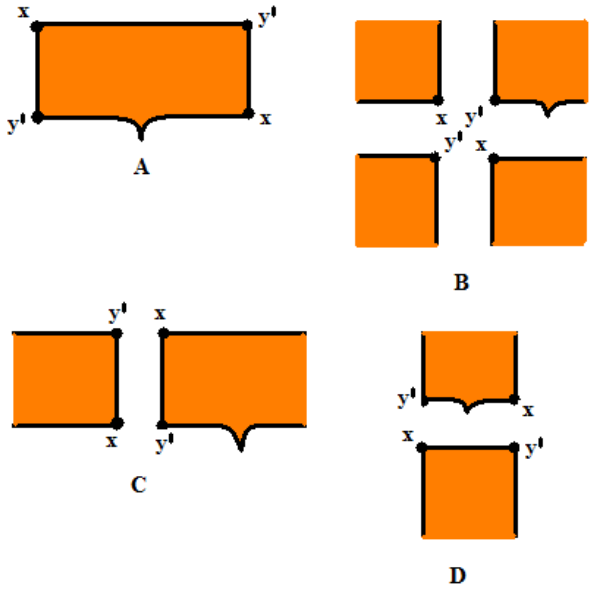

Figure 5.7: Different types of pentagons sending $\boldsymbol{x}$ to $\boldsymbol{y'}$.

- when a cut line connecting two basepoints partitions a pentagon, then each of the adjoining parts gets an opposite sign.
- if there is a coordinate $x_{mn} = y'_{mn}$ in the pentagon (including the boundary of the pentagon), then the sign of x_{mn} is opposite to the sign of the smaller domain it sits in.

The first two conditions ensure that all the corner points of a pentagon are compatible with each other, so that there is a pentagon in the lift connecting the generators. The third condition implies that if a cut line partitions a pentagon, which is in the positive region, then the portion of the pentagon after meeting the cut line comes out from the negative region and vice versa. These conditions ensure that the pentagon in the grid is the projection of the pentagon in $\Sigma \subset Y$ and contains no basepoint and no other coordinates of $\boldsymbol{x}$ and $\boldsymbol{y'}$.

We discuss Figure 5.7 C and D. The last three conditions in A remain the same for other types of pentagons (B,C,D). In C, the conditions for an empty pentagon are the following:

- $k_{tj} = (-1)^{N_{x_{ij}y'_{tj}}} k_{ij}, k_{is} = (-1)^{N_{y'_{is}x_{ts}}} k_{ts},$

- $k_{is} = (-1)^{N_{y'_{is}x_{ij}}} k_{ij}$, if x_{ij} and y'_{is} are on the old β-curve.
- $k_{is} = (-1)^{(N_{y'_{is}x_{ij}}+1)} k_{ij}$, if x_{ij} and y'_{is} are on the new β-curve.

The last condition holds because there are odd number of intersections of the cut lines with the new curves. Hence, if there are N cut lines between y'_{is} and x_{ij}, then there will be $N+1$ cut lines between x_{ij} and y'_{is}.

In case D, the conditions for an empty pentagon are the following:

- $k_{is} = (-1)^{N_{x_{ij}y'_{is}}} k_{ij}$
- $k_{tj} = (-1)^{N_{y'_{tj}x_{ij}}} k_{ij}$, if x_{ij} and y'_{tj} are on the old α-curve.
- $k_{tj} = (-1)^{(N_{y'_{tj}x_{ij}}+1)} k_{ij}$, if x_{ij} and y'_{tj} are on the new α-curve.
- $k_{is} = (-1)^{N_{x_{ts}y'_{is}}} k_{ts}$, if x_{ts} and y'_{is} are on the old α-curve.
- $k_{is} = (-1)^{(N_{x_{ts}y'_{is}}+1)} k_{ts}$, if x_{ts} and y'_{is} are on the new α-curve.

In case B, the conditions for an empty pentagon are the following:

- $k_{tj} = (-1)^{N_{x_{ts}y'_{tj}}} k_{ts}$, if x_{ts} and y'_{tj} are on the old β-curve.
- $k_{tj} = (-1)^{(N_{x_{ts}y'_{tj}}+1)} k_{ts}$, if x_{ts} and y'_{tj} are on the new β-curve.
- $k_{tj} = (-1)^{N_{x_{ij}y'_{tj}}} k_{ij}$, if x_{ij} and y'_{tj} are on the old α-curve.
- $k_{tj} = (-1)^{(N_{x_{ij}y'_{tj}}+1)} k_{ij}$, if x_{ij} and y'_{tj} are on the new α-curve.
- $k_{is} = (-1)^{N_{y'_{is}x_{ts}}} k_{ts}$, if x_{ts} and y'_{is} are on the old α-curve.
- $k_{is} = (-1)^{(N_{y'_{is}x_{ts}}+1)} k_{ts}$, if x_{ts} and y'_{is} are on the new α-curve.

We define a map $\phi_2 : EGC(H_1) \longrightarrow EGC(H_2)$ by counting pentagons:

$$\phi_2(\boldsymbol{x}) = \sum_{\boldsymbol{y'} \in S(H_2)} \sum_{p \in pent_b^\circ(\boldsymbol{x}, \boldsymbol{y'})} \boldsymbol{y'}$$

Analogously, we define an "inverse map"

$$\phi_2' : EGC(H_2) \longrightarrow EGC(H_1)$$

by counting pentagons from generators in $\widetilde{H_2}$ to generators in $\widetilde{H_1}$ with a vertex at "a". In other words,

$$\phi_2'(\boldsymbol{x'}) = \sum_{\boldsymbol{y} \in S(H_1)} \sum_{p \in pent_a^\circ(\boldsymbol{x'}, \boldsymbol{y})} \boldsymbol{y}$$

Lemma 5.2.1. *The maps ϕ_2 and ϕ_2' are chain maps.*

Proof. The proof is similar to Lemma 5.1.4 in [14]. We prove the lemma for ϕ_2. The proof is similar for ϕ_2'. The map ϕ_2 is well-defined, i.e., ϕ_2 maps generators to generators because if there exists a pentagon which connects $\boldsymbol{x}$ to $\boldsymbol{y'}$, then the conditions for the pentagon make it compatible with the conditions for the generators. We need to show ϕ_2 commutes with the boundary map i.e., we need to verify the identity

$$\partial \circ \phi_2 = \phi_2 \circ \partial$$

We have

$$\partial \circ \phi_2(\boldsymbol{x}) = \partial\Big(\sum_{\boldsymbol{y'} \in S(H_2)} \sum_{p \in pent_b^\circ(\boldsymbol{x}, \boldsymbol{y'})} \boldsymbol{y'}\Big) = \sum_{\boldsymbol{y'} \in S(H_2)} \sum_{p \in pent_b^\circ(\boldsymbol{x}, \boldsymbol{y'})} \sum_{\boldsymbol{z'} \in S(H_2)} \sum_{rect^o(\boldsymbol{y'}, \boldsymbol{z'})} \boldsymbol{z'}$$

and

$$\phi_2 \circ \partial(\boldsymbol{x}) = \phi_2\Big(\sum_{\boldsymbol{y} \in S(H_1)} \sum_{rect^o(\boldsymbol{x}, \boldsymbol{y})} \boldsymbol{y}\Big) = \sum_{\boldsymbol{y} \in S(H_1)} \sum_{rect^o(\boldsymbol{x}, \boldsymbol{y})} \sum_{\boldsymbol{z'} \in S(H_2)} \sum_{p \in pent_b^\circ(\boldsymbol{y}, \boldsymbol{z'})} \boldsymbol{z'}.$$

Hence, combining both, we get

$$(\partial \circ \phi_2 + \phi_2 \circ \partial)\boldsymbol{x} = \sum_{\boldsymbol{z'} \in S(H_2)} \sum_{\{\tau \in \pi(\boldsymbol{x}, \boldsymbol{z'}) \mid \boldsymbol{z'} \cap Int(\tau) = \emptyset = \boldsymbol{x} \cap Int(\tau), \mathbb{X} \cap \tau = \emptyset = \mathbb{O} \cap \tau\}} N(\tau)\boldsymbol{z'}. \tag{5.1}$$

where $\pi(\boldsymbol{x}, \boldsymbol{z'})$ is the set of regions connecting $\boldsymbol{x}$ and $\boldsymbol{z'}$ and $N(\tau)$ denotes the number of ways a region τ can be decomposed as a justaposition of a rectangle and a pentagon in any order. τ can be decomposed either to an empty rectangle first and then to an empty pentagon or first decompose into an empty pentagon and then to a rectangle. Figure 5.8 shows some of the possible choices for the domain τ. If a pentagon or a rectangle crosses cut lines, the cut lines cross the top and

the bottom the same number of times as pentagons and rectangles do not contain any basepoints. Except for the case 3 in Figure 5.8, there is no wrapping around and overlap of any region as the regions are free from basepoints. In addition, there is no overlap of the rectangles or the pentagons as they are free from interior points. There can be at most four points where $\boldsymbol{x}$ and $\boldsymbol{z'}$ could differ

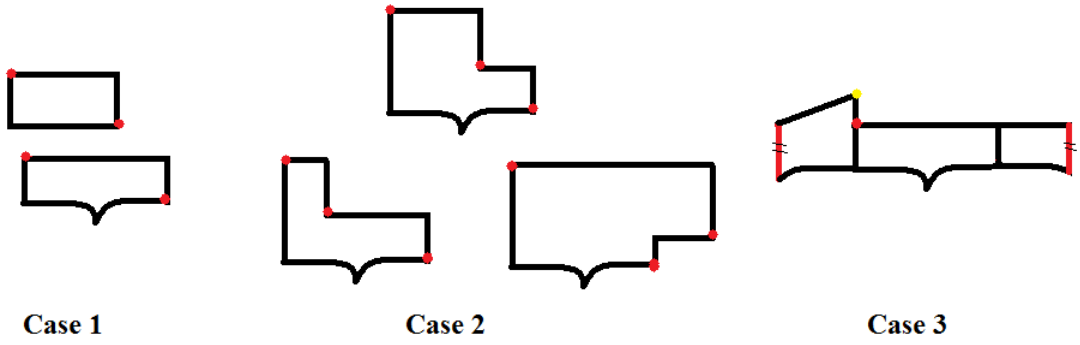

Figure 5.8: Some of the possible choices for the domain τ.

since a rectangle switches two points and a pentagon switches two points. $\boldsymbol{x} - (\boldsymbol{x} \cap \boldsymbol{z'})$ can contain either four, three or one points. We note that $\boldsymbol{x} - (\boldsymbol{x} \cap \boldsymbol{z'})$ cannot contain two points. The reason for this is that the pentagon and the rectangle would have exactly one edge in common, hence, two coordinates of $\boldsymbol{x}$ would come from the same $\boldsymbol{\beta}$ curve in the lift.

One can decompose the domain τ in three different ways:

Case 1: $\boldsymbol{x} - (\boldsymbol{x} \cap \boldsymbol{z'})$ contains exactly four distinct points. In this case, the region consists of a disjoint rectangle and a pentagon (Figure 5.9). A schematic diagram is shown in case 1 in Figure 5.8, with vertices belonging to $\boldsymbol{x}$ marked in red. In this case, there are exactly two ways to decompose τ, either by decomposing into rectangle first and then to a pentagon or to a pentagon first and then to a rectangle. Hence, we have $N(\tau)= 2$.

Case 2: $\boldsymbol{x} - (\boldsymbol{x} \cap \boldsymbol{z'})$ contains exactly three points. There are different choices for τ, some are shown in case 2 of Figure 5.8 and others are mirror images of those in case 2 of Figure 5.8. In all the cases, τ has seven corners in the lift, of which six of them are right-angled corners (including the intersection point b) and one of the corners is 270°.

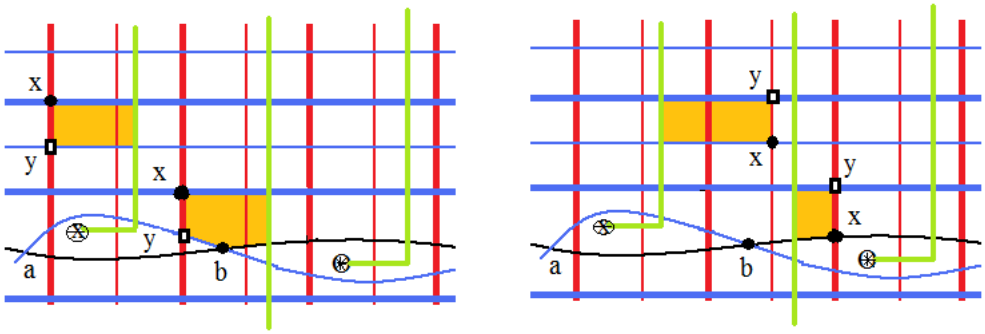

Figure 5.9: Disjoint pentagon and a rectangle in the lift of the extended grid diagram.

Subcase 1: Here τ as in bottom left figure in case 2 in Figure 5.8. It looks like the picture as shown in Figure 5.10. We can decompose τ along the 270° corner in two different ways. We give a schematic diagram for the decomposition of τ (Figure 5.11). The cut lines break the domain into smaller and smaller chunks and place those chunks alternately in the adjacent copies of the lift as the domain is free from basepoints. Using cut lines, we show the decomposition of τ: the first way is to use the pentagon first as shown in Figure 5.12 and then use the rectangle (Figure 5.13). The second way is to use the rectangle first (Figure 5.14) and then the pentagon (Figure 5.15). This gives two different decomposition of τ. Hence, $N(\tau)= 2$.

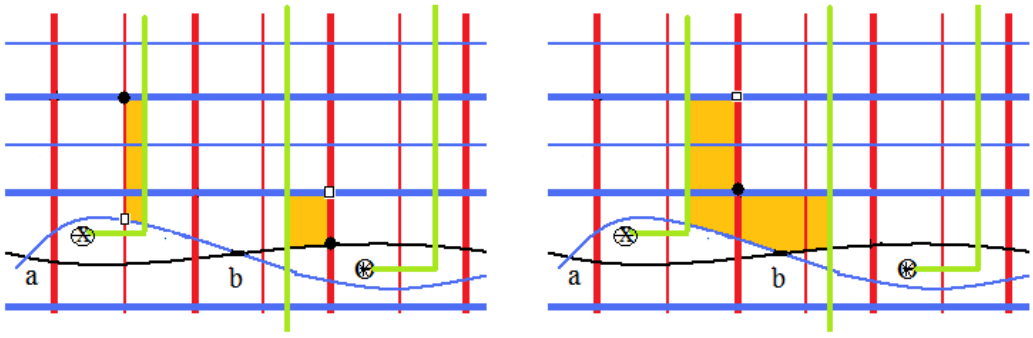

Figure 5.10: $\boldsymbol{x}$ and $\boldsymbol{z'}$ shown in the lift, $\boldsymbol{x}$ with black dots and $\boldsymbol{z'}$ with hollow squares.

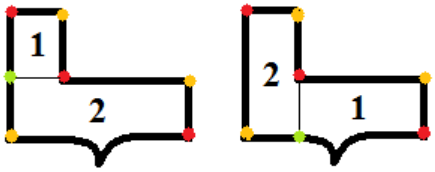

Figure 5.11: Subcase 1: Decomposing the domain τ in two different ways. The red dots represent $\boldsymbol{x}$ and the yellow dots represent $\boldsymbol{z'}$. The green dot represents a point $\boldsymbol{y}$ in $S(H_1)$.

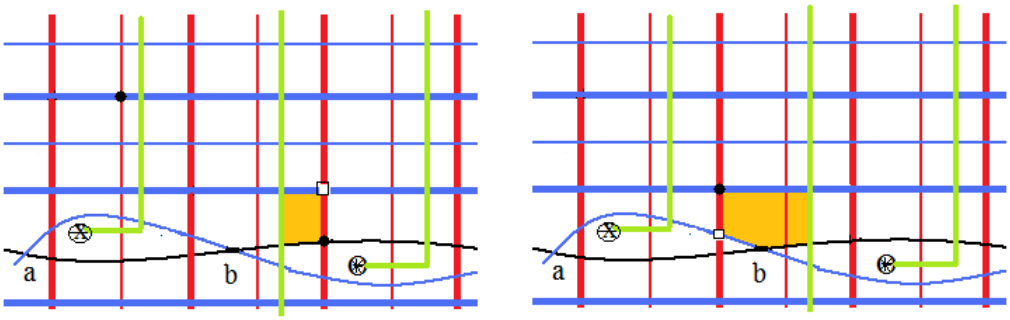

Figure 5.12: Using pentagon first to go from $\boldsymbol{x}$ to $\boldsymbol{y'}$.

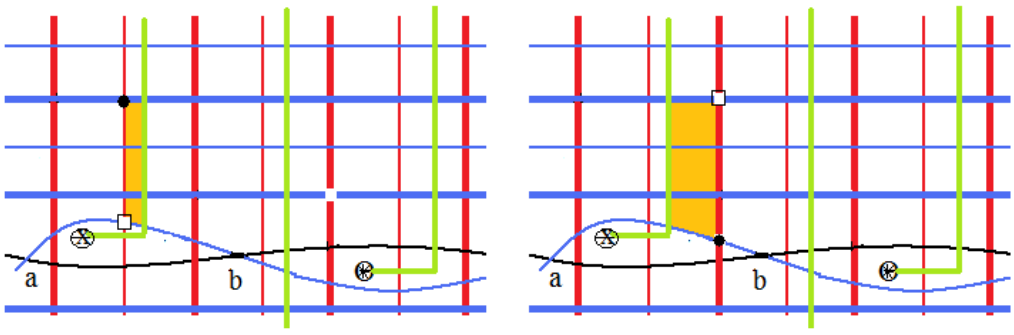

Figure 5.13: Using rectangle to go from $\boldsymbol{y'}$ to $\boldsymbol{z'}$.

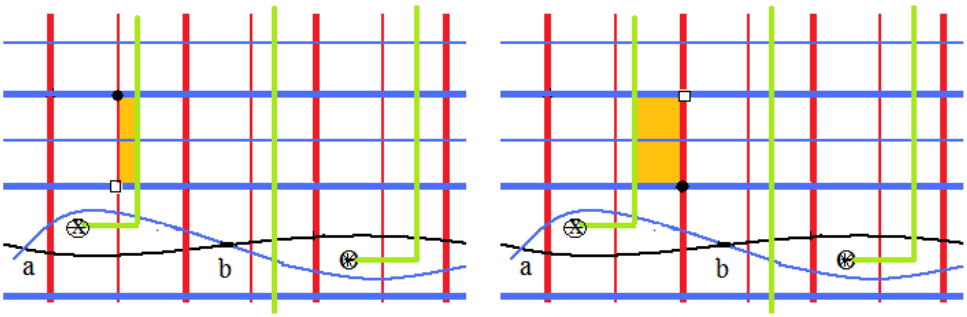

Figure 5.14: Using rectangle to go from $\boldsymbol{x}$ to $\boldsymbol{y}$.

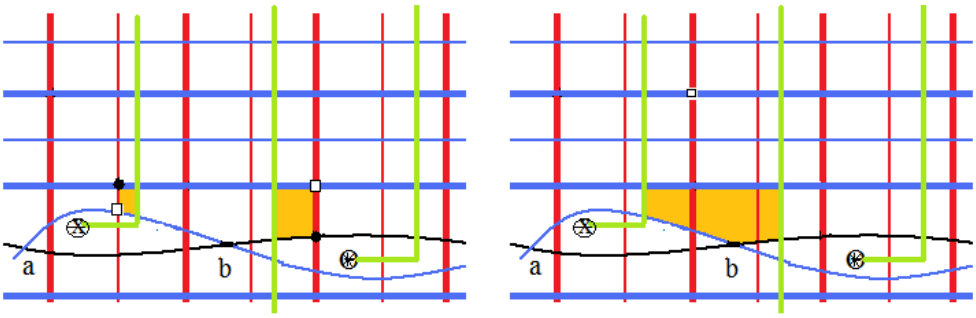

Figure 5.15: Using pentagon to go from $\boldsymbol{y}$ to $\boldsymbol{z'}$.

Subcase 2: Here τ as in the top figure in case 2 in Figure 5.8. It looks like the picture as shown in Figure 5.16. We cut the 270° corner in two different ways. We give a schematic diagram for the decomposition of τ (Figure 5.17).

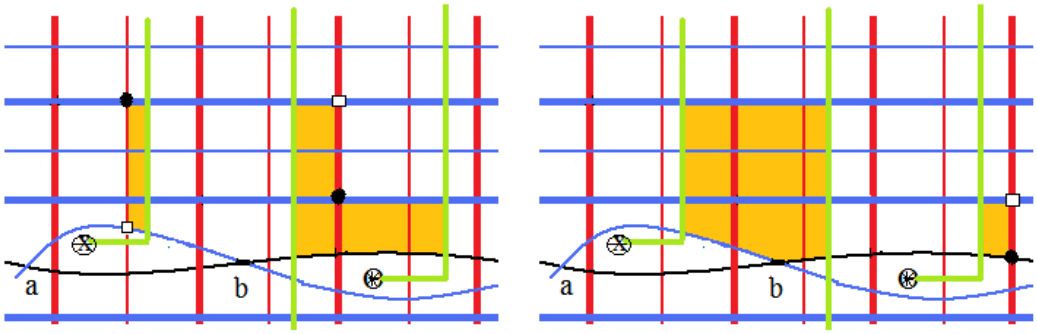

Figure 5.16: Subcase 2: $\boldsymbol{x}$ and $\boldsymbol{z'}$ shown in the lift, $\boldsymbol{x}$ with black dots and $\boldsymbol{z'}$ with hollow squares.

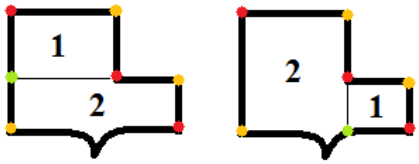

Figure 5.17: Subcase 2: Decomposing the domain τ in two different ways. The red dots represent $\boldsymbol{x}$ and the yellow dots represent $\boldsymbol{z'}$. The green dot represents a point $\boldsymbol{y}$ in $S(H_1)$.

Using cut lines, we show the decomposition of τ: both ways we use the rectangle first and then we use the pentagon (see Figures 5.18, 5.19, 5.20, 5.21). There are exactly two different ways to decompose τ, hence $N(\tau) = 2$.

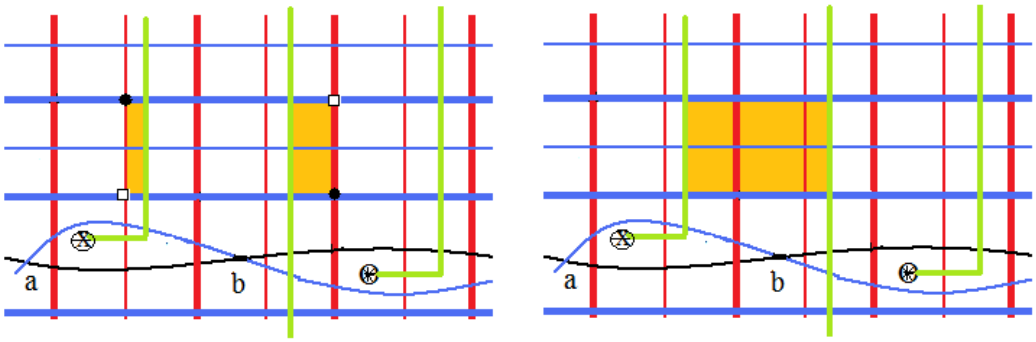

Figure 5.18: Subcase 2: Using rectangle to go from $\boldsymbol{x}$ to $\boldsymbol{y}$ in the lift. Here $\boldsymbol{x}$ is denoted by black dots and $\boldsymbol{y}$ with hollow squares.

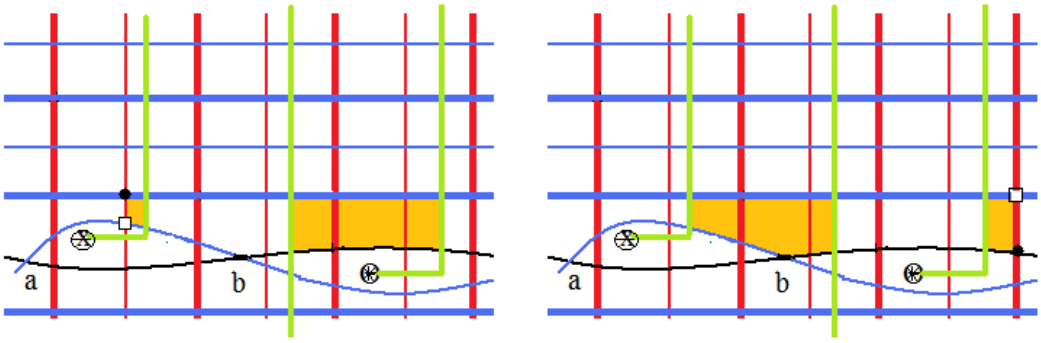

Figure 5.19: Subcase 2: Using pentagon to go from $\boldsymbol{y}$ to $\boldsymbol{z'}$ in the lift. Here $\boldsymbol{y}$ is denoted with black dots and $\boldsymbol{z'}$ with hollow squares.

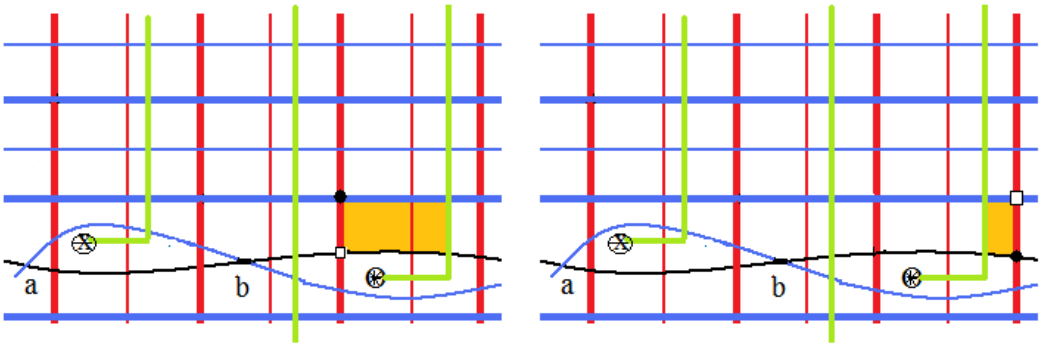

Figure 5.20: Second way of decomposing: Using rectangle to go from $\boldsymbol{x}$ to $\boldsymbol{y}$ in the lift. Here $\boldsymbol{x}$ is denoted by black dots and $\boldsymbol{y}$ with hollow squares.

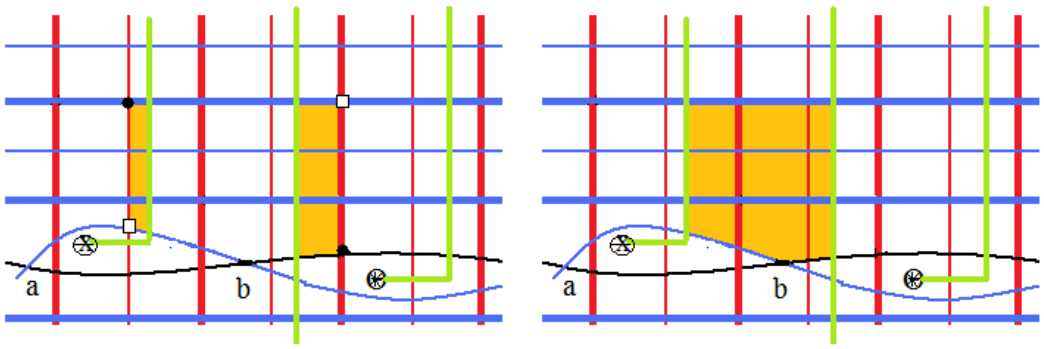

Figure 5.21: Second way of decomposing: Using pentagon to go from $\boldsymbol{y}$ to $\boldsymbol{z'}$ in the lift. Here $\boldsymbol{y}$ is denoted with black dots and $\boldsymbol{z'}$ with hollow squares.

Subcase 3: Here τ as in the bottom right figure in case 2 in Figure 5.8. It looks like the picture as shown in Figure 5.22. We give a schematic diagram for decomposition of τ (Figure 5.23).

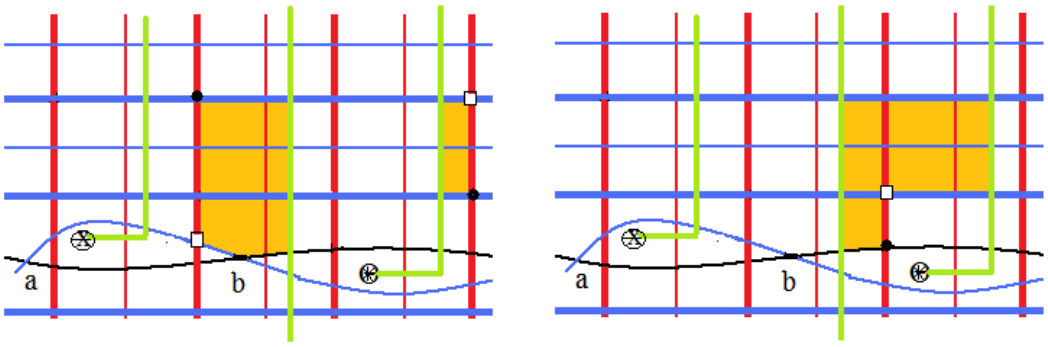

Figure 5.22: Subcase 3: $\boldsymbol{x}$ and $\boldsymbol{z'}$ shown in the lift, $\boldsymbol{x}$ with black dots and $\boldsymbol{z'}$ with hollow squares.

Using cut lines, we show the decomposition of τ in two different ways: in the first way, we decompose ψ into pentagon first (Figure 5.24) and then the rectangle (Figure 5.25). In the second way, we decompose ψ into a rectangle first (Figure 5.26) and then into a pentagon (Figure 5.27). There are exactly two different ways to decompose τ. Hence, $N(\tau) = 2$.

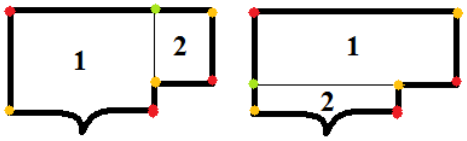

Figure 5.23: Subcase 3: Decomposing the domain τ in two different ways. The red dots represent $\boldsymbol{x}$ and the yellow dots represent $\boldsymbol{z'}$. The green dot represents a point $\boldsymbol{y'}$ in $S(H_2)$ in the first figure, and a point $\boldsymbol{y}$ in $S(H_1)$ in the second figure.

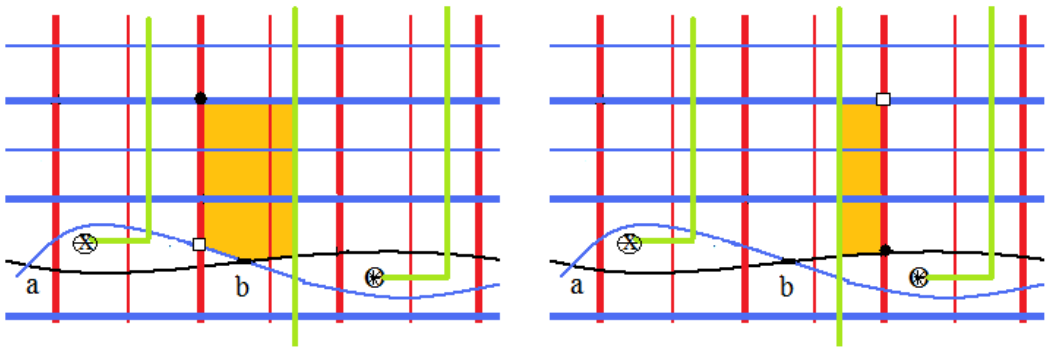

Figure 5.24: Subcase 3: Using pentagon to go from $\boldsymbol{x}$ to $\boldsymbol{y'}$ in the lift. Here $\boldsymbol{x}$ is denoted by black dots and $\boldsymbol{y'}$ with hollow squares.

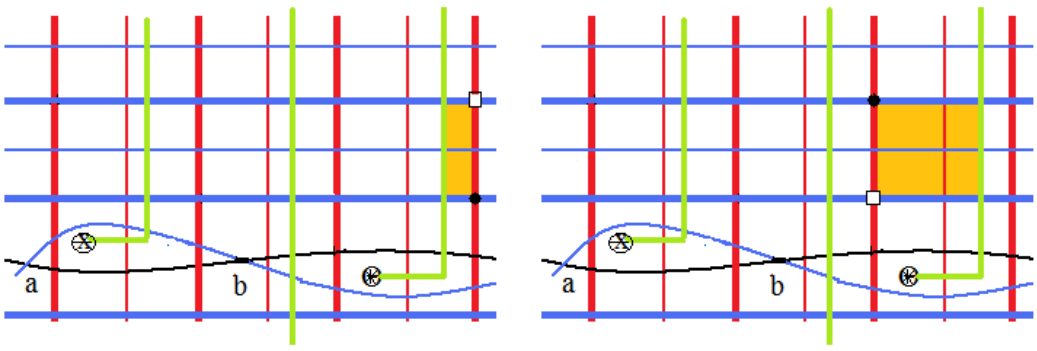

Figure 5.25: Subcase 3: Using rectangle to go from $\boldsymbol{y'}$ to $\boldsymbol{z'}$ in the lift. Here $\boldsymbol{y'}$ is denoted with black dots and $\boldsymbol{z'}$ with hollow squares.

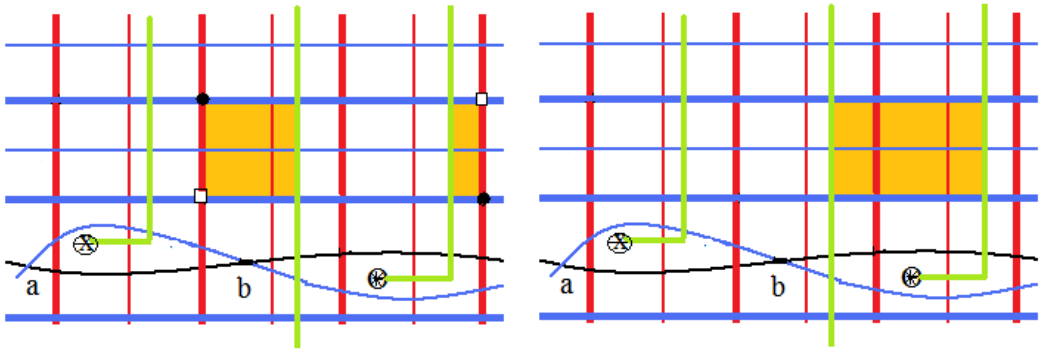

Figure 5.26: Subcase 3: Second way of decomposing: Using rectangle to go from $\boldsymbol{x}$ to $\boldsymbol{y}$ in the lift. Here $\boldsymbol{x}$ is denoted by black dots and $\boldsymbol{y}$ with hollow squares.

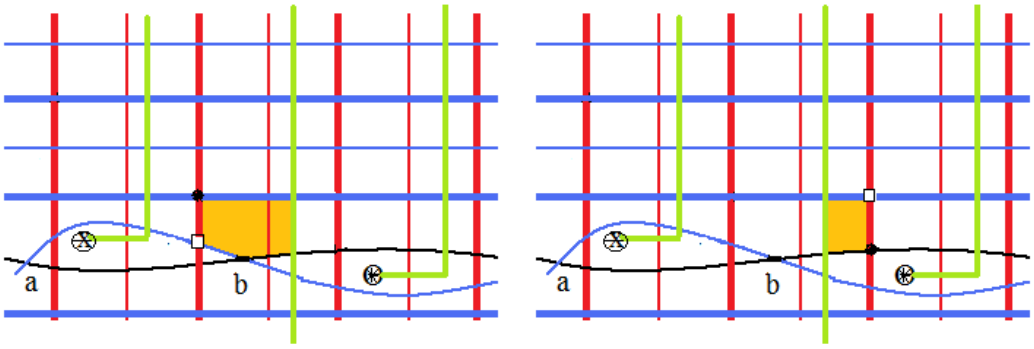

Figure 5.27: Subcase 3: Second way of decomposing: Using pentagon to go from $\boldsymbol{y}$ to $\boldsymbol{z'}$ in the lift. Here $\boldsymbol{y}$ is denoted with black dots and $\boldsymbol{z}$ with hollow squares.

Case 3: $\boldsymbol{x} - (\boldsymbol{x} \cap \boldsymbol{z'})$ contains exactly one point. Figure 5.28 shows one such domain. Schematically, the domain looks like case 3 in Figure 5.8.

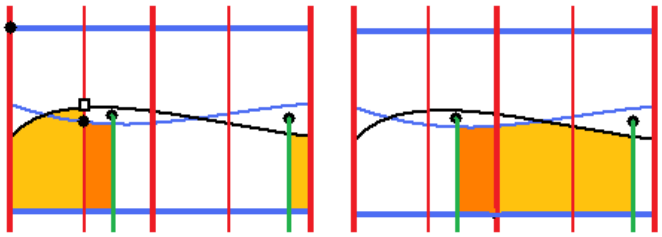

Figure 5.28: Case 3: Using rectangle and pentagon to go from $\boldsymbol{x}$ to $\boldsymbol{z'}$ in the lift. Here $\boldsymbol{x}$ is denoted with black dots and $\boldsymbol{z'}$ with hollow squares.

We show that for each generator $\boldsymbol{x} \in S(H_1)$, there are exactly two domains τ_1 and τ_2 that connect $\boldsymbol{x}$ to $\boldsymbol{z'}$ such that $\boldsymbol{x} - (\boldsymbol{x} \cap \boldsymbol{z'})$ contains exactly one point.

In the lower half of the intersections of β_{i_0} and γ_{i_0}, the domain τ_1 has a unique decomposition as a "thin" rectangle and a pentagon (Figures 5.28, 5.29, 5.30). By thin we mean that the domain will be in between the old curves $\beta^{\pm}_{i_0-1}$ and $\beta^{\pm}_{i_0+1}$, where β_{i_0} is replaced by γ_{i_0}. If there is a domain starting in the positive region, which decomposes as a rectangle followed by a pentagon (or the other way round) and there is no 270° corner, then it has to wrap around as there is already a coordinate of $\boldsymbol{x}$ in the bottom curve $\beta^{+}_{i_0+1}$. Since there are basepoints in the annulus below the old curve β_{i_0+1}, we cannot find an empty annular domain free from basepoints below β_{i_0+1}.

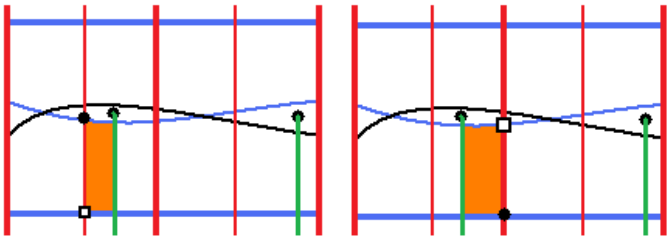

Figure 5.29: Case 3: Using rectangle to go from $\boldsymbol{x}$ to $\boldsymbol{y}$ in the lift. Here $\boldsymbol{x}$ is denoted with black dots and $\boldsymbol{y}$ with hollow squares.

In addition, we have a domain τ_2 in the upper half of the intersection of β_{i_0} and γ_{i_0}, which has a unique decomposition as a rectangle and a pentagon (Figure 5.31, Figure 5.32, Figure 5.33).

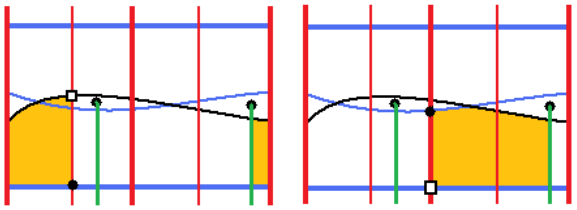

Figure 5.30: Case 3: Using pentagon to go from $\boldsymbol{y}$ to $\boldsymbol{z'}$ in the lift. Here $\boldsymbol{y}$ is denoted with black dots and $\boldsymbol{z'}$ with hollow squares.

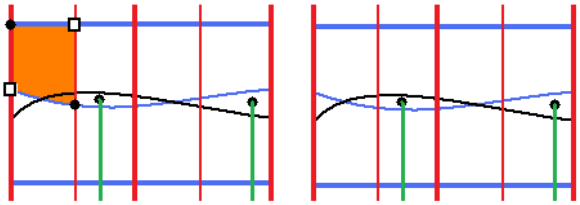

Figure 5.31: Case 3: Another way of using rectangle to go from $\boldsymbol{x}$ to $\boldsymbol{y}$ in the lift. Here $\boldsymbol{x}$ is denoted with black dots and $\boldsymbol{y}$ with hollow squares.

Another way to decompose the domain τ_1 and τ_2, is to decompose the domain first to a pentagon and then to a rectangle (Figure 5.34, Figure 5.35, Figure 5.36, Figure 5.37). The decomposition having pentagon or rectangle first depends on where the point of $\boldsymbol{x}$ is on the bottom β_{i_0+1} curve for τ_1 and on the top β_{i_0-1} curve for τ_2.

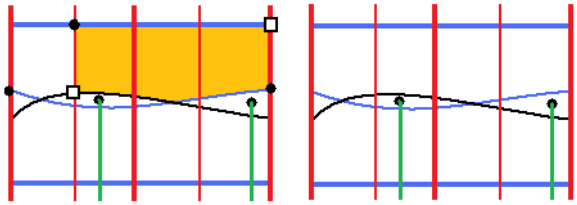

Figure 5.32: Case 3: Another way of using pentagon to go from $\boldsymbol{y}$ to $\boldsymbol{z'}$ in the lift. Here $\boldsymbol{y}$ is denoted with black dots and $\boldsymbol{z'}$ with hollow squares.

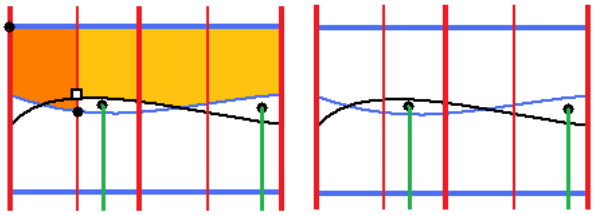

Figure 5.33: Case 3: Another way of using rectangle and pentagon to go from $\boldsymbol{x}$ to $\boldsymbol{z'}$ in the lift. Here $\boldsymbol{x}$ is denoted with black dots and $\boldsymbol{z'}$ with hollow squares.

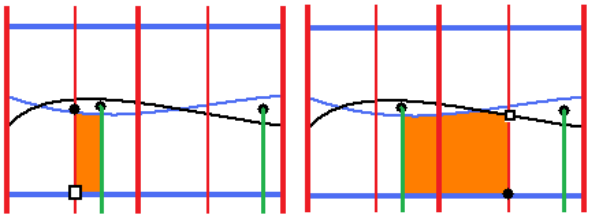

Figure 5.34: Case 3: Another way of using pentagon to go from $\boldsymbol{x}$ to $\boldsymbol{y'}$ in the lift. Here $\boldsymbol{x}$ is denoted with black dots and $\boldsymbol{y'}$ with hollow squares.

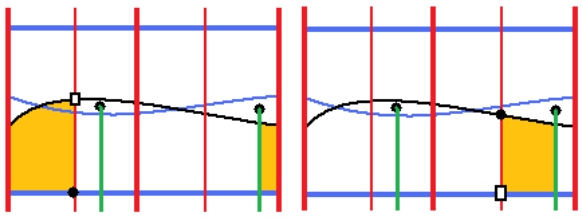

Figure 5.35: Case 3: Another way of using rectangle to go from $\boldsymbol{y'}$ to $\boldsymbol{z'}$ in the lift. Here $\boldsymbol{y'}$ is denoted with black dots and $\boldsymbol{z'}$ with hollow squares.

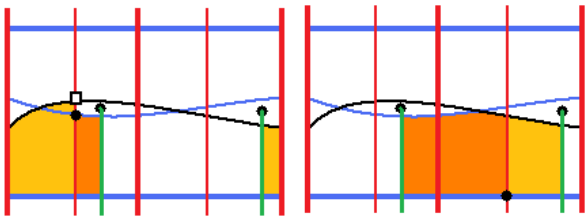

Figure 5.36: Case 3: Both pentagon and rectangle in the lift.

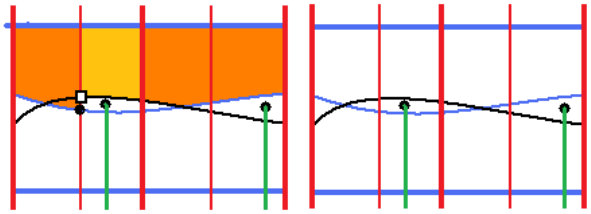

Figure 5.37: Case 3: Both pentagon and rectangle in the lift in the upper half of the intersection.

Hence for each generator $\boldsymbol{x} \in S(H_1)$, there are exactly two domains τ_1 and τ_2 that contribute to $\boldsymbol{z'}$ so that the mod two count for $\boldsymbol{z'}$ in the sum is zero.

Therefore, in all the cases, $(\partial^-_{\mathbb{X}} \circ \phi_2 + \phi_2 \circ \partial^-_{\mathbb{X}})\boldsymbol{x} = 0$. □

ϕ_2 preserves the relative grading since ϕ_2 is a chain map. Next, we want to show that $\phi_2' \circ \phi_2$ is homotopic to the identity map on $EGC(H_1)$. For that, we introduce hexagon counting map that appeared in [14].

Definition 5.2.2. *(Embedded hexagon [14]) Let $\boldsymbol{x}, \boldsymbol{y} \in S(H_1)$. An embedded hexagon h (Figure 5.38) in $H_{1,2}$ with boundary in $\boldsymbol{\alpha} \cup \boldsymbol{\beta} \cup \gamma_{i_0}$ is a hexagon from $\boldsymbol{x}$ to $\boldsymbol{y}$ if $\partial((\partial h) \cap \boldsymbol{\alpha}) = \boldsymbol{y} - \boldsymbol{x}$.*

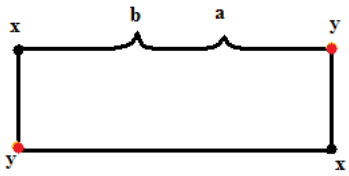

Figure 5.38: An hexagon connecting $\boldsymbol{x}$ and $\boldsymbol{y}$.

An hexagon in $H_{1,2}$ lifts to an hexagon from $\boldsymbol{x}$ to $\boldsymbol{y}$ in the double cover $\widetilde{H_{1,2}}$ such that $\boldsymbol{x}, \boldsymbol{y}$ have exactly (3n-2) coordinates in common. We denote the set of hexagons from $\boldsymbol{x}$ to $\boldsymbol{y}$ by $hex(\boldsymbol{x}, \boldsymbol{y})$.

The hexagon $h \in hex(\boldsymbol{x}, \boldsymbol{y})$ is empty if h does not contain any point of $\boldsymbol{x}$ and $\boldsymbol{y}$ in its interior (respectively boundary) and does not contain any basepoint in its interior. The set of empty hexagons from $\boldsymbol{x}$ to $\boldsymbol{y}$ is denoted by $hex^{\circ}(\boldsymbol{x}, \boldsymbol{y})$.

The conditions for the hexagon in the extended grid is similar to the conditions for the pentagon. We define a map $H : EGC(H_1) \longrightarrow EGC(H_1)$ by

$$H(\boldsymbol{x}) = \sum_{\boldsymbol{y} \in S(H_1)} \sum_{h \in hex^{\circ}(\boldsymbol{x}, \boldsymbol{y})} \boldsymbol{y}$$

We define analogously a map $H' : EGC(H_2) \longrightarrow EGC(H_2)$ by counting suitable hexagons from $\widetilde{H_2}$ to itself,

$$H'(\boldsymbol{x'}) = \sum_{\boldsymbol{y'} \in S(H_2)} \sum_{h' \in hex^{\circ}(\boldsymbol{x'}, \boldsymbol{y'})} \boldsymbol{y'}$$

The map H maps generators to generators as the conditions for the hexagon is compatible with the conditions for the generator.

Lemma 5.2.2. *The map $H : EGC(H_1) \longrightarrow EGC(H_1)$ is a chain homotopy between the identity map on $EGC(H_1)$ and the composite map $\phi_2' \circ \phi_2$.*

Proof. The idea of the proof is similar to Lemma 5.1.7 in [14]. We will show that

$$\partial \circ H + H \circ \partial = Id + \phi_2' \circ \phi_2$$

Now,

$$\partial \circ H(\boldsymbol{x}) = \sum_{\boldsymbol{y} \in S(H_1)} \sum_{h \in hex^{\circ}(\boldsymbol{x}, \boldsymbol{y})} \sum_{\boldsymbol{z} \in S(H_1)} \sum_{rect^{o}(\boldsymbol{y}, \boldsymbol{z})} \boldsymbol{z}$$

$$H \circ \partial(\boldsymbol{x}) = \sum_{\boldsymbol{y} \in S(H_1)} \sum_{rect^{o}(\boldsymbol{x}, \boldsymbol{y})} \sum_{\boldsymbol{z} \in S(H_1)} \sum_{h \in hex^{\circ}(\boldsymbol{y}, \boldsymbol{z})} \boldsymbol{z}$$

$$\phi_2' \circ \phi_2(\boldsymbol{x}) = \sum_{\boldsymbol{y'} \in S(H_2)} \sum_{pent_b^{\circ}(\boldsymbol{x}, \boldsymbol{y'})} \sum_{\boldsymbol{z} \in S(H_1)} \sum_{h \in pent_a^{\circ}(\boldsymbol{y'}, \boldsymbol{z})} \boldsymbol{z}$$

By combining all the terms, we can write

$$(\partial \circ H + H \circ \partial + \phi_2' \circ \phi_2)(\boldsymbol{x}) = \sum_{\boldsymbol{z} \in S(H_1)} \sum_{\{\psi \in \pi(\boldsymbol{x}, \boldsymbol{z}) | \boldsymbol{z} \cap Int(\psi) = \emptyset, \boldsymbol{z} \cap \mathbb{X} = \boldsymbol{z} \cap \mathbb{O} = \emptyset\}} N(\psi).\boldsymbol{z} \qquad (5.2)$$

where $N(\psi)$ denote the number of ways to decompose domain ψ. The analysis needed here relies on understanding how rectangles and hexagons interact with each other and also, on how pentagons interact with each other. One can decompose ψ in three different ways: first decompose ψ in to an empty rectangle r and then to an empty hexagon h, we denote this decomposition as $r * h$; first decompose ψ in to an empty hexagon h and then to an empty rectangle r, we denote this decomposition as $h * r$; first decompose ψ in to an empty pentagon p from $\widetilde{H_1}$ to $\widetilde{H_2}$ and then to an empty pentagon p' from $\widetilde{H_2}$ to $\widetilde{H_1}$, we denote this decomposition as $p * p'$ (for H', we do $p^{'} * p$). If a hexagon or a rectangle cross cut lines, the cut lines cross the top and the bottom the same number of times as hexagons and rectangles do not contain any basepoints.

We have at most 4 points where $\boldsymbol{x}$ and $\boldsymbol{z}$ differ since a rectangle switches two points and an hexagon switches two points. Here $\boldsymbol{x} - (\boldsymbol{x} \cap \boldsymbol{z})$ contains four, three or no points. We note that $\boldsymbol{x} - (\boldsymbol{x} \cap \boldsymbol{z})$ cannot contain two points as it would happen only if two of the $\boldsymbol{x}$ components that differ from the $\boldsymbol{z}$ components are on the same curve β_{i_0}. Also, $\boldsymbol{x} - (\boldsymbol{x} \cap \boldsymbol{z})$ cannot contain one point as hexagons (or rectangles) switch two points, where one of the point that is in the β_{i_0} is replaced by another point on β_{i_0}. We consider 3 cases for $\psi \in \pi(\boldsymbol{x}, \boldsymbol{y})$:

Case 1: $\boldsymbol{x} - (\boldsymbol{x} \cap \boldsymbol{z})$ contains exactly 4 points. In this case, the region consists of a disjoint union of a rectangle and a hexagon. There are exactly two decompositions for ψ, either $r * h$ or $h * r$ (Figure 5.39). Hence $N(\psi) = 2$.

Case 2: $\boldsymbol{x} - (\boldsymbol{x} \cap \boldsymbol{z})$ contains exactly 3 points. In this case, ψ has eight corners. Out of eight, seven corners are 90° and one is 270°. We will consider three different cases for how the domains ψ would look like, others are mirror images of these three (Figure 5.40).

Subcase 1: ψ looks as in Figure 5.41. The 270° corner can be decomposed in two different ways. The first way is to decompose ψ into a rectangle and then to an hexagon (Figure 5.42) or to decompose ψ into an hexagon and then to a rectangle (Figure 5.43). There are exactly two ways to decompose ψ. Hence, $N(\psi) = 2$.

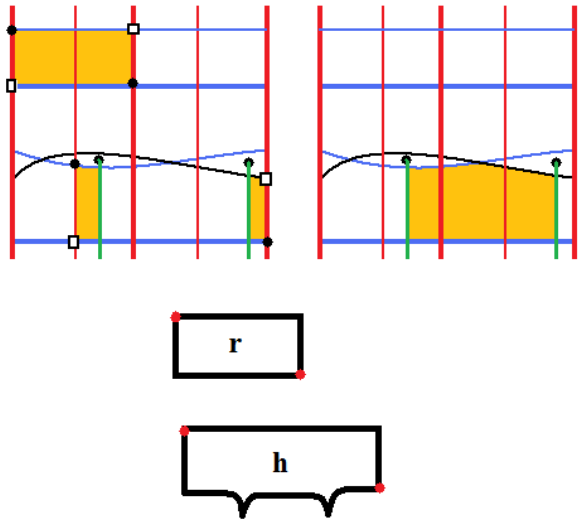

Figure 5.39: Case 1: A disjoint rectangle and an hexagon in the lift. The bottom figure shows a schematic diagram for the decomposition of ϕ.

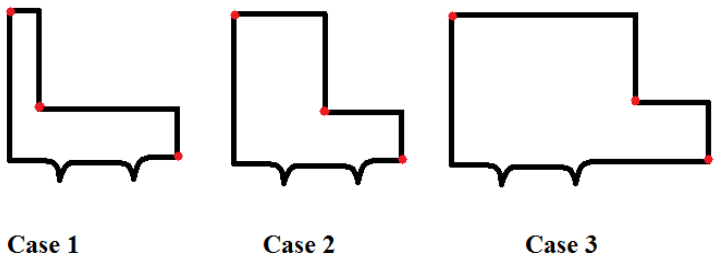

Figure 5.40: Schematic diagram for the possible domains for ϕ.

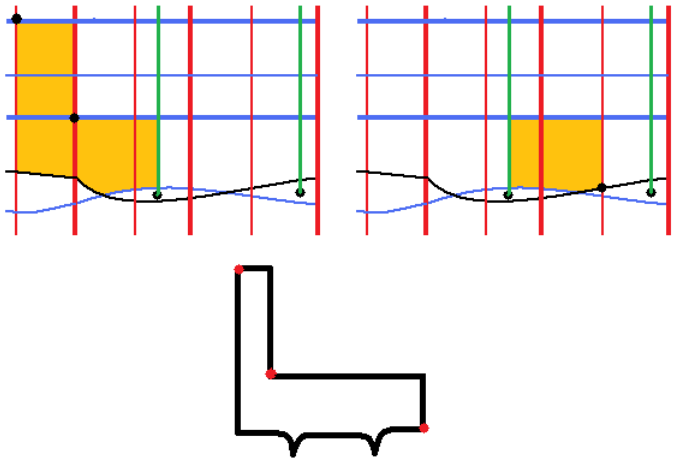

Figure 5.41: Subcase 1: Domain in the lift.

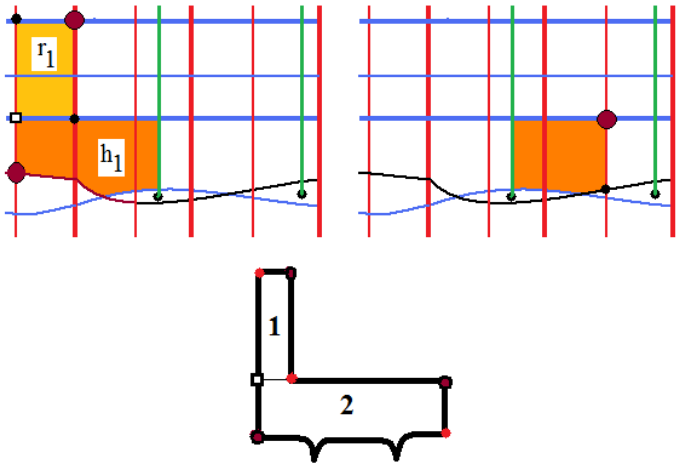

Figure 5.42: Subcase 1: Decomposing the domain into first a rectangle and then a hexagon in the lift.

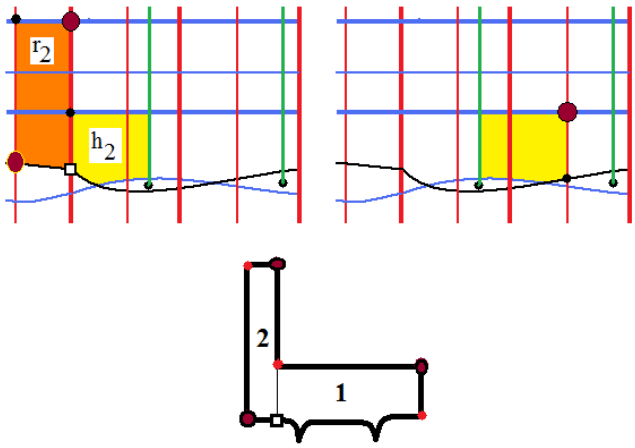

Figure 5.43: Subcase 1: Decomposing the domain first into a hexagon and then to a rectangle in the lift.

Subcase 2: ψ looks as in Figure 5.44. ψ can be decomposed in two different ways. We can decompose ψ as a rectangle and an hexagon (Figure 5.45) or as two pentagons P_1 and P_2' in $\widetilde{H_{1,2}}$ (Figure 5.46). Thus, $N(\psi) = 2$.

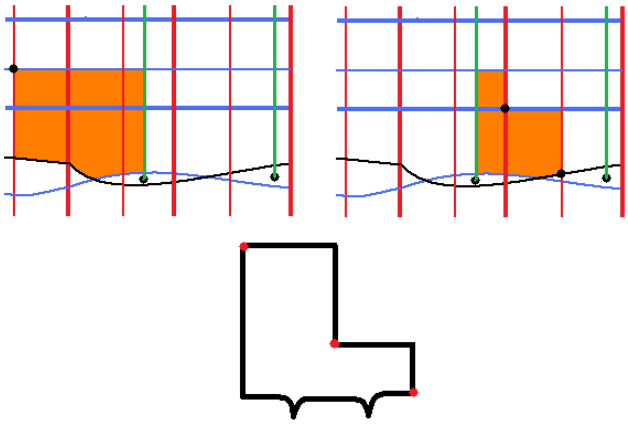

Figure 5.44: Subcase 2: Domain in the lift.

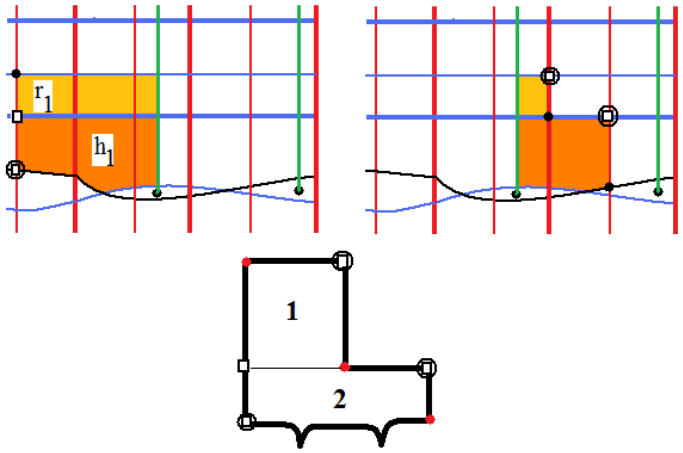

Figure 5.45: Subcase 2: Decomposing the domain first into a rectangle and then to an hexagon in the lift.

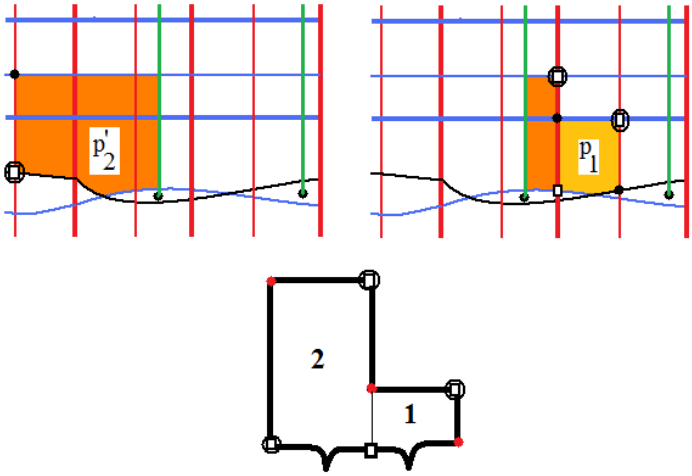

Figure 5.46: Subcase 2: Decomposing the domain into two pentagons.

Subcase 3: ψ looks as in Figure 5.47. We can decompose ψ as a rectangle and an hexagon in two different ways (Figure 5.48, Figure 5.49). Thus, $N(\psi) = 2$.

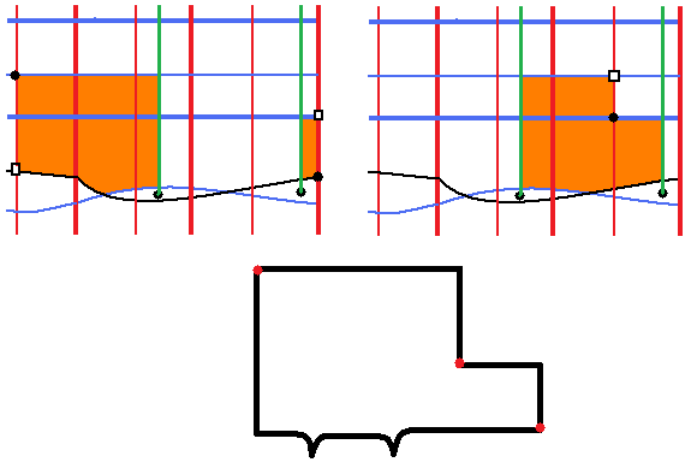

Figure 5.47: Subcase 3: Domain in the lift.

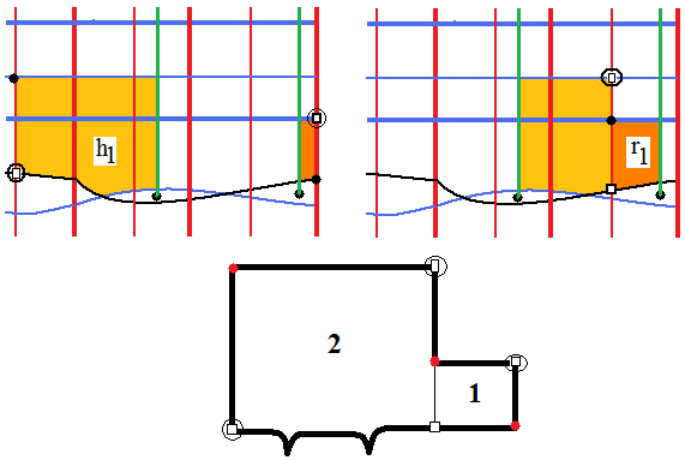

Figure 5.48: Subcase 3: Decomposing the domain first into a rectangle and then to an hexagon.

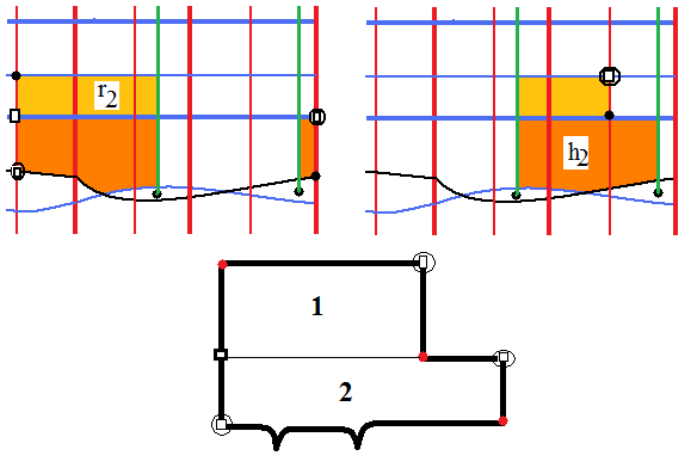

Figure 5.49: Subcase 3: Decomposing the domain first into a rectangle and then to an hexagon in the lift.

Case 3: $\boldsymbol{x} - (\boldsymbol{x} \cap \boldsymbol{z'})$ contains no points. Depending on the initial generator $\boldsymbol{x}$, there is a unique region next to β_{i_0} and γ_{i_0}. This region has a unique decomposition as a juxtaposition of a rectangle with a hexagon or two pentagons (Figure 5.50, Figure 5.51, Figure 5.52, Figure 5.53, Figure 5.54, Figure 5.55). ψ could be any one of these decompositions, it depends on the position of the point of $\boldsymbol{x}$ that is on the old curve. Hence, $N(\psi) = 1$ and this case contributes to the identity map. We note here that this case is different from the case 3 of lemma 5.2.1 as there is no basepoint free domain in the other half.

All these cases, verifies the identity $\partial \circ H + H \circ \partial = Id + \phi_2' \circ \phi_2$. □

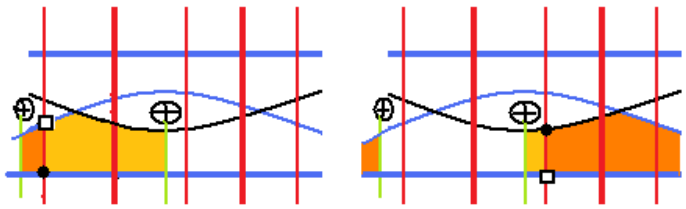

Figure 5.50: Case 3: Juxtaposition of two pentagons.

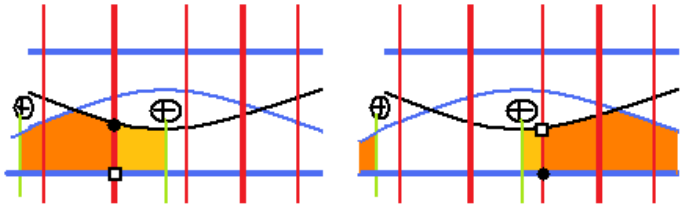

Figure 5.51: Case 3: Juxtaposition of a rectangle and an hexagon. The initial coordinates of the generators are marked with black dots.

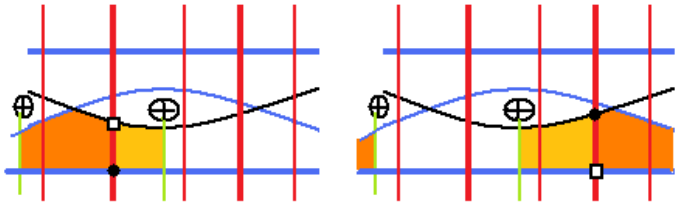

Figure 5.52: Case 3: Juxtaposition of an hexagon and a rectangle. The initial coordinates of the generators are marked with black dots.

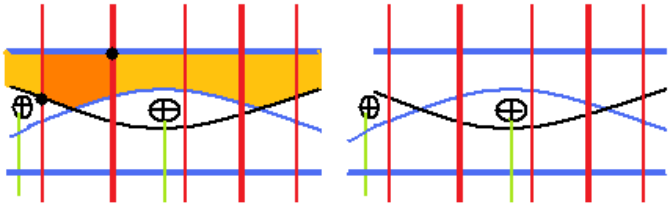

Figure 5.53: Case 3: Juxtaposition of two pentagons. The lighter shade is the first pentagon and the darker shade is the second pentagon.

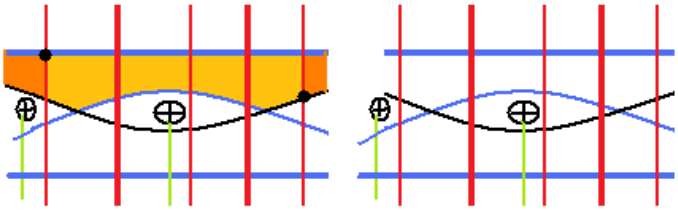

Figure 5.54: Case 3: Juxtaposition of an hexagon and a rectangle. The lighter shade denotes the first in the decomposition.

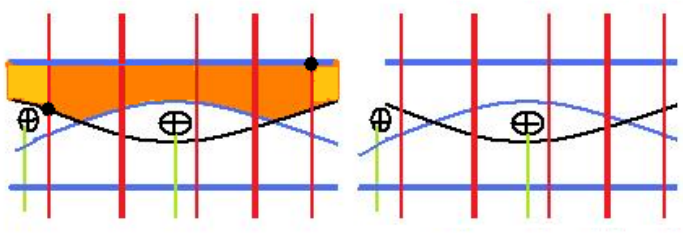

Figure 5.55: Case 3: Juxtaposition of a rectangle and an hexagon. The lighter shade denotes the first in the decomposition.

Proof of proposition 5.2.1. The map $\phi_2 : EGC(H_1) \longrightarrow EGC(H_2)$ is a chain map and applying the previous lemma to $\phi_2' \circ \phi_2$ and H; $\phi_2 \circ \phi_2'$ and H', we have a chain homotopy equivalence. A chain homotopy equivalence induces an isomorphism on homology, hence $EGH(H_1) \cong EGH(H_2)$.

Theorem 5.2.1. *If H_1 and H_2 are the extended grid diagrams of a link L in S^3 branched along L, where H_2 differs from H_1 by the choice of the new β-curves, then there is an isomorphism between $EGH(H_1)$ and $EGH(H_2)$.*

Proof. We apply proposition 5.2.1 repeatedly to switch, one at a time, to all new β curves. □

Similarly, we can show that EGH is independent of the choice of the new $\boldsymbol{\alpha}$-curves. We will define the pentagon counting maps in the same way as before. Figure 5.56 shows the pentagons.

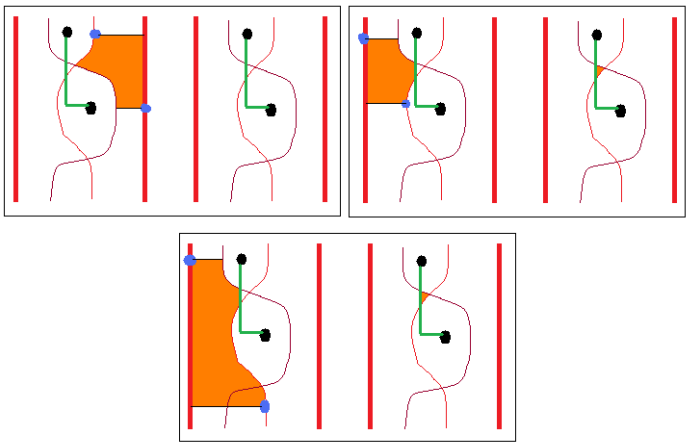

Figure 5.56: Possible pentagons.

Theorem 5.2.2. *If H_1 and H_2 are the extended grid diagrams of a link L in S^3 branched along L, where H_2 differs from H_1 by the choice of the new α-curves, then there is an isomorphism between $EGH(H_1)$ and $EGH(H_2)$.*

Proof. The proof is similar to the proof of Theorem 5.2.1. □

5.3 Invariance of EGH under Cyclic Permutation

Let G_1 be an extended grid diagram for a link $L \subset S^3$ and $\widetilde{G_1}$ be a lift of G_1. Let G_2 be obtained from G_1 by cyclically permuting two consecutive rows of the extended grid diagram corresponding to L, such that the i-th row becomes $(i-2)$ mod $2n$-th row. Note that this corresponds to a one-step cyclic pemutation of the original grid. Then we have,

Theorem 5.3.1. *If G_1 and G_2 are extended grid diagrams of a link L in S^3, where G_2 is obtained from G_1 by a cyclic permutation moving two consecutive rows from top to bottom, then there is an isomorphism between $EGH(G_1)$ and $EGH(G_2)$.*

To prove Theorem 5.3.1, we define a map $\phi_3 : EGC(G_1) \longrightarrow EGC(G_2)$ by

$$\phi_3(\{x_{ij}^k\}) = \{x_{tj}^l\}$$

where $t = i - 2 \pmod{2n}$, $l = k + N_{i,j}^1 - N_{t,j}^2 \pmod 2$ and $N_{i,j}^1 =$ # intersection points of β_i with the cut lines that lie between $\alpha_0 \cap \beta_i$ and $\alpha_j \cap \beta_i$ in G_1, $N_{t,j}^2 =$ # intersection points of β_t with the cut lines that lie between $\alpha_0 \cap \beta_t$ and $\alpha_j \cap \beta_t$ in G_2, and for generators x_{ij}^k we refer to remark 4.2.1.

The leftmost figure in Figure 5.57 shows a generator in the extended grid diagram for the Hopf link and the rightmost figure shows its image under the map ϕ_3.

Lemma 5.3.1. *ϕ_3 maps generators to generators.*

Proof. We need to check all the conditions for generators. It is clear from the definition of ϕ_3 that $\phi_3(\{x_{ij}^k\})$ has 3n-tuples of entries with each old curve (both $\boldsymbol{\alpha}$ and $\boldsymbol{\beta}$) containing two entries and the new curves (both $\boldsymbol{\alpha}$ and $\boldsymbol{\beta}$) containing exactly one entry. Also, for the coordinates of $\boldsymbol{x}$ for which the exponent is both 0 and 1, ϕ_3 will retain the exponents 0 and 1 for the corresponding entry.

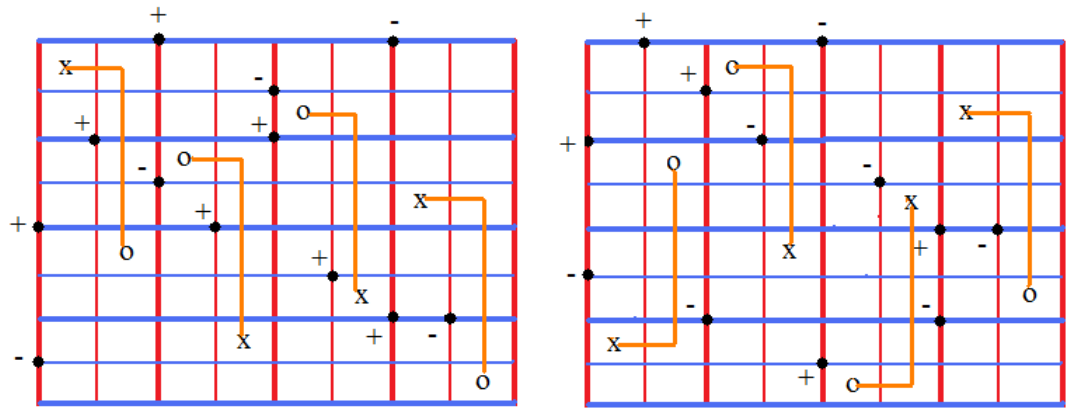

Figure 5.57: A generator in the extended grid diagram for the Hopf link and its image under the map ϕ_3.

We check here that the condition "if there are two entries on an old $\boldsymbol{\alpha}$ curve in G_2, then they must have opposite signs" is satisfied for the image of ϕ_3. Let x_{tj} and x_{dj} be two entries on α_j in G_2 such that their corresponding preimages in G_1 are x_{ij} and x_{pj} respectively, with l_1 and l_2 exponents of x_{tj} and x_{dj}, and k_1 and k_2 exponents of x_{ij} and x_{pj} respectively. We assume that k_1 and k_2 are different, i.e $k_2 = k_1 + 1 \pmod 2$. From the definition of ϕ_3, we have $l_1 = k_1 + N^1_{i,j} - N^2_{t,j} \pmod 2$, $l_2 = k_2 + N^1_{p,j} - N^2_{d,j} \pmod 2$.

Lemma 5.3.2 below gives us that $N^1_{i,j} - N^1_{p,j} = N^2_{t,j} - N^2_{d,j} \pmod 2$. Therefore, $l_2 = k_2 + N^1_{p,j} - N^2_{d,j} = k_1 + 1 + N^1_{p,j} - N^2_{d,j} = k_1 + 1 + N^1_{i,j} - N^2_{t,j} \pmod 2 = l_1 + 1 \pmod 2$. This shows that any two entries on an old $\boldsymbol{\alpha}$-curve in the image set of ϕ_3 have opposite signs.

We check that if there are two entries of a generator on an old $\boldsymbol{\beta}$ curve in G_2, then the exponents are compatible with the condition that is required for them to be in generator. Let $x^{p_1}_{ij}$ and $x^{p_2}_{is}$ be two points on β_i in G_1 and $x^{q_1}_{tj}$ and $x^{q_2}_{ts}$ respectively, be their corresponding images on β_t in G_2. Then if the exponents of these grid points are l_1 and l_2 for x_{tj} and x_{dj}, and k_1 and k_2 for x_{ij} and x_{pj} respectively, the relationship between the exponents $q_1 = p_1 + N^1_{i,j} - N^2_{t,j} \pmod 2$, $q_2 = p_2 + N^1_{i,s} - N^2_{t,s} \pmod 2$, and $p_2 = p_1 + N^1_{i,s} - N^1_{i,j} + 1 \pmod 2$.

Therefore, $q_2 = p_2 + N^1_{i,s} - N^2_{t,s} \pmod 2 = p_1 + N^1_{i,s} - N^1_{i,j} + 1 + N^1_{i,s} - N^2_{t,s} \pmod 2 = p_1 - N^1_{i,j} + 1 - N^2_{t,s} \pmod 2 = p_1 + N^1_{i,j} + 1 + N^2_{t,s} \pmod 2 = p_1 + N^1_{i,j} + 1 + N^2_{t,s} - N^2_{tj} - N^2_{tj} \pmod 2 = p_1 + N^1_{i,j} - N^2_{tj} + 1 + N^2_{t,s} - N^2_{tj} \pmod 2 = q_1 + 1 + N^2_{t,s} - N^2_{tj} \pmod 2$. This shows that the exponents of any pair of entries on an old β-curve in the image set are compatible with the conditions of the generators.

Hence, this shows that ϕ_3 maps generators to generators. □

Lemma 5.3.2. *Let $x^{l_1}_{tj}$ and $x^{l_2}_{dj}$ be two entries on α_j in G_2 such that their corresponding preimages in G_1 are $x^{k_1}_{ij}$ and $x^{k_2}_{pj}$ respectively, then*

$$N^1_{i,j} - N^1_{p,j} = N^2_{t,j} - N^2_{d,j} \text{ (mod 2)}$$

Proof. Assume that there is only one cut line to the left of α_j in G_1. We consider three cases:

Case 1: If there is a cut line to the left of both $x_{i,j}$ and $x_{p,j}$, then a cyclic permutation of the rows either leaves the cut line unchanged or it moves the cut line to the other side of the torus. In the former case, both $x_{t,j}$ and $x_{d,j}$ will have a cut line on the left; in the latter case, neither $x_{t,j}$ nor $x_{d,j}$ will have a cut line on the left. Hence the differences $N^1_{i,j} - N^1_{p,j}$ and $N^2_{t,j} - N^2_{d,j}$ are equal mod 2.

Case 2: If there is a cut line only to the left of $x_{i,j}$ and no cut line to the left of $x_{p,j}$, then a cyclic permutation of the rows either leaves the cut line unchanged or it moves the cut line to the other side of the torus. In the former case, $x_{t,j}$ will have a cut line on the left; in the latter case, $x_{d,j}$ will have a cut line on the left. Hence the differences $N^1_{i,j} - N^1_{p,j}$ and $N^2_{t,j} - N^2_{d,j}$ are equal mod 2.

Case 3: If there is no cut line to the left of both $x_{i,j}$ and $x_{p,j}$, then a cyclic permutation of the rows either leaves the cut line unchanged or it moves the cut line to the other side of the torus. In the former case, neither $x_{t,j}$ nor $x_{d,j}$ will have a cut line on the left; in the latter case, both $x_{t,j}$ and $x_{d,j}$ will have a cut line on the left. Hence the differences $N^1_{i,j} - N^1_{p,j}$ and $N^2_{t,j} - N^2_{d,j}$ are equal mod 2. □

Lemma 5.3.3. *The map $\phi_3 : EGC(G_1) \longrightarrow EGC(G_2)$ is a chain map.*

Proof. We need to show ϕ_3 commutes with the boundary map ∂. Recalling the rules for the rectangles, it is clear that the sign of the exponents are compatible under the map ϕ_3. Geometrically, we can see that the composite map $\phi_3 \circ \partial$ moves rectangles two rows up within the same columns in the extended grid diagram (Figure 5.58). □

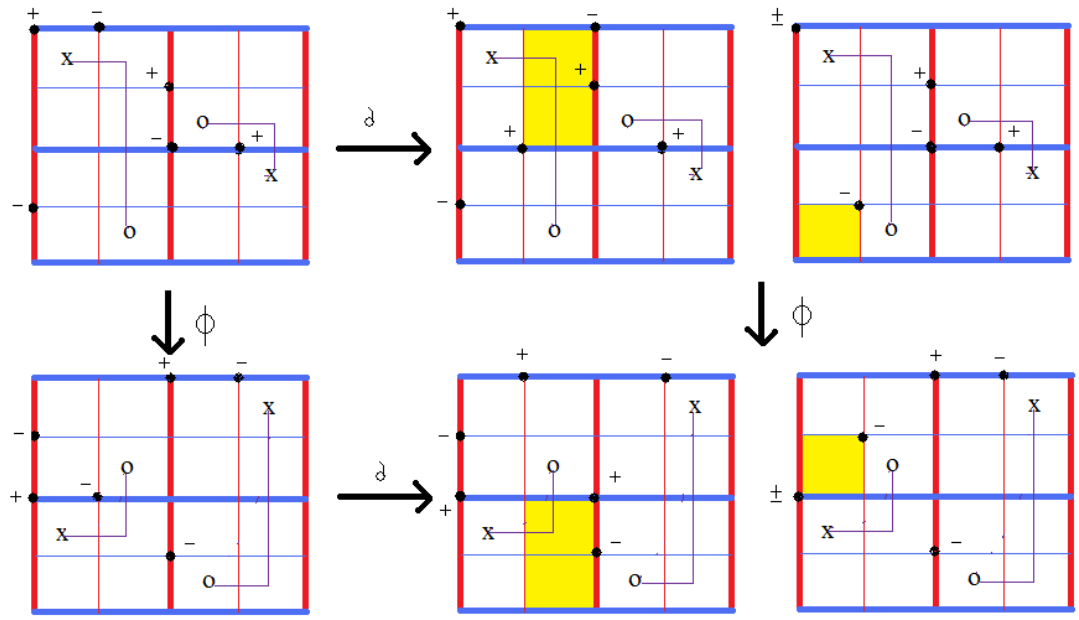

Figure 5.58: Picture showing how rectangles are moved using the map ϕ_3.

Similarly, we define an inverse map $\phi_3' : EGC(G_2) \longrightarrow EGC(G_1)$ by

$$\phi_3'(\{x_{ij}^k\}) = \{x_{tj}^l\}$$

where $t = i - 2 \pmod{2n}$, $l = k + N_{i,j}^1 - N_{t,j}^2 \pmod 2$ and $N_{i,j}^1$= # intersection points of β_i with the cut lines that lie between $\alpha_0 \cap \beta_i$ and $\alpha_j \cap \beta_i$ in G_1, and $N_{t,j}^2$ = # intersection points of β_t with the cut lines that lie between $\alpha_0 \cap \beta_t$ and $\alpha_j \cap \beta_t$ in G_2.

Proof of Theorem 5.3.1. ϕ_3' is a chain map and is the inverse of ϕ_3. Hence, $EGH(G_1) \cong EGH(G_2)$.

Similarly one can prove the invariance of EGH under the cyclic permutation of columns. Let G' be obtained from G by cyclically permuting two consecutive columns of G, such that the j-th

column becomes $(j-2)$ mod $2n$-th column. One can define a chain map $\phi : EGC(G) \longrightarrow EGC(G')$ by

$$\phi(\{x_{ij}^k\}) = \{x_{it}^l\}$$

where $t = j - 2 \pmod{2n}$, $l = k + N_{i,j}^1 - N_{i,t}^2 \pmod 2$ and $N_{i,j}^1$= # intersection points of β_i with the cut lines that lie between $\alpha_0 \cap \beta_i$ and $\alpha_j \cap \beta_i$ in G, and $N_{i,t}^2$ = # intersection points of β_i with the cut lines that lie between $\alpha_0 \cap \beta_i$ and $\alpha_t \cap \beta_i$ in G'. This chain map induces an isomorphism on the homology.

5.4 Discussion

In future, we are hoping to prove the commutation and stabilization invariance.

Commutation: Let G_3 be an extended grid diagram for a link $L \subset S^3$. Let $\widetilde{G_3}$ be a lift of G_3 and the set of generators $S(G_3)$ be the set of unordered 3n-tuples of intersection points between the α- and β-curves satisfying the conditions for the generators.

Let G_3' be obtained from G_3 by commutation of the columns (see Figure 5.59). Here the red α-curves are replaced by the green α-curves.

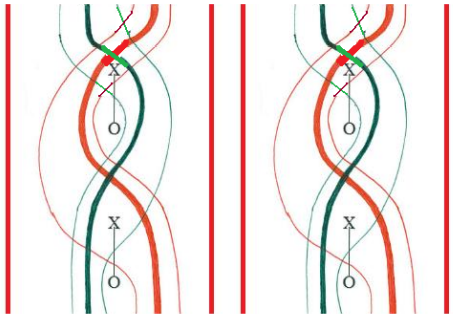

Figure 5.59: The commutation move in the extended grid diagram. Three of the red α-curves are replaced by three other green α-curves. Among the three to be replaced, one is an old α-curve and other two are new α-curves.

Theorem 5.4.1. *If G_3 and G'_3 are extended grid diagrams of a link L in S^3 branched along L, where G'_3 differs from G_3 by a commutation move, then there is an isomorphism between $EGH(G_3)$ and $EGH(G'_3)$.*

Stabilization: We consider the stabilization as shown in Figure 5.60.

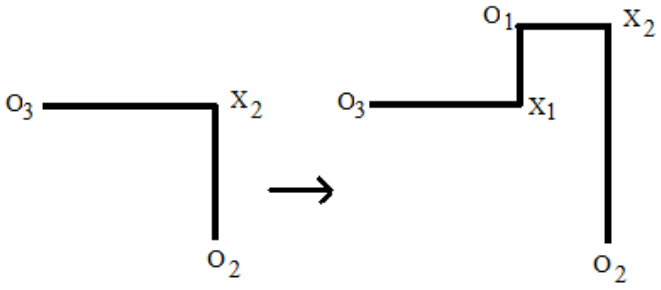

Figure 5.60: Figure showing stabilization at X_2. O_1 and X_1 are the new entries after the stabilization.

Figure 5.61 shows the extended grid diagram for a stabilized unknot. Here we notice that we have introduced two new $\boldsymbol{\alpha}$ (similarly $\boldsymbol{\beta}$)-curves in the extended grid, one of them is a thickened (old) curve, and the other one is a thin (new) curve. This means that there will be two thickened curves and one thin curve extra in the lift.

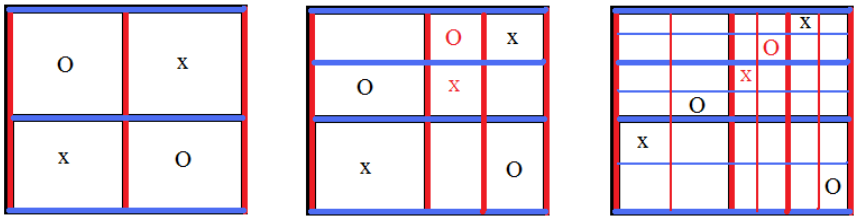

Figure 5.61: Extended grid diagram for stabilized unknot.

Let $\mathbb{G}$ be an adapted diagram for Y and $\mathbb{G}_s$ be its stabilization as described above. We draw the adapted diagram as a lift of the extended grid diagram which has two copies of the extended grid such that each new curve (one that is introduced into the grid diagram to obtain an extended grid diagram) goes over from one grid to the other, forming a single curve and each of the old

curves (ones that are the original curves in the grid diagram) lifts to two copies of the same curve (Figure 5.62). Hence, there are total of (3n+3) $\boldsymbol{\alpha}$ (similarly $\boldsymbol{\beta}$)-curves.

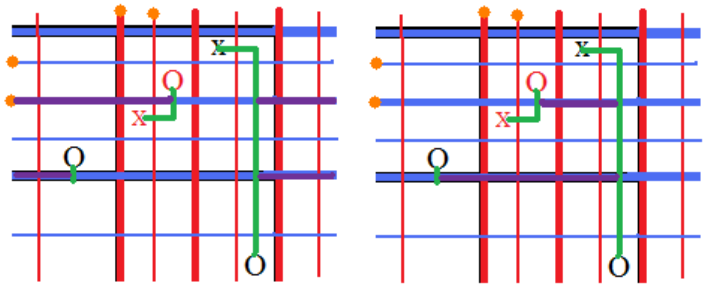

Figure 5.62: The extended grid diagram in the lift. The lines with the orange dots are the newly introduced lines after the stabilization. Thin red and blue lines respectively, in the extended grid are connected, representing a single curve. Therefore, in the lift we have 3 new α-(similarly β-) curves, a total of (3n+3) $\boldsymbol{\alpha}$ (similarly $\boldsymbol{\beta}$)-curves. The red colored X and O represents X_1 and O_1.

Theorem 5.4.2. *If G and G' are extended grid diagrams of a link L in S^3 branched along L, where G' differs from G by a stabilization move (as described above), then there is an isomorphism between $EGH(G')$ and $EGH(G) \otimes (\mathbb{Z}/2 \oplus \mathbb{Z}/2)^2$.*

Chapter 6

The Coding Algorithm

In this chapter we present a representation for a grid diagram in a matrix form. We use this matrix interpretation of the adapted diagram to present an algorithm we use in the computer code we developed to compute extended grid homology of double branched covers of S^3 along links in S^3.

Description of a grid as a matrix: For an extended grid diagram of grid size $2n \times 2n$, we will use as a representative of a generator a matrix $M = [m_{ij}]_{0 \leq i,j \leq (2n-1)}$ of size $2n \times 2n$. The $\boldsymbol{\alpha}$-curves are represented by columns and the $\boldsymbol{\beta}$-curves are represented by rows in the matrix. The intersection points of $\boldsymbol{\alpha}$ and $\boldsymbol{\beta}$-curves in the grid are represented by corresponding entry positions in a matrix. The intersection of α_i and β_j corresponds to m_{ji} entry in the matrix.

Description of a knot in a matrix: A knot in a grid is represented by basepoints. A basepoint in the grid lies in a portion of the grid bounded by $(\beta_i, \beta_{i+1}) \times (\alpha_j, \alpha_{j+1})$. We represent such a point by a pair $(i + \frac{1}{2}, j + \frac{1}{2})$. For example, in Figure 6.1, we have the basepoints (0+ $\frac{1}{2}$, 2+ $\frac{1}{2}$), (1+ $\frac{1}{2}$, 6+ $\frac{1}{2}$), (2+ $\frac{1}{2}$, 0+ $\frac{1}{2}$), (3+ $\frac{1}{2}$, 5+ $\frac{1}{2}$), (4+ $\frac{1}{2}$, 7+ $\frac{1}{2}$), (5+ $\frac{1}{2}$, 3+ $\frac{1}{2}$), (6+ $\frac{1}{2}$, 4+ $\frac{1}{2}$), (7+ $\frac{1}{2}$, 1+ $\frac{1}{2}$). We will use this example to illustrate how to represent an intersection of a cut line with a row. In Figure 6.1, there are 0 cut lines in the 0-th row, so we assign $\{0\}$ to this row. There is one cutline in the 1st row, which appears right after the 3rd column, so we assign $\{3 + \frac{1}{2}\}$. There are two cut line intersections in the 2nd row, so we assign $\{3 + \frac{1}{2}, 7 + \frac{1}{2}\}$. Similarly, we assign

$\{1+\frac{1}{2}, 3+\frac{1}{2}, 7+\frac{1}{2}\}$ to the 3rd, $\{1+\frac{1}{2}, 3+\frac{1}{2}, 5+\frac{1}{2}, 7+\frac{1}{2}\}$ to the 4-th, $\{1+\frac{1}{2}, 3+\frac{1}{2}, 5+\frac{1}{2}\}$ to the 5-th, $\{1+\frac{1}{2}, 5+\frac{1}{2}\}$ to the 6-th, and $\{1+\frac{1}{2}\}$ to the 7-th row. In general, a cut line that appeared in the i-th row in between the j-th and $(j+1)$-th columns will be assigned a value $\{j+\frac{1}{2}\}$. Similarly, a cut line that appeared in the j-th column in between the i-th and $(i+1)$-th rows will be assigned a value $\{i+\frac{1}{2}\}$.

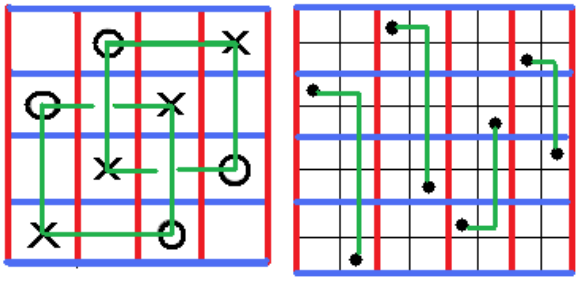

Figure 6.1: Extended grid diagram for Hopf link.

Description of generators in matrix form: We discuss generators $\{x_{ij}^{k_{ij}}\}$ for $EGC(G)$ that appeared in the definition 4.2.1. We will form a matrix where an entry in the corresponding i-th row and j-th column corresponds to the assignment of a certain value to the exponent k_{ij}. The entries will be $[1,0], [-1,0]$, or $[1,-1]$ at the positions that are present in the generator, and $[0,0]$ otherwise.

- If there is exactly one point in an even row, then that point also appears in the even column and is the only point in that even column as well. That point has position $m_{2i,2j'}$ and we assign $k_{2i,2j'} = [1,-1]$. This corresponds to the case when lifts of two old curves intersect in such a way that their intersections project to the same point in the extended grid.

- Except in case above, each even row and column in the grid contains two points for each generator, and we have exactly two positions in the matrix that are not $[0,0]$, i.e there are two points m_{ij} assigned one of the two values $k_1 = [1,0]$ or $k_2 = [-1,0]$. In the double cover of the extended grid, [1, 0] represents an intersection point of $\boldsymbol{\alpha}$ and $\boldsymbol{\beta}$ in the positive region G^+ and [-1, 0] represents an intersection point of $\boldsymbol{\alpha}$ and $\boldsymbol{\beta}$ in the negative region G^-.

- Two different non-zero positions in any even numbered column are such that adding the two entries gives zero, i.e. if one entry in the even numbered column is [1, 0], then the other has to be [-1, 0]. This corresponds to the fact that two entries on an old $\boldsymbol{\alpha}$-curve in the extended grid lift to two distinct intersection points.

- The exponent relationship for two distinct positions in M in an even numbered row depends on the number of intersections of the cut lines with the row between the two positions. If m_{ij} is the first entry in the i-th row, we assign either k_1 or k_2. Call the value k_{ij}. As the row is even, there exists another entry m_{ip}, with $p > j$, such that k_{ip} must satisfy the equation,

$$k_{ij} = (-1)^{N+1} k_{ip} \tag{6.1}$$

  where N is the number of intersections of the cut lines with the i-th row in between m_{ij} and m_{ip} and thus k_{ip} is uniquely determined by k_{ij}.

- For position m_{ij}, i, j odd, there are no conditions on what k_{ij} we can assign. If one coordinate is odd and the other even, the conditions in the even coordinate are as above.

Hence, for a generator of $EGH(G)$ we have a matrix $M_k = [k_{ij}]$. Figure 6.2 shows a generator in the matrix form.

Description of the rectangles in the boundary map: We describe the rectangles that appeared in equation 4.2. We take two generators $M_k = [k_{ij}]$ and $M_{k'} = [k'_{ij}]$. These generators have $3n$ non-zero entries. To obtain a rectangle, the code calculates $M_k - M_{k'}$. We require $M_k - M_{k'}$ to have precisely four non-zero positions in the matrix such that the four non-zero positions create a rectangle. Suppose the four corners of the rectangle are $c_{ij}, c_{ip}, c_{dj}, c_{dp}$ where $c_{ij} := k_{ij} - k'_{ij}$. Figure 6.3 shows two rectangles with four nonzero corner positions in the matrix obtained by subtracting the two generators.

The algorithm in the code checks whether the rectangle is a type A, type B or type C, type D rectangle (as discussed in section 4.2.2). For that, consider the sum $s_{ij} = k_{ij} + k'_{ij}$ at the four corner points. There are five possibilities for the sum - it can be either [0, 0], [1, 0], [-1, 0], [1, -1],

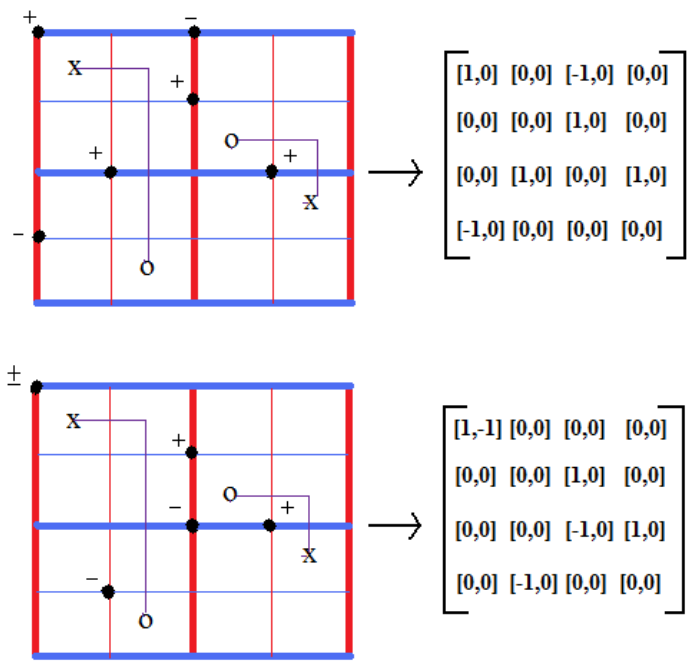

Figure 6.2: Generators in the matrix form. The left hand side diagram shows two generators in the extended grid diagram for an unknot and the right hand side shows their corresponding matrix form.

[2, -1] or [0, -1]. For example, in Figure 6.3, the first rectangle has four corners at c_{00}, c_{01}, c_{20} and c_{21}. For those four corner points, the code calculates the sum of the entries from the two generators (Figure 6.4) and sets all the other entries in the matrix to be [0,0].

If the sum entry is [2, -1], then one of the entries at that corner point from one of the generators had to be [1, -1] and the other [1, 0], and the corner point of the rectangle in the same column has to have the value [-1, 0] (Figure 6.5) for the rectangle to exist. If the sum is [0, -1], then one of the entries at that corner point from one of the generators is [1, -1] and the other is [-1, 0], and the other corner point of the rectangle in the same column has to have the value [1, 0] for the rectangle to exist.

If the sum is one of [1, 0], [-1, 0] or [-1, 1], then one of the entries at that position is [1, 0], [-1, 0] or [-1, 1] and the other one is [0, 0]. If the sum is [0, 0], the code discards the choice.

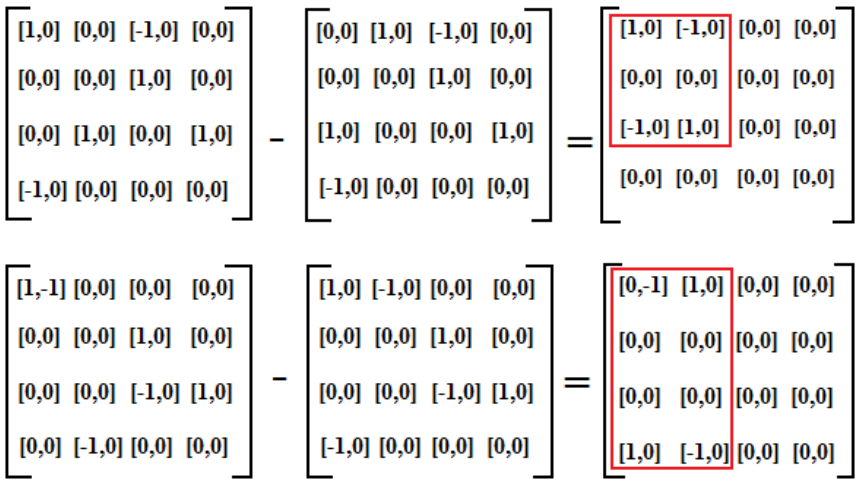

Figure 6.3: Two rectangles in the matrix are shown, which are formed by four non-zero positions, obtained by subtracting two generators.

Next the code checks from where the four corner points come. The code allows only those rectangles whose top-left and bottom-right corners are from the first generator and the other two from the second generator or vice versa. In the case when the sum of the entries from the two generators at the vertex of the rectangle is [2, -1] or [0, -1], the entry [1, -1] decides the type of the rectangle. If it is a top-left corner point in the rectangle and [1, -1] is the entry from the first generator, then the rectangle is either a type A or type B rectangle (Figure 6.4, Figure 6.5), otherwise it is of type C or type D.

For the rest of the code for finding appropriate rectangles, we assign a positive sign to [1, 0] and a negative sign to [-1, 0]. If a corner point has [1, -1] assignment, then the code checks for both [1, 0] and [-1, 0].

We have two sets of rectangles that might appear depending on the upper left (UL) corner of the rectangle. If UL is coming from M_k, then it is either a type A or type B rectangle, otherwise it is a type C or D rectangle (refer to section 4.2.2).

In the next paragraph, we illustrate the code that checks for type A rectangles. Other types are similarly coded in the program.

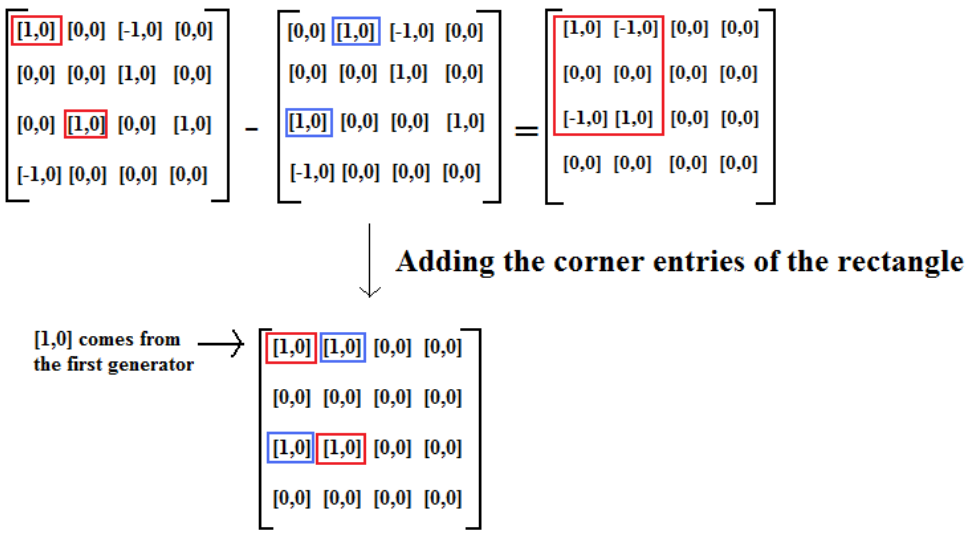

Figure 6.4: Proper assignment at the corners of the rectangle. Since the top-left corner point comes from the first generator, the rectangle is either of type A or of type B.

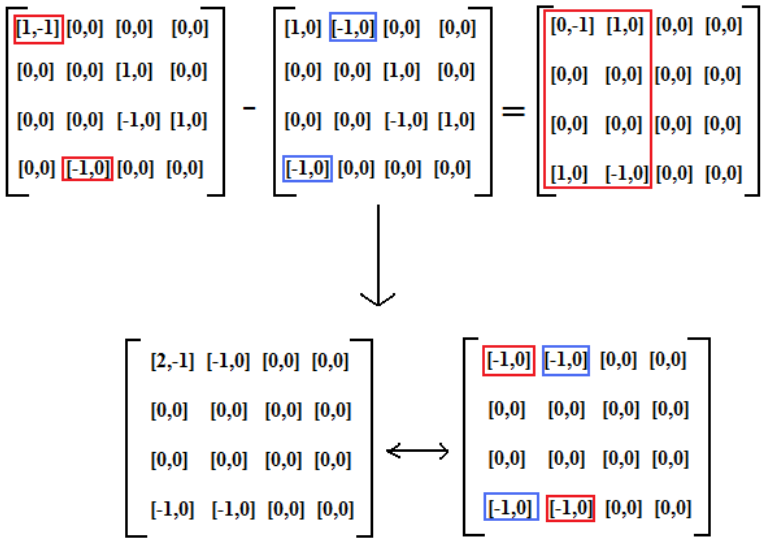

Figure 6.5: Proper assignment at the corners of the rectangle. The rectangle is either of type A or of type B as the top-most corner point gets the value from the first generator.

Type A rectangles: Pick a basepoint (a, b) (Figure 6.6). The basepoint (a, b) has the form $(i + \frac{1}{2}, j + \frac{1}{2})$, where i denotes the i-th row and j denotes the j-th column. Let U, D be the top and bottom rows of the rectangle and L, R denote the left and the right columns of the rectangle.

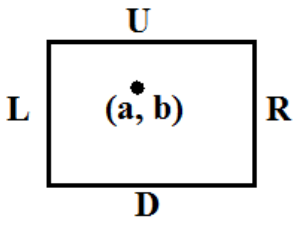

Figure 6.6: A type A rectangle with rows U, D and columns L, R in the matrix with a basepoint (a, b).

The code checks if $U < a < D$ and $L < b < R$. If there is a rectangle which contains a basepoint, then the code discards that rectangle. Next the code checks for positions in M_k and $M_{k'}$ that are in the interior of the rectangle. For that the code checks if there are points in the rows of the matrix between columns L and R and for rows between U and D. The following describes how the code detects appropriate sign for the interior points. All these conditions make sure that the point lies outside the rectangle in the lift.

We refer to Figure 6.7 for the notation.

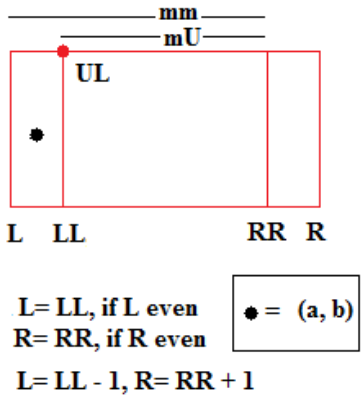

Figure 6.7: mU refers to the number of intersections of the cut lines with row U in between LL and RR. mm refers to the number of intersections of the cut lines with row U in between L and RR.

We consider the following cases:

Case 1: If $mU = 0$, the sign of the interior point p_* has to be the negative of the sign of UL to guarantee that the interior point is not in the interior of the rectangle in the lift.

Case 2: If $mU \neq 0$, then we have the following cases:

Subcase 2.1: If $mm = mU$.

Subcase 2.1.1: There is a basepoint (a, b) in the rectangle bounded by U, D, L and LL (Figure 6.8). If the row of $p_* < a$, then sign of p_* is $(-1)^{N_m+1}\times$ (sign of UL), where N_m is the number of intersections of the cut lines with the row, where p_* lies in between L and column of p_*. Otherwise, sign of p_* is $(-1)^{N_m}\times$ (sign of UL).

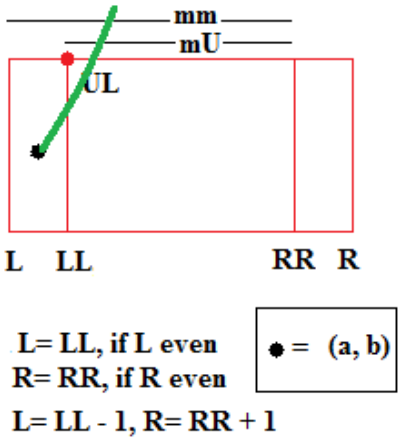

Figure 6.8: Basepoint in between the U, D rows and L, LL columns.

Subcase 2.1.2: There is no basepoint in the rectangle bounded by U, D, L and LL (Figure 6.9). Then the sign of p_* is $(-1)^{N_m+1}\times$ (sign of UL).

Subcase 2.2: If $mm \neq mU$.

Subcase 2.2.1: There is a basepoint (a, b) in the rectangle bounded by U, D, L and LL (Figure 6.10). If the row of $p_* < a$, then the sign of p_* is $(-1)^{N_m}\times$ (sign of UL). Otherwise, sign of p_* is $(-1)^{N_m+1}\times$ (sign of UL).

Subcase 2.2.2: There is no basepoint in the rectangle bounded by U, D, L and LL (Figure 6.11). Then the sign of p_* is $(-1)^{N_m}\times$ (sign of UL).

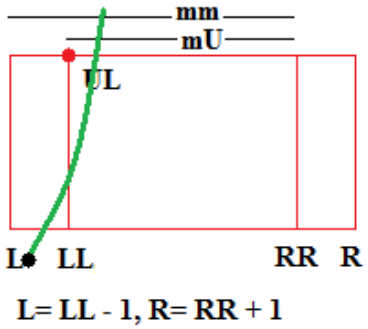

Figure 6.9: No basepoint in between the U, D rows and L, LL columns.

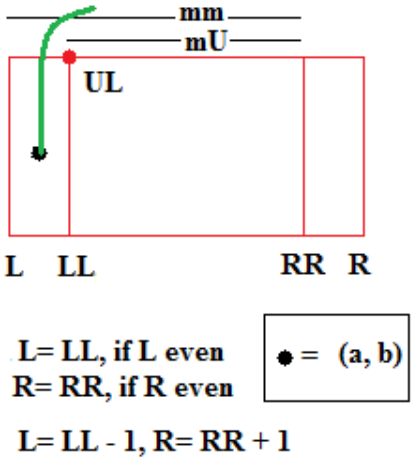

Figure 6.10: Subcase 2.2.1: Basepoint in between the U, D rows and L, LL columns.

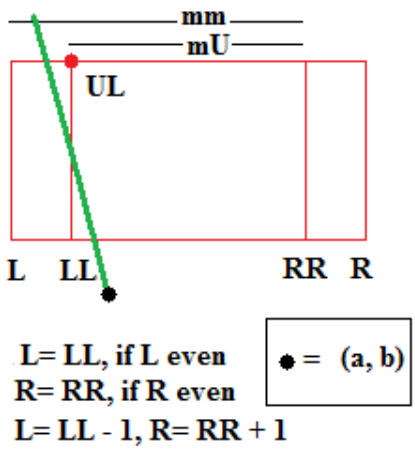

Figure 6.11: Subcase 2.2.2: No basepoint in between the U, D rows and L, LL columns.

Compatible boundary points: Boundary point refers to the point on the boundary of the rectangle. We want to make sure if there is a point on the boundary of the rectangle in the extended grid, then it has appropriate sign so that it does not lie on the boundary of the rectangle in the lift. In the row U, sign of a boundary point p_1 is $(-1)^{N+1}\times$ (sign of UL), where N is the number of intersections of the cut lines with the row U in between L and column of p_1. Similarly, the other boundary points on the left and right columns and the lower row is determined in the code.

Proper signs for the four corners of the rectangle: Finally, the code checks for the proper signs for the four corner points of the rectangle to ensure the region is a valid rectangle in the lift. We fix the top left corner position UL. Then the sign of the top right corner UR is $(-1)^{n_1}$ (sign of UL) and the sign of bottom left corner DL is $(-1)^{n_2}$ sign of UL, where n_1 is the number of intersections of the cut lines with the row U in between L and the column of UR, and n_2 is the number of intersections of the cut lines with the column L in between U and the row of DL. The code requires $(-1)^{n_3}$ (sign of DL) to be equal to $(-1)^{n_4}$ (sign of UR), where n_3 is the number of intersections of the cut lines with the row D in between L and the column of DR, and n_4 is the number of intersections of the cut lines with the column R in between U and the row of the down right corner DR. Then sign of DR is $(-1)^{n_3}$ (sign of DL).

In a similar manner, the code is written for other types of rectangles. A differential matrix is written where rows and columns are the generators and an $ij-$th entry in the matrix is 1, if there exists an empty rectangle connecting one generator M_i to the other generator M_j or 0, if such rectangle does not exist.

We have calculated the extended grid homology for the double branched cover of S^3 branched along an unknot. For an unknot the extended grid number is 4. The number of generators is 224. At this moment, the code is in the developmental stage. Due to memory issues, the code is able to generate the generators only for extended grid number 6. There are 57120 generators of the chain complex EGC of the double branched cover of S^3 branched along an unknot with extended grid number 6.

The code is available upon request.

Chapter 7

Bibliography

[1] Birman, J.S., Menasco, W., *Special positions for essential tori in link complements*, Topology, 33(3):525-556, 1994.

[2] Brunn, H. *Über verknotete Kurven*. Verhandlungen des Internationalen Math. Kongresses (Zurich 1897), pp. 256-259, 1898.

[3] Cromwell, P. R., *Embedding knots and links in an open book. I. Basic Properties*, Topology Appl., 64(1):37-58, 1995.

[4] Cromwell, P. R., *Knots and links*, Cambridge University Press, Cambridge, 2004.

[5] Douroudian, F., *Combinatorial knot Floer homology and cyclic double branched covers*, preprint, math.GT/ 1107.1363.

[6] Dynnikov, I., *Arc-presentations of links: monotonic simplification*, Fund. Math., 190: 29 - 76, 2006.

[7] Floer, A., *Morse theory for Lagrangian intersections*, J. Differential Geometry, 28:513-547, 1988.

[8] Fox, R. H., *A note on branched cyclic covering of spheres*, Rev. Mat. Hisp.- Amer. (4), 32: 158-166, 1972.

[9] Lipshitz, R., *A cylindrical reformulation of Heegaard Floer homology*, Geom. Topol. 10 (2006), 955- 1097.

[10] Lipshitz, R., Manolescu, C., Wang, J., *Combinatorial cobordism maps in hat Heegaard Floer theory*, Duke Math. J. 145 (2008).

[11] MacDonald, I. G., *Symmetric products of an algebraic curve*, Topology, 1:319-343,1962.

[12] Manolescu, C., Ozsváth, P. and Sarkar, S., *A combinatorial description of knot Floer homology*, Ann. of Math. 169 (2009), 633-660.

[13] Manolescu, C., Ozsváth, P., Szabó, Z., Thurston, D., *On Combinatorial Link Floer Homology*, Geom. Topol, 11: 2339-2412, 2007.

[14] Ozsváth, P., Stipsicz, A., Szabó, Z., *Grid homology for knots and links*, in preparation.

[15] Ozsváth, P., Stipsicz, A., Szabó, Z., *Combinatorial Heegaard Floer homology and nice Heegaard diagrams*, preprint, math.GT/0912.0830.

[16] Ozsváth, P., Szabó, Z., *Holomorphic disks and three-manifold invariants: properties and applications*, math.SG/0105202, 2001.

[17] Ozsváth, P., Szabó, Z., *An introduction to Heegaard Floer homology*, Clay Mathematics Proceedings.

[18] Ozsváth, P. and Szabó, Z., *Holomorphic disks and topological invariants for closed three-manifolds*, Ann. of Math., 159 (2004) 1027-1158.

[19] Ozsváth, P. and Szabó, Z., *Holomorphic disks and knot invariants*, Adv. Math., 186(1):58116, 2004.

[20] Ozsváth, P. and Szabó, Z., *Holomorphic disks, link invariants and the multi-variable Alexander polynomial*, arXiv:math.GT/0512286, 2005.

[21] Ozsváth, P., Szabó, Z., *Heegaard diagrams and holomorphic disks*, Different Faces of Geometry, 301-348, International Mathematical Series (New York), 3, Kluwer/Plenum, New York, 2004.

[22] Sarkar, S. and Wang, J., *An algorithm for computing some Heegaard Floer homologies*, Ann. of Math., Volume 171 (2010), Issue 2, 1213-1236.

[23] Singer, J., *Three-dimensional manifolds and their Heegaard diagrams*, Trans. Amer. Math. Soc., 35(1): 88-111, 1933.

[24] Stipsicz, A., *Computations of Heegaard Floer Homology Groups*, MATHEMATICA, Tome 52(75), N° 1, 2010, pp. 55-74.

[25] Weibel, C., *An introduction to homological algebra*, Cambridge University Press, 1994.